TASOPT 2.16
Transport Aircraft System OPTimization
Technical Description

Mark Drela
26 Nov 16

TASOPT is a program for optimizing the airframe of a wing+tube transport aircraft, together with the engine parameters and operating parameters. The target objective is minimum fleet fuel burn for a set of given payload and range missions, possibly in the presence of field length constraints.

This document derives the physical models used to represent the structural, aerodynamic, propulsion, and performance elements of the overall combined model. It also presents the resulting relations and their convergence iteration strategy as used in TASOPT's code implementation.

Contents

1 Introduction

1.1 Background

There is a vast body of work on conceptual and preliminary aircraft design. The more traditional approaches of e.g. Roskam [1], Torrenbeek [2], Raymer [3], have relied heavily on historical weight correlations, empirical drag build-ups, and established engine performance data for their design evaluations. The ACSYNT program [4],[5] likewise relies on such models, with a more detailed treatment of the geometry via its PDCYL [6] extension.

More recently, optimization-based approaches such as those of Knapp [7], the WINGMOD code of Wakayama [8],[9], and in particular the PASS program of Kroo [10] perform tradeoffs in a much more detailed geometry parameter space, but still rely on simple drag and engine performance models.

The recent advent of turbofan engines with extremely high bypass ratios (Pratt geared turbofan), advanced composite materials (Boeing 787), and possibly less restrictive operational restrictions (Free-Flight ATC concept), make it of great interest to re-examine the overall aircraft/engine/operation system to maximize transportation efficiency. NASA's N+1,2,3 programs are examples of research efforts towards this goal. In addition, greater emphasis on limiting noise and emissions demands that such aircraft design examination be done under possibly stringent environmental constraints. Optimally exploiting these new factors and constraints on transport aircraft is a major motivation behind TASOPT's development.

1.2 Summary

1.2.1 Overall approach

To examine and evaluate future aircraft with potentially unprecedented airframe, engine, or operation parameters, it is desirable to dispense with as many of the historically-based methods as possible, since these cannot be relied on outside of their data-fit ranges. The approach used by TASOPT is to base most of the weight, aerodynamic, and engine-performance prediction on low-order models which implement fundamental structural, aerodynamic, and thermodynamic theory and associated computational methods. Historical correlations will be used only where absolutely necessary, and in particular only for some of the secondary structure and for aircraft equipment. Modeling the bulk of the aircraft structure, aerodynamics, and propulsion by fundamentals gives considerable confidence that the resulting optimized design is realizable, and not some artifact of inappropriate extrapolated data fits.

1.2.2 Airframe structure and weight

The airframe structural and weight models used by TASOPT treat the primary structure elements as simple geometric shapes, with appropriate load distributions imposed at critical loading cases. The fuselage is assumed to be a pressure vessel with one or more "bubbles", with added bending loads, with material gauges sized to obtain a specified stress at specified load situations. The wing is assumed to be cantilevered or to have a single support strut,

whose material gauges are also sized to obtain a specified stress. The resulting fuselage, wing, and tail material volumes, together with specified material density, then gives the primary structural weight. Only the secondary structural weights and non-structural and equipment weights are estimated via historical weight fractions.

1.2.3 Aerodynamic performance

The wing airfoil performance is represented by a parameterized transonic airfoil family spanning a range of thicknesses, whose performance is determined by 2D viscous/inviscid CFD calculation for a range of lift coefficients and Mach numbers. Together with suitable sweep corrections, this gives reliable profile+wave drag of the wing in cruise and high climb and high descent. The fuselage drag is likewise obtained from compressible viscous/inviscid CFD, suitably simplified with axisymmetric-based approximations. A side benefit is that detailed knowledge of the fuselage boundary layers makes it possibly for TASOPT to reliably predict the benefits of boundary layer ingestion in fuselage-mounted engines.

The drag of only the minor remaining components such as nacelles is obtained by traditional wetted area methods, but corrected for supervelocities estimated with vortex sheet models. Induced drag is predicted by fairly standard Trefftz-Plane analysis.

The primary use of CFD-level results in the present TASOPT method makes it more widely applicable than the previous more traditional approaches which have typically relied on wetted-area methods for major components of the configuration.

1.2.4 Engine performance

A fairly detailed component-based turbofan model, such as described by Kerrebrock [11], is used to both size the engines for cruise, and to determine their off-design performance at takeoff, climb, and descent. The model includes the effects of turbine cooling flows, allowing realistic simultaneous optimization of cycle pressure ratios and operating temperatures together with the overall airframe and its operating parameters. The overall aircraft and engine system is actually formulated in terms of dissipation and power rather than drag and thrust [12], which allows a rigorous examination of advanced propulsion systems using boundary layer ingestion.

The use of component-based engine simulation in the present TASOPT method differs from previous approaches which typically have relied on simple historical regressions or established engine performance maps. The more detailed treatment is especially important for examining designs with extreme engines parameters which fall outside of historical databases.

1.2.5 Mission profiles

Integration of standard trajectory equations over a parameterized mission profile provides the required mission weight, which completes the overall sizing approach. The end result is a defined aircraft and engine combination which achieves the specified payload and range mission. Off-design missions are also addressed, allowing the possibility of minimizing fuel burn for a collection of fleet missions rather than for just the aircraft-sizing mission.

1.2.6 Takeoff and noise

A takeoff performance model is used to determine the normal takeoff distance and the balanced field length of any given design. The balanced field length can be included as a constraint in overall TASOPT optimization. Noise estimates are also calculated using a few published methods, e.g. [13], [14], [15]. These are used only for run-time rough estimates, and are not well suited for use as constraints. Much more detailed noise analyses can typically be performed as a post-processing step using the ANOPP method, for example.

1.2.7 Restriction to wing+tube aircraft

The description of the structural and aerodynamic models above explains why TASOPT is restricted to tube+wing configurations — most other configurations would be quite difficult or impossible to treat with these models. For example, a joined-wing configuration [16] has a relatively complex structure with out-of-plane deformations and the possibility of coupled twist/bend buckling in the presence of eccentricity from the airloads, which requires a greatly more complex structural analysis than straightforward beam theory. A blended-wing-body configuration [17] with non-circular cabin cross sections likewise has non-obvious critical load cases and load paths, and its transonic aerodynamics are dominated by 3D effects. For these reasons such non-traditional configurations are simply outside the scope of the present work.

2 Model Derivation

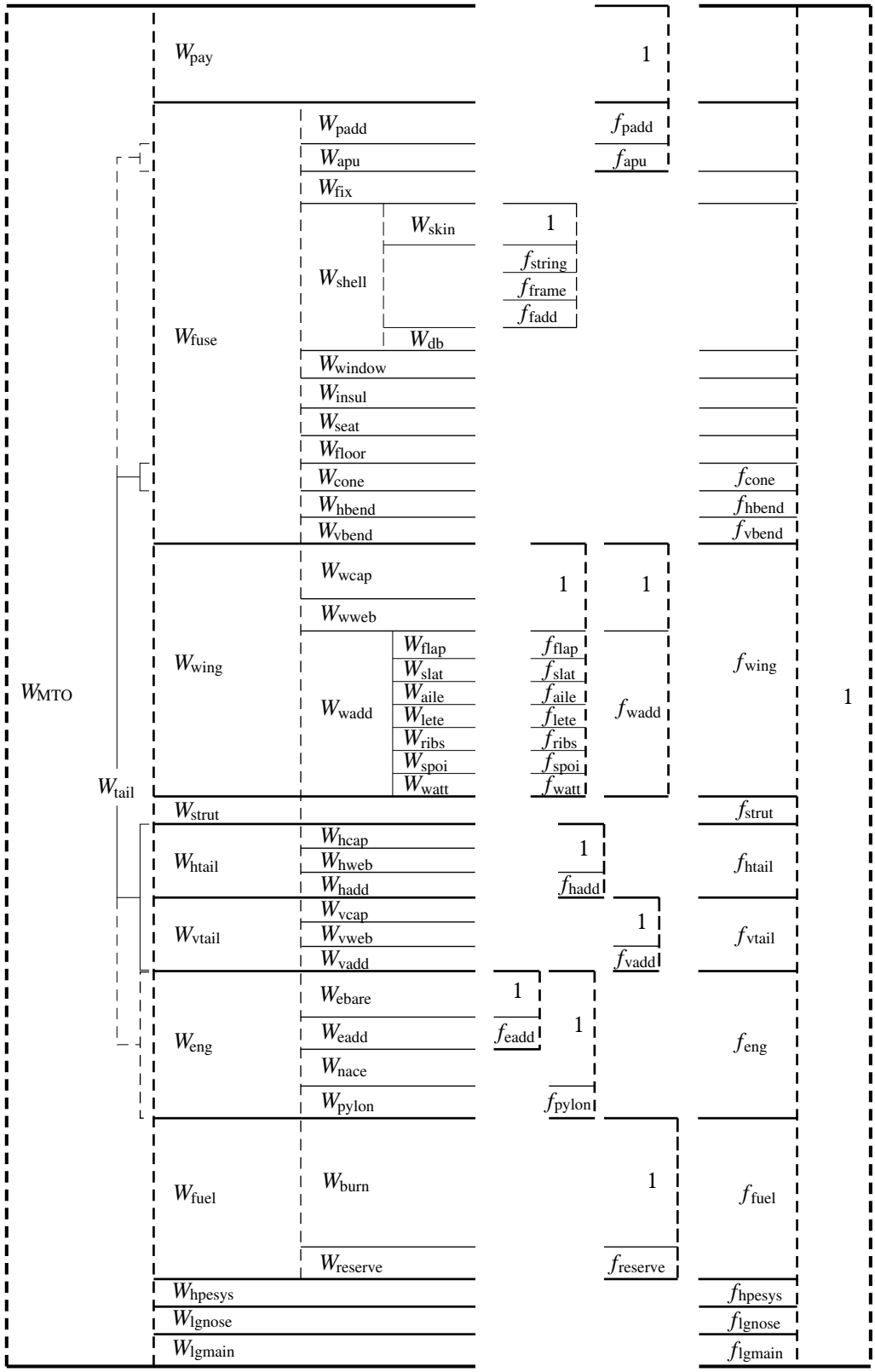

Figure 1: Aircraft weights and weight fractions breakdown.

2.1 Weight Breakdown

The weight breakdown is summarized in Figure 1, to serve as a convenient reference.

2.2 Fuselage pressure and torsion loads

The fuselage is modeled as a side-by-side "multi-bubble" pressure vessel with an ellipsoidal nose endcap and a hemispherical tail endcap, which is subjected to pressurization, bending, and torsion loads, as shown in Figures 2 and 3. The loaded cylindrical length of the pressure vessel shell is from $x_{\text{shell}\,1}$ to $x_{\text{shell}\,2}$.

$$l_{\text{shell}} \;=\; x_{\text{shell}\,2} \;-\; x_{\text{shell}\,1} \tag{1}$$

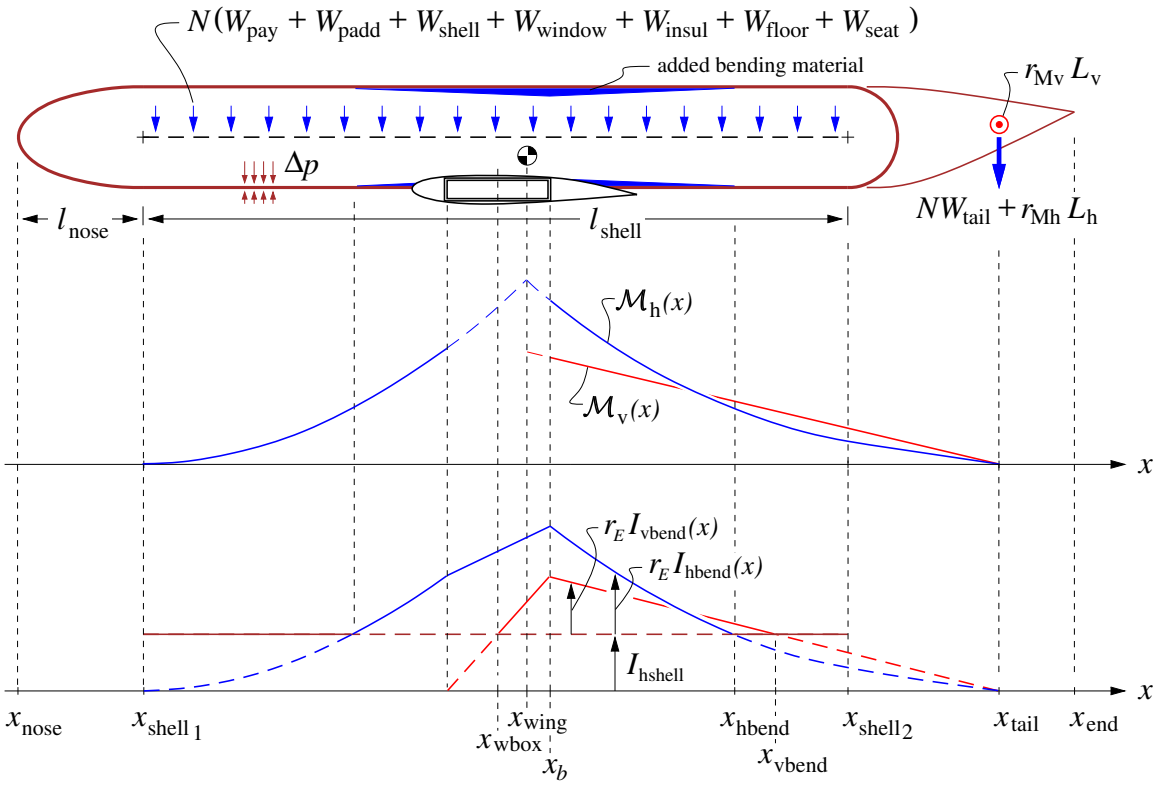

Figure 2: Fuselage layout, loads, and bending moment and inertia distributions. Bending material and $r_E I_{\text{hbend}(x)}$ is added wherever the horizontal-axis bending moment $\mathcal{M}_{\text{h}(x)}$ exceeds the capability of the pressure vessel's bending inertia I_{hshell}, and likewise for the vertical-axis moment and inertia.

The horizontal-axis moment $\mathcal{M}_{\text{h}(x)}$ distributions on the front and back bending fuselage are assumed to match at location x_{wing}, as shown in Figure 2. Theoretically this is the wing's net lift–weight centroid, which varies somewhat depending the fuel fraction in the wings, the wing's profile pitching moment and hence the flap setting, and on the aircraft C_L. For simplicity it will be approximated as the wing's area centroid. Note that for a swept wing the wing box location x_{wbox} will be centered somewhat ahead of x_{wing}, but it will then also

impart a pitch-axis moment at its location, so that the front and back $\mathcal{M}_{\mathrm{h}(x)}$ distributions must still match at x_{wing}.

Figure 3 shows the fuselage cross section for the case of a "double-bubble", or two tubes. Figure 4 compares to alternative possible cross sections with three or four tubes, each specified by the number of webs n_{fweb}. The pressure-vessel skin and endcaps have a uniform thickness t_{skin}, while each of the n_{fweb} tension web(s) has an average thickness t_{fweb}. The cross-sectional area of the skin is A_{skin}, and has stiffening stringers which have a "smeared" average area $A_{\mathrm{skin}} f_{\mathrm{string}} \rho_{\mathrm{skin}} / \rho_{\mathrm{bend}}$, specified via the empirical stringer/skin weight fraction f_{string}. The enclosed area S_{skin} enters the torsional stiffness and strength calculations. The fuselage cross section also shows the possibility of added bottom bubbles or fairings, extended downward by the distance ΔR_{fuse}.

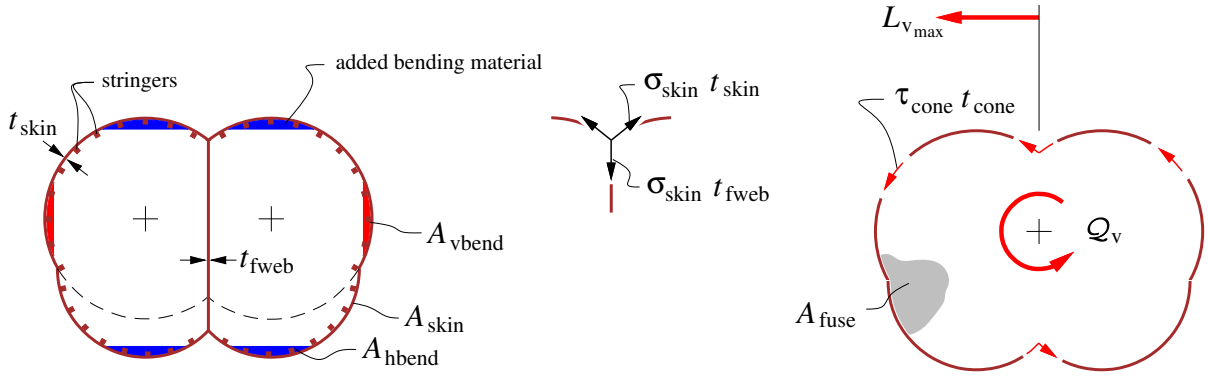

Figure 3: Fuselage cross-section, shell/web junction tension flows, and torsion shear flow from vertical tail load, for the double-bubble case $n_{\mathrm{fweb}} = 1$. An optional bottom fairing extends down by the distance ΔR_{fuse}. Fuselage frames are not shown.

The skin and stringers constitute the "shell", which has bending inertias $I_{\mathrm{hshell}}, I_{\mathrm{vshell}}$ about the horizontal and vertical axes. Figure 3 does not show any hoop-stiffening frames which are typically required, and whose weight is a specified fraction f_{frame} of the skin weight. These typically may be offset from the skin inside of the stringers, and hence are assumed to not contribute to the skin's circumferential tensile strength.

To address the weight and aerodynamic loads of the tail group on the fuselage, the horizontal and vertical tails, the tailcone, and any rear-mounted engines are treated as one lumped mass and aero force at location x_{tail}, shown in Figure 2.

The bending loads on the shell may require the addition of vertical-bending material concentrated on top and bottom of the fuselage shell (typically as skin doublers or additional stringers). The total added cross sectional area is $A_{\mathrm{hbend}(x)}$, and the associated added bending inertia is $I_{\mathrm{hbend}(x)}$. Corresponding added material on the sides has $A_{\mathrm{vbend}(x)}$ and $I_{\mathrm{vbend}(x)}$. Because the wing box itself will contribute to the fuselage bending strength, these added areas and bending inertias do not match the $\mathcal{M}_{(x)}$ distribution there, but are made linear over the wing box extent, as shown in Figure 2.

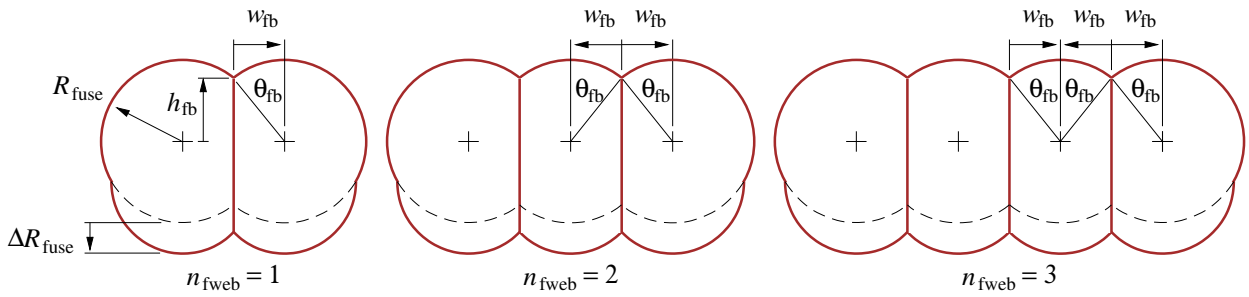

Figure 4: Two-bubble, three-bubble and four-bubble optional cross-sections, specified by the number of webs $n_{\rm fweb}$. Each bubble has the same center-to-web width $w_{\rm fb}$ and subtended half-angle $\theta_{\rm fb}$.

2.2.1 Cross-section relations

The fuselage pressure shell has the following geometric relations and beam quantities.

$$\theta_{\rm fb} = \arcsin(w_{\rm fb}/R_{\rm fuse}) \tag{2}$$

$$h_{\rm fb} = \sqrt{R_{\rm fuse}^2 - w_{\rm fb}^2} \tag{3}$$

$$A_{\rm skin} = (2\pi + 4n_{\rm fweb}\theta_{\rm fb})\, R_{\rm fuse}\, t_{\rm skin} \;+\; 2\Delta R_{\rm fuse}\, t_{\rm skin} \tag{4}$$

$$A_{\rm fweb} = n_{\rm fweb}(2h_{\rm fb} + \Delta R_{\rm fuse})\, t_{\rm fweb} \tag{5}$$

$$A_{\rm fuse} = [\pi + n_{\rm fweb}\,(2\theta_{\rm fb} + \sin 2\theta_{\rm fb})]\, R_{\rm fuse}^2 \;+\; 2\,[R_{\rm fuse} + n_{\rm fweb} w_{\rm fb}]\,\Delta R_{\rm fuse} \tag{6}$$

The skin has some modulus and density $E_{\rm skin}, \rho_{\rm skin}$, while the stringers have some possibly different values $E_{\rm bend}, \rho_{\rm bend}$. The effective modulus-weighted "shell" thickness $t_{\rm shell}$ can then be defined as follows, assuming that only the skin and stringers contribute to bending, but not the frames.

$$t_{\rm shell} = \frac{(Et)_{\rm skin}}{E_{\rm skin}} = t_{\rm skin}\left(1 + r_E\, f_{\rm string}\frac{\rho_{\rm skin}}{\rho_{\rm bend}}\right) \tag{7}$$

$$\text{where} \qquad r_E = \frac{E_{\rm bend}}{E_{\rm skin}} \tag{8}$$

This is then convenient for determining the modulus-weighted horizontal-axis and vertical-axis bending inertias. The fuselage webs, if any, are assumed to be made of the same material as the skin. The passenger-access cutouts will not extend all the way to the skin/web junctions, so that the webs' contributions are included in the overall shell bending inertia.

$$\begin{aligned} I_{\rm hshell} &= \frac{(EI)_{\rm hshell}}{E_{\rm skin}} \\ &= 4\int_0^{\pi/2} (R_{\rm fuse}\sin\theta + \Delta R_{\rm fuse}/2)^2\; R_{\rm fuse}\, t_{\rm shell}\; {\rm d}\theta \\ &+ 4n_{\rm fweb}\int_{\pi/2}^{\pi/2+\theta_{\rm fb}} (R_{\rm fuse}\sin\theta + \Delta R_{\rm fuse}/2)^2\; R_{\rm fuse}\, t_{\rm shell}\; {\rm d}\theta \;+\; \frac{2}{3} n_{\rm fweb}(h_{\rm fb} + \Delta R_{\rm fuse}/2)^3 t_{\rm fweb} \\ &= \Big\{\, [\,\pi + n_{\rm fweb}(2\theta_{\rm fb} + \sin 2\theta_{\rm fb})]\, R_{\rm fuse}^2 \\ &\quad + 8n_{\rm fweb}\cos\theta_{\rm fb}\,(\Delta R_{\rm fuse}/2)\, R_{\rm fuse} \end{aligned}$$

$$+ [2\pi + 4n_{\text{fweb}}\theta_{\text{fb}}] \, (\Delta R_{\text{fuse}}/2)^2 \, \Big\} \, R_{\text{fuse}} \, t_{\text{shell}} \quad + \quad \frac{2}{3} n_{\text{fweb}} (h_{\text{fb}} + \Delta R_{\text{fuse}}/2)^3 t_{\text{fweb}} \tag{9}$$

$$\begin{aligned}
I_{\text{vshell}} &= \frac{(EI)_{\text{vshell}}}{E_{\text{skin}}} \\
&= 4 \int_0^{\pi/2} (R_{\text{fuse}} \cos\theta + n_{\text{fweb}} w_{\text{fb}})^2 \; R_{\text{fuse}} \, t_{\text{shell}} \; \mathrm{d}\theta \\
&+ 4 n_{\text{fweb}} \int_{\pi/2}^{\pi/2+\theta_{\text{fb}}} (R_{\text{fuse}} \cos\theta)^2 \; R_{\text{fuse}} \, t_{\text{shell}} \; \mathrm{d}\theta \; + \; \sum_{k=1}^{n_k} 4 R_{\text{fuse}} t_{\text{shell}} \theta_{\text{fb}} w_{\text{fb}}^2 (2k - i_k)^2 \\
&= \Big[[\, \pi + n_{\text{fweb}} (2\theta_{\text{fb}} - \sin 2\theta_{\text{fb}})] \, R_{\text{fuse}}^2 \\
&\quad + 8 \cos\theta_{\text{fb}} \, n_{\text{fweb}} w_{\text{fb}} \, R_{\text{fuse}} \\
&\quad + (2\pi + 4\theta_{\text{fb}}) \, (n_{\text{fweb}} w_{\text{fb}})^2 \\
&\quad + 4\theta_{\text{fb}} w_{\text{fb}}^2 \sum_{k=1}^{n_k} (2k - i_k)^2 \Big] \, R_{\text{fuse}} \, t_{\text{shell}}
\end{aligned} \tag{10}$$

$$n_k = \text{int}(n_{\text{fweb}}/2) \tag{11}$$

$$i_k = \text{mod}(n_{\text{fweb}} + 1 \, , \, 2) \tag{12}$$

It's useful to note that for the particular case of $n_{\text{fweb}} = 0, w_{\text{fb}} = 0$, together with $\Delta R_{\text{fuse}} = 0$, there is only one circle. The areas and bending inertias then reduce to those for a single circular cross-section.

$$A_{\text{skin}} = 2\pi R_{\text{fuse}} \, t_{\text{skin}} \qquad (\text{if } n_{\text{fweb}} = 0, \; w_{\text{fb}} = 0, \; \Delta R_{\text{fuse}} = 0) \tag{13}$$

$$S_{\text{skin}} = \pi R_{\text{fuse}}^2 \qquad (\text{if } n_{\text{fweb}} = 0, \; w_{\text{fb}} = 0, \; \Delta R_{\text{fuse}} = 0) \tag{14}$$

$$I_{\text{hshell}} = I_{\text{vshell}} = \pi R_{\text{fuse}}^3 \, t_{\text{shell}} \qquad (\text{if } n_{\text{fweb}} = 0, \; w_{\text{fb}} = 0, \; \Delta R_{\text{fuse}} = 0) \tag{15}$$

Hence, no generality is lost with this multiple-bubble cross-section model.

2.2.2 Pressure shell loads

The pressurization load from the Δp pressure difference produces the following axial and hoop stresses in the fuselage skin, with the assumption that the stringers share the axial loads, but the frames do not share the hoop loads. This assumes a typical aluminum fuselage structure, where the stringers are contiguous and solidly riveted to the skin, but the frames are either offset from the skin or have clearance cutouts for the stringers which interrupt the frames' hoop loads.

$$\sigma_x = \frac{\Delta p}{2} \frac{R_{\text{fuse}}}{t_{\text{shell}}} \tag{16}$$

$$\sigma_\theta = \Delta p \, \frac{R_{\text{fuse}}}{t_{\text{skin}}} \tag{17}$$

An isotropic (metal) fuselage skin thickness t_{skin} and the web thickness t_{fweb} will therefore be sized by the larger σ_θ value in order to meet an allowable stress σ_{skin}.

$$t_{\text{skin}} = \frac{\Delta p \, R_{\text{fuse}}}{\sigma_{\text{skin}}} \tag{18}$$

$$t_{\text{fweb}} = 2 \, \frac{\Delta p \, w_{\text{fb}}}{\sigma_{\text{skin}}} \tag{19}$$

This particular $t_{\rm fweb}$ value is obtained from the requirement of equal circumferential stress in the skin and the web, and tension equilibrium at the 3-point web/skin junction.

The volume of the skin material $\mathcal{V}_{\rm skin}$ is obtained from the cross-sectional skin area, plus the contribution of the ellipsoidal nose endcap and the spherical rear bulkhead. The nose uses Cantrell's approximation for the surface area of an ellipsoid.

$$S_{\rm nose} \simeq [2\pi + 4n_{\rm fweb}\theta_{\rm fb}]\, R_{\rm fuse}^2 \left[\frac{1}{3} + \frac{2}{3}\left(\frac{l_{\rm nose}}{R_{\rm fuse}}\right)^{8/5}\right]^{5/8} \tag{20}$$

$$S_{\rm bulk} \simeq [2\pi + 4n_{\rm fweb}\theta_{\rm fb}]\, R_{\rm fuse}^2 \tag{21}$$

$$\mathcal{V}_{\rm cyl} = A_{\rm skin}\, l_{\rm shell} \tag{22}$$

$$\mathcal{V}_{\rm nose} = S_{\rm nose}\, t_{\rm skin} \tag{23}$$

$$\mathcal{V}_{\rm bulk} = S_{\rm bulk}\, t_{\rm skin} \tag{24}$$

$$\mathcal{V}_{\rm fweb} = A_{\rm fweb}\, l_{\rm shell} \tag{25}$$

$$x\mathcal{V}_{\rm cyl} = \tfrac{1}{2}(x_{\rm shell\,1} + x_{\rm shell\,2})\, \mathcal{V}_{\rm cyl} \tag{26}$$

$$x\mathcal{V}_{\rm nose} = \tfrac{1}{2}(x_{\rm nose} + x_{\rm shell\,1})\, \mathcal{V}_{\rm nose} \tag{27}$$

$$x\mathcal{V}_{\rm bulk} = (x_{\rm shell\,2} + \tfrac{1}{2}\Delta R_{\rm fuse})\, \mathcal{V}_{\rm bulk} \tag{28}$$

$$x\mathcal{V}_{\rm fweb} = \tfrac{1}{2}(x_{\rm shell\,1} + x_{\rm shell\,2})\, \mathcal{V}_{\rm fweb} \tag{29}$$

The total fuselage shell weight then follows by specifying a material density $\rho_{\rm skin}$ for the skin and web. The assumed skin-proportional added weights of local reinforcements, stiffeners, and fasteners are represented by the $f_{\rm fadd}$ fraction, and stringers and frames are represented by the $f_{\rm string}, f_{\rm frame}$ fractions.

$$W_{\rm skin} = \rho_{\rm skin}\, g\, (\mathcal{V}_{\rm cyl} + \mathcal{V}_{\rm nose} + \mathcal{V}_{\rm bulk}) \tag{30}$$

$$W_{\rm fweb} = \rho_{\rm skin}\, g\, \mathcal{V}_{\rm fweb} \tag{31}$$

$$xW_{\rm skin} = \rho_{\rm skin}\, g\, (x\mathcal{V}_{\rm cyl} + x\mathcal{V}_{\rm nose} + x\mathcal{V}_{\rm bulk}) \tag{32}$$

$$xW_{\rm fweb} = \rho_{\rm skin}\, g\, x\mathcal{V}_{\rm fweb} \tag{33}$$

$$W_{\rm shell} = W_{\rm skin}(1 + f_{\rm string} + f_{\rm frame} + f_{\rm fadd}) \;+\; W_{\rm fweb} \tag{34}$$

$$xW_{\rm shell} = xW_{\rm skin}(1 + f_{\rm string} + f_{\rm frame} + f_{\rm fadd}) \;+\; xW_{\rm fweb} \tag{35}$$

2.2.3 Cabin volume and Buoyancy weight

At this point it's convenient to calculate the pressurized cabin volume.

$$\mathcal{V}_{\rm cabin} = A_{\rm fuse}\,(l_{\rm shell} \;+\; 0.67\, l_{\rm nose} \;+\; 0.67\, R_{\rm fuse}) \tag{36}$$

The air in the cabin is pressurized to either the specified minimum cabin pressure $p_{\rm cabin}$, or the ambient pressure at altitude $p_{0(h)}$, whichever is greater. The resulting negative cabin buoyancy increases the effective instantaneous weight of the aircraft by the added buoyancy weight $W_{{\rm buoy}(h)}$ which varies with altitude.

$$\rho_{{\rm cabin}(h)} = \frac{1}{RT_{\rm cabin}}\, \max(\, p_{\rm cabin}\,,\; p_{0(h)}\,) \tag{37}$$

$$W_{\rm buoy} = (\rho_{{\rm cabin}(h)} \;-\; \rho_{0(h)})\, g\, \mathcal{V}_{\rm cabin} \tag{38}$$

This is then added to the physical weight to give the net effective aircraft weight used for cruise wing sizing and performance calculations.

$$\bar{W} \;=\; W \,+\, W_{\text{buoy}} \tag{39}$$

2.2.4 Windows and Insulation

The window weight is specified by their assumed net weight/length density W'_{window}, together with the cabin length l_{shell}.

$$W_{\text{window}} \;=\; W'_{\text{window}}\, l_{\text{shell}} \tag{40}$$

$$x\!W_{\text{window}} \;=\; \tfrac{1}{2}(x_{\text{shell}\,1} + x_{\text{shell}\,2})\, W_{\text{window}} \tag{41}$$

The W'_{window} value represents the actual window weight, minus the weight of the skin and insulation cutout which is eliminated by the window.

The fuselage insulation and padding weight is specified by its assumed weight/area density W''_{insul}, together with the cabin+endcap shell surface area.

$$W_{\text{insul}} \;=\; W''_{\text{insul}} \left[\, (1.1\pi + 2\theta_{\text{fb}}) R_{\text{fuse}}\, l_{\text{shell}} \;+\; 0.55\,(S_{\text{nose}} + S_{\text{bulk}}) \,\right] \tag{42}$$

$$x\!W_{\text{insul}} \;=\; \tfrac{1}{2}(x_{\text{shell}\,1} + x_{\text{shell}\,2})\, W_{\text{insul}} \tag{43}$$

The 1.1 and 0.55 factors assume that 55% of the fuselage circle is over the cabin, and the remaining 45% is over the cargo hold which has no insulation.

2.2.5 Payload-proportional weights

The APU weight W_{apu} is assumed to be proportional to the payload weight, and is treated as a point weight at some specified location x_{apu}.

$$W_{\text{apu}} \;=\; W_{\text{pay}}\, f_{\text{apu}} \tag{44}$$

$$x\!W_{\text{apu}} \;=\; x_{\text{apu}}\, W_{\text{apu}} \tag{45}$$

The seat weight is also assumed to be proportional to the payload weight, uniformly distributed along the cabin for a single-class aircraft.

$$W_{\text{seat}} \;=\; W_{\text{pay}}\, f_{\text{seat}} \tag{46}$$

$$x\!W_{\text{seat}} \;=\; \tfrac{1}{2}(x_{\text{shell}\,1} + x_{\text{shell}\,2})\, W_{\text{seat}} \tag{47}$$

Another payload-proportional weight W_{padd} is used to represent all remaining added weight: flight attendants, food, galleys, toilets, luggage compartments and furnishings, doors, lighting, air conditioning systems, in-flight entertainment systems, etc. These are also assumed to be uniformly distributed on average.

$$W_{\text{padd}} \;=\; W_{\text{pay}}\, f_{\text{padd}} \tag{48}$$

$$x\!W_{\text{padd}} \;=\; \tfrac{1}{2}(x_{\text{shell}\,1} + x_{\text{shell}\,2})\, W_{\text{padd}} \tag{49}$$

The proportionality factors $f_{\text{apu}}, f_{\text{seat}}, f_{\text{padd}}$ will depend on generator technology, seat technology, passenger class, and slightly on long-haul versus short-haul aircraft.

2.2.6 Fixed weight

A specified fixed weight contribution W_{fix} is assumed. This represents the pilots, cockpit windows, cockpit seats and control mechanisms, flight instrumentation, navigation and communication equipment, antennas, etc., which are expected to be roughly the same total weight for any transport aircraft. To get the associated weight moment, a specified weight centroid x_{fix} is also specified. Typically this will be located in the nose region.

$$W_{\text{fix}} = \ldots \text{ specified} \tag{50}$$

$$xW_{\text{fix}} = x_{\text{fix}}\, W_{\text{fix}} \tag{51}$$

2.2.7 Floor

The weight of the transverse floor beams is estimated by assuming the payload weight is distributed uniformly over the floor, producing the shear and bending moment distributions shown in Figure 5. The weight of the floor itself is typically much smaller than the payload and is neglected. The floor beams are assumed to by sized by some load factor N_{land}, which

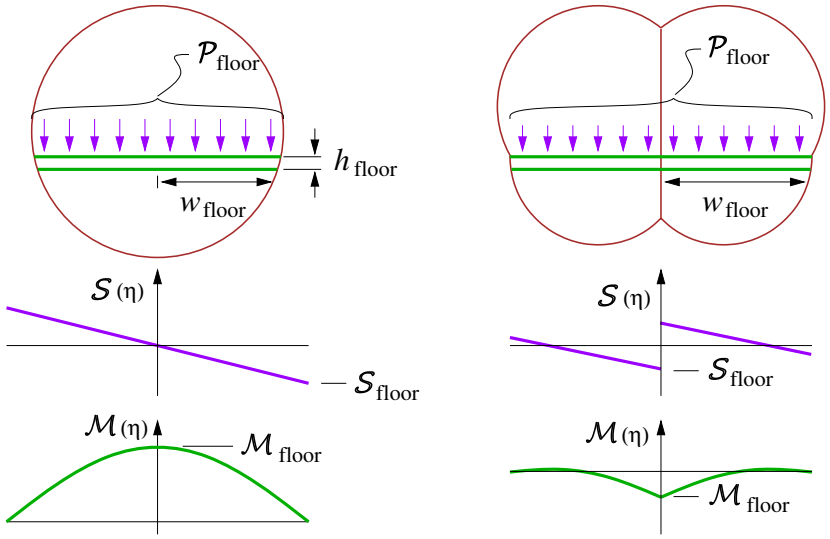

Figure 5: Distributed floor load $¶_{\text{floor}}$, resulting in maximum shear $\mathcal{S}_{\text{floor}}$ and maximum bending moment $\mathcal{M}_{\text{floor}}$ in all the floor beams, without and with a center support.

is typically the emergency landing case and greater than the usual in-flight load factor N_{lift} which sizes most of the airframe. This gives to following total distributed load on the floor.

$$¶_{\text{floor}} = N_{\text{land}}(W_{\text{pay}} + W_{\text{seat}}) \tag{52}$$

The floor/wall joints are assumed to be pinned, with the double-bubble fuselage having an additional center floor support. The single-bubble fuselage can of course also have center supports under the floor. The maximum shear and bending moment seen by all the floor beams put together are then readily obtained from simple beam theory.

$$\mathcal{S}_{\text{floor}} = \frac{1}{2}¶_{\text{floor}} \qquad \text{(w/o support)} \tag{53}$$

$$\mathcal{S}_{\text{floor}} = \frac{5}{16}\,\P_{\text{floor}} \qquad \text{(with support)} \tag{54}$$

$$\mathcal{M}_{\text{floor}} = \frac{1}{4}\,\P_{\text{floor}}\,w_{\text{floor}} \qquad \text{(w/o support)} \tag{55}$$

$$\mathcal{M}_{\text{floor}} = \frac{9}{256}\,\P_{\text{floor}}\,w_{\text{floor}} \qquad \text{(with support)} \tag{56}$$

$$w_{\text{floor}} \simeq w_{\text{fb}} + R_{\text{fuse}} \tag{57}$$

Note that $w_{\text{fb}}=0$ for a single-bubble fuselage, so that the expression for the floor half-width w_{floor} above is valid in general.

For a given floor I-beam height h_{floor}, and max allowable cap stress σ_{floor} and shear-web stress τ_{floor}, the beams' total average cross-sectional area and corresponding weight are then determined. The added weight of the floor planking is determined from a specified weight/area density W''_{floor}.

$$A_{\text{floor}} = \frac{2.0\,\mathcal{M}_{\text{floor}}}{\sigma_{\text{floor}}\,h_{\text{floor}}} + \frac{1.5\,\mathcal{S}_{\text{floor}}}{\tau_{\text{floor}}} \tag{58}$$

$$\mathcal{V}_{\text{floor}} = 2\,\left[n_{\text{fweb}} w_{\text{floor}} + R_{\text{fuse}}\right]\,A_{\text{floor}} \tag{59}$$

$$l_{\text{floor}} = x_{\text{shell}\,2} - x_{\text{shell}\,1} + 2R_{\text{fuse}} \tag{60}$$

$$W_{\text{floor}} = \rho_{\text{floor}}\,g\,\mathcal{V}_{\text{floor}} + 2\,w_{\text{floor}}\,l_{\text{floor}}\,W''_{\text{floor}} \tag{61}$$

$$x W_{\text{floor}} = \tfrac{1}{2}(x_{\text{shell}\,1} + x_{\text{shell}\,2})W_{\text{floor}} \tag{62}$$

Relation (58) assumes the beams are uniform in cross-section. Suitable taper of the cross section would reduce the 2.0 and 1.5 coefficients substantially, especially for the center-supported case for which the bending moment rapidly diminishes away from the center.

It's also important to recognize that if clamped ends rather than the assumed pinned end joints are used, and if the center support is present, then the hoop compliance of the fuselage frame cross-section shape will become important. Without doing the much more complicated deformation analysis of the entire fuselage frame + floor cross section, the conservative pinned-end and uniform beam assumptions are therefore deemed appropriate.

2.2.8 Tail cone

The tail cone average wall thickness is assumed to be sized by the torsion moment $\mathcal{Q}_{\text{v}}$ imparted by the vertical tail, defined in terms of its maximum lift $L_{\text{v}_{\text{max}}}$, span b_{v}, and taper ratio λ_{v}.

$$L_{\text{v}_{\text{max}}} = q_{NE}\,S_{\text{v}}\,C_{L\text{v}_{\text{max}}} \tag{63}$$

$$\mathcal{Q}_{\text{v}} = \frac{L_{\text{v}_{\text{max}}}\,b_{\text{v}}}{3}\,\frac{1+2\lambda_{\text{v}}}{1+\lambda_{\text{v}}} \tag{64}$$

Referring to Figure 3, this $\mathcal{Q}_{\text{v}}$ produces a shear flow $\tau_{\text{cone}}\,t_{\text{cone}}$ according to the torsion-shell relation

$$\mathcal{Q}_{\text{v}} = 2A_{\text{cone}}\,\tau_{\text{cone}}\,t_{\text{cone}} \tag{65}$$

where the cone's enclosed area $A_{\rm cone}$ is assumed to taper linearly with a taper ratio of $\lambda_{\rm cone}^2$. The cone radius $R_{\rm cone}$ then tapers to a ratio of $\lambda_{\rm cone}$, but nonlinearly. The taper extends from $x_{\rm shell\,2}$ to $x_{\rm conend}$, the latter being the endpoint of the cone's primary structure, roughly at the horizontal or vertical tail attachment.

$$A_{\rm cone(}x{\rm)} = A_{\rm fuse}\left[1+(\lambda_{\rm cone}^2-1)\frac{x-x_{\rm shell\,2}}{x_{\rm conend}-x_{\rm shell\,2}}\right] \tag{66}$$

$$R_{\rm cone(}x{\rm)} = R_{\rm fuse}\left[1+(\lambda_{\rm cone}^2-1)\frac{x-x_{\rm shell\,2}}{x_{\rm conend}-x_{\rm shell\,2}}\right]^{1/2} \tag{67}$$

Setting $\mathcal{Q}_{\rm v}$ to the moment imparted by the vertical tail lift gives the cone wall thickness $t_{\rm cone}$ and corresponding material volume and weight.

$$t_{\rm cone(}x{\rm)} = \frac{\mathcal{Q}_{\rm v}}{2\tau_{\rm cone}A_{\rm cone(}x{\rm)}} \tag{68}$$

$$\begin{aligned}\mathcal{V}_{\rm cone} &= \int_{x_{\rm shell\,2}}^{x_{\rm conend}} 2\left[\pi+2n_{\rm fweb}\theta_{\rm fb}\right]R_{\rm cone}\,t_{\rm cone}\;{\rm d}x \\ &= \frac{\mathcal{Q}_{\rm v}}{\tau_{\rm cone}}\,\frac{\pi+2n_{\rm fweb}\theta_{\rm fb}}{\pi+n_{\rm fweb}(2\theta_{\rm fb}+\sin 2\theta_{\rm fb})}\,\frac{x_{\rm conend}-x_{\rm shell\,2}}{R_{\rm fuse}}\,\frac{2}{1+\lambda_{\rm cone}}\end{aligned} \tag{69}$$

$$W_{\rm cone} = \rho_{\rm cone}\,g\,\mathcal{V}_{\rm cone}(1+f_{\rm string}+f_{\rm frame}+f_{\rm fadd}) \tag{70}$$

$$x_{W_{\rm cone}} = \tfrac{1}{2}(x_{\rm shell\,2}+x_{\rm conend})\,W_{\rm cone} \tag{71}$$

2.3 Fuselage Bending Loads

In addition to the pressurization and torsion loads, the fuselage also sees bending loads from its distributed weight load plus the tail weight and airloads. In the case where the pressurization-sized shell is not sufficient to withstand this, additional bending material area is assumed to be added at the top and bottom (total of $A_{\rm hbend(}x{\rm)}$), and also sides of the shell (total of $A_{\rm vbend(}x{\rm)}$), as shown in Figure 3. If the shell is sufficiently strong, then these areas will be zero.

2.3.1 Lumped tail weight and location for fuselage stresses

For simplicity in the fuselage bending stress analysis to be considered next, both the horizontal and vertical tails, the tailcone, and any APU or rear-engine weight loads (if present) are lumped into their summed weight $W_{\rm tail}$, which is assumed to be located at the corresponding mass centroid location $x_{\rm tail}$. The tail aero loads are also assumed to act at this point.

$$W_{\rm tail} = W_{\rm htail}+W_{\rm vtail}+W_{\rm cone}\;[\,+W_{\rm apu}+W_{\rm eng}] \tag{72}$$

$$x_{\rm tail} = \frac{x_{\rm htail}W_{\rm htail}+x_{\rm vtail}W_{\rm vtail}+\frac{1}{2}(x_{\rm shell\,2}+x_{\rm conend})W_{\rm cone}\;[\,+x_{\rm apu}W_{\rm apu}+x_{\rm eng}W_{\rm eng}]}{W_{\rm tail}} \tag{73}$$

For the overall aircraft pitch balance and pitch stability analyses to be presented later, this lumping simplification will not be invoked.

2.3.2 Tail aero loads

An impulsive load on the horizontal or vertical tail will produce a direct static bending load on the aft fuselage. It will also result in an overall angular acceleration of the aircraft, whose distributed inertial-reaction loads will tend to alleviate the tail's static bending loads. These effects are captured by the inertial-relief factor r_{M} evaluated just to the right of the wingbox, which takes on the two different values r_{Mh} and r_{Mv} due to the different wing inertias about the horizontal and vertical axes. Typical values are $r_{\mathrm{Mh}} \simeq 0.4$ and $r_{\mathrm{Mv}} \simeq 0.7$, with the latter applied only over the rear fuselage. The resulting net bending moment distributions are shown in Figure 6, where the static case is the limit for an infinitely massive wing.

The maximum tail loads are set at a specified never-exceed dynamic pressure q_{NE}, and some assumed max-achievable lift coefficient for each surface.

$$L_{\mathrm{h_{max}}} = q_{NE}\, S_{\mathrm{h}}\, C_{L\mathrm{h_{max}}} \tag{74}$$

$$L_{\mathrm{v_{max}}} = q_{NE}\, S_{\mathrm{v}}\, C_{L\mathrm{v_{max}}} \tag{75}$$

$$(\mathcal{M}_{\mathrm{h}})_{\mathrm{aero}} = \begin{cases} r_{\mathrm{Mh}}\, L_{\mathrm{h_{max}}}\, (x_{\mathrm{tail}} - x) & , \quad x > x_{\mathrm{wing}} \\ r_{\mathrm{Mh}}\, L_{\mathrm{h_{max}}}\, (x + x_{\mathrm{tail}} - 2x_{\mathrm{wing}}) & , \quad x < x_{\mathrm{wing}} \end{cases} \tag{76}$$

$$(\mathcal{M}_{\mathrm{v}})_{\mathrm{aero}} = \begin{cases} r_{\mathrm{Mv}}\, L_{\mathrm{v_{max}}}\, (x_{\mathrm{tail}} - x) & , \quad x > x_{\mathrm{wing}} \\ 0.0 & , \quad x < x_{\mathrm{wing}} \end{cases} \tag{77}$$

$$r_{\mathrm{M}} = 1 - \frac{I_{\mathrm{fuse}}/2}{I_{\mathrm{fuse}} + I_{\mathrm{wing}}} - \frac{m_{\mathrm{fuse}}/4}{m_{\mathrm{fuse}} + m_{\mathrm{wing}}} \tag{78}$$

$$r_{\mathrm{Mh}} \simeq 0.4 \tag{79}$$

$$r_{\mathrm{Mv}} \simeq 0.7 \tag{80}$$

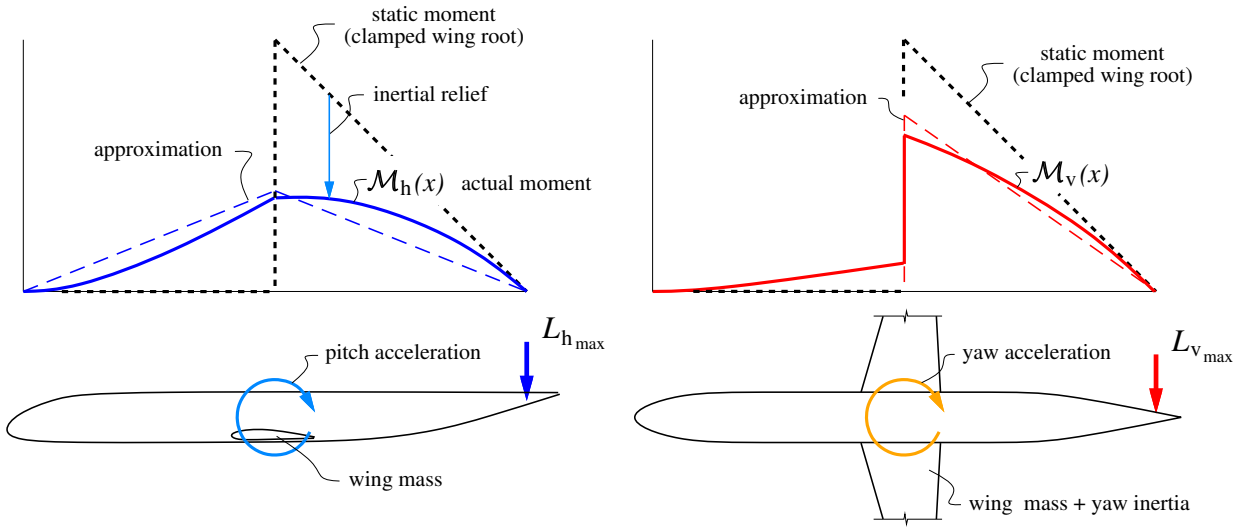

Figure 6: Fuselage bending moments due to unbalanced horizontal and vertical tail aero loads. The static bending moment (dashed lines) is partly relieved by reaction loads from the overall angular acceleration.

2.3.3 Landing gear loads

The maximum vertical load on the landing gear typically occurs in the emergency landing case, and subjects the fuselage to some vertical acceleration $N = N_{\text{land}}$ which is specified. The fuselage distributed mass will then subject the fuselage to a bending load shown in Figure 2.

2.3.4 Distributed and point weight loads

The fuselage is loaded by the payload weight W_{pay}, plus its own component weights W_{padd}, $W_{\text{shell}} \ldots$ etc. which are all assumed to be uniformly distributed over the fuselage shell length l_{shell}. The overall tail weight W_{tail} is assumed to be a point load at x_{tail}. With all weights scaled up by a load factor N, plus the impulsive horizontal-tail aero load moment (76), gives the following quadratic+linear horizontal-axis fuselage bending moment distribution, also sketched in Figure 2.

$$\begin{aligned} \mathcal{M}_{\text{h}(x)} &= N \frac{W_{\text{pay}}+W_{\text{padd}}+W_{\text{shell}}+W_{\text{window}}+W_{\text{insul}}+W_{\text{floor}}+W_{\text{seat}}}{2\,l_{\text{shell}}} (x_{\text{shell}\,2} - x)^2 \\ &+ (NW_{\text{tail}} + r_{\text{Mh}} L_{\text{h}})\,(x_{\text{tail}} - x) \end{aligned} \tag{81}$$

Expression (81) has been constructed to represent the bending moment over the rear fuselage. Since the wing's inertial-reaction pitching moments are small compared to those of the tail and fuselage, the horizontal-axis bending moment is assumed to be roughly symmetric about the wing's center of lift at x_{wing}, as sketched in Figure 2, so that (81) if reflected about x_{wing} also gives the bending moment over the front fuselage. For the same reason, the fixed weight W_{fix} is assumed to be concentrated near the aircraft nose, and hence it does not impose either a distributed load or a point load on the rear fuselage, and hence does not appear in (81).

2.3.5 Added horizontal-axis bending material

The total bending moment $\mathcal{M}_{\text{h}(x)}$ defined by (81) is used to size the added horizontal-axis bending area $A_{\text{hbend}(x)}$. Two loading scenarios are considered:

1. Maximum load factor at V_{NE}

$$N = N_{\text{lift}} \tag{82}$$
$$L_{\text{h}} = L_{\text{h}_{\text{max}}} \tag{83}$$

2. Emergency landing impact

$$N = N_{\text{land}} \tag{84}$$
$$L_{\text{h}} = 0 \tag{85}$$

The scenario which gives the larger added structural weight will be selected.

The maximum axial stress, which is related to the sum of the bending and pressurization strains, is limited everywhere to some maximum allowable value σ_{bend}.

$$E_{\text{bend}}\epsilon_{x(x)} \;=\; E_{\text{bend}}\left(\epsilon_{\text{bend}(x)} \;+\; \epsilon_{\text{press}}\right) \;\leq\; \sigma_{\text{bend}} \tag{86}$$

$$r_{_E}\left(\frac{\mathcal{M}_{\text{h}(x)}\, h_{\text{fuse}}}{I_{\text{hshell}} + r_{_E}\, I_{\text{hbend}(x)}} \;+\; \frac{\Delta p}{2}\,\frac{R_{\text{fuse}}}{t_{\text{shell}}}\right) \;\leq\; \sigma_{\text{bend}} \tag{87}$$

$$\text{where} \qquad h_{\text{fuse}} \;=\; R_{\text{fuse}} + \tfrac{1}{2}\Delta R_{\text{fuse}} \tag{88}$$

Relation (87) can then be solved for the required $I_{\text{hbend}(x)}$ and the associated $A_{\text{hbend}(x)}$.

$$I_{\text{hbend}(x)} \;=\; \max\left(\frac{\mathcal{M}_{(x)}\, h_{\text{fuse}}}{\sigma_{\text{Mh}}} \;-\; \frac{I_{\text{hshell}}}{r_{_E}} \;\;,\;\; 0\right) \tag{89}$$

$$\text{where} \qquad \sigma_{\text{Mh}} \;=\; \sigma_{\text{bend}} \;-\; r_{_E}\,\frac{\Delta p}{2}\,\frac{R_{\text{fuse}}}{t_{\text{shell}}} \tag{90}$$

$$A_{\text{hbend}(x)} \;=\; \frac{I_{\text{hbend}(x)}}{h_{\text{fuse}}^2} \;=\; A_2(x_{\text{shell}\,2} - x)^2 \;+\; A_1(x_{\text{tail}} - x) \;+\; A_0 \tag{91}$$

$$\text{where} \qquad A_2 \;=\; \frac{N(W_{\text{pay}} + W_{\text{padd}} + W_{\text{shell}} + W_{\text{window}} + W_{\text{insul}} + W_{\text{floor}} + W_{\text{seat}})}{2\, l_{\text{shell}}\, h_{\text{fuse}}\, \sigma_{\text{Mh}}} \tag{92}$$

$$A_1 \;=\; \frac{NW_{\text{tail}} + r_{\text{Mh}} L_{\text{h}}}{h_{\text{fuse}}\, \sigma_{\text{Mh}}} \tag{93}$$

$$A_0 \;=\; -\frac{I_{\text{hshell}}}{r_{_E}\, h_{\text{fuse}}^2} \tag{94}$$

The volume and weight of the added bending material is defined by integration of A_{hbend}, from the wing box to the location $x = x_{\text{hbend}}$ where $A_{\text{hbend}} = 0$ in the quadratic definition (91). If this quadratic has no real solution, then the inequality (81) holds for $\mathcal{M}_{\text{h}(x)} = 0$ everywhere, and no added bending material is needed.

Two separate integration limits are used for the front and back fuselage, to account for the shifted wing box for a swept wing. The integral for $\mathcal{V}_{\text{hbend}_f}$ for the front fuselage is actually computed over the back, by exploiting the assumed symmetry of $\mathcal{M}_{\text{h}(x)}$ and $A_{\text{hbend}(x)}$ about $x = x_{\text{wing}}$. The wing box offset Δx_{wing} is computed later in the wing-sizing section, so here it is taken from the previous iteration.

$$x_f \;=\; x_{\text{wing}} \;+\; \Delta x_{\text{wing}} \;+\; \tfrac{1}{2} c_o \bar{w} \tag{95}$$

$$x_b \;=\; x_{\text{wing}} \;-\; \Delta x_{\text{wing}} \;+\; \tfrac{1}{2} c_o \bar{w} \tag{96}$$

$$\begin{aligned}
\mathcal{V}_{\text{hbend}_f} \;&=\; \int_{x_f}^{x_{\text{hbend}}} A_{\text{hbend}(x)}\; \mathrm{d}x \\
&=\; A_2\,\frac{1}{3}\left[(x_{\text{shell}\,2} - x_f)^3 - (x_{\text{shell}\,2} - x_{\text{hbend}})^3\right] \\
&+\; A_1\,\frac{1}{2}\left[(x_{\text{tail}} - x_f)^2 - (x_{\text{tail}} - x_{\text{hbend}})^2\right] \\
&+\; A_0\,(x_{\text{hbend}} - x_f)
\end{aligned} \tag{97}$$

$$\begin{aligned}
\mathcal{V}_{\text{hbend}_b} \;&=\; \int_{x_b}^{x_{\text{hbend}}} A_{\text{hbend}(x)}\; \mathrm{d}x \\
&=\; A_2\,\frac{1}{3}\left[(x_{\text{shell}\,2} - x_b)^3 - (x_{\text{shell}\,2} - x_{\text{hbend}})^3\right]
\end{aligned}$$

$$
\begin{aligned}
&+ \quad A_1 \frac{1}{2}\left[(x_{\text{tail}}-x_b)^2 - (x_{\text{tail}}-x_{\text{hbend}})^2\right] \\
&+ \quad A_0\,(x_{\text{hbend}}-x_b) \qquad (98)\\
\mathcal{V}_{\text{hbend}_c} &= \frac{1}{2}\left[A_{\text{hbend}(x_b)} + A_{\text{hbend}(x_f)}\right] c_o \bar{w} \qquad (99)\\
\mathcal{V}_{\text{hbend}} &= \mathcal{V}_{\text{hbend}_f} + \mathcal{V}_{\text{hbend}_c} + \mathcal{V}_{\text{hbend}_b} \qquad (100)\\
W_{\text{hbend}} &= \rho_{\text{bend}}\, g\, \mathcal{V}_{\text{hbend}} \qquad (101)\\
xW_{\text{hbend}} &= x_{\text{wing}} W_{\text{hbend}} \qquad (102)
\end{aligned}
$$

2.3.6 Added vertical-axis bending material

The vertical-axis bending moment on the rear fuselage is entirely due to the airload on the vertical tail (77), reduced by the r_{Mv} factor to account for inertial relief.

$$\mathcal{M}_{\text{v}(x)} = r_{\text{Mv}}\, L_{\text{v}_{\text{max}}}\,(x_{\text{tail}} - x) \qquad (103)$$

Since the wing is assumed to react the local $\mathcal{M}_{\text{v}}$ via its large yaw inertia, as sketched in Figure 6, the moment distribution (103) is imposed only on the rear fuselage. The required bending inertia $I_{\text{vbend}(x)}$ and area $A_{\text{vbend}(x)}$ are then sized to keep the axial stress constant. The defining relations follow the ones for the horizontal-axis case above.

$$
\begin{aligned}
E_{\text{bend}}\epsilon_{x(x)} &= r_E\left(\frac{\mathcal{M}_{\text{v}(x)}\, w_{\text{fuse}}}{I_{\text{vshell}} + r_E\, I_{\text{vbend}(x)}} + \frac{\Delta p}{2}\frac{R_{\text{fuse}}}{t_{\text{shell}}}\right) \le \sigma_{\text{bend}} \qquad (104)\\
&\text{where} \qquad w_{\text{fuse}} = R_{\text{fuse}} + n_{\text{fweb}} w_{\text{fb}} \qquad (105)
\end{aligned}
$$

$$
\begin{aligned}
I_{\text{vbend}(x)} &= \max\left(\frac{\mathcal{M}_{\text{v}(x)}\, w_{\text{fuse}}}{\sigma_{\text{Mv}}} - \frac{I_{\text{vshell}}}{r_E}\ ,\ 0\right) \qquad (106)\\
\text{where} \qquad \sigma_{\text{Mv}} &= \sigma_{\text{bend}} - r_E\frac{\Delta p}{2}\frac{R_{\text{fuse}}}{t_{\text{shell}}} \qquad (107)\\
A_{\text{vbend}(x)} &= \frac{I_{\text{vbend}(x)}}{w_{\text{fuse}}^2} = B_1(x_{\text{tail}} - x) + B_0 \qquad (108)\\
\text{where} \qquad B_1 &= \frac{r_{\text{Mv}} L_{\text{v}}}{w_{\text{fuse}}\,\sigma_{\text{Mv}}} \qquad (109)\\
B_0 &= -\frac{I_{\text{vshell}}}{r_E\, w_{\text{fuse}}^2} \qquad (110)
\end{aligned}
$$

The volume and weight of the added bending material is defined by integration of $A_{\text{vbend}(x)}$ over the rear fuselage, from the rear of the wing box x_b, up to the point $x = x_{\text{vbend}}$ where $A_{\text{vbend}} = 0$ in definition (108).

$$
\begin{aligned}
\mathcal{V}_{\text{vbend}_b} &= \int_{x_b}^{x_{\text{vbend}}} A_{\text{vbend}(x)}\ \mathrm{d}x \\
&= B_1\frac{1}{2}\left[(x_{\text{tail}}-x_b)^2 - (x_{\text{tail}}-x_{\text{vbend}})^2\right] + B_0\,(x_{\text{vbend}}-x_b) \qquad (111)\\
\mathcal{V}_{\text{vbend}_c} &= \frac{1}{2} A_{\text{vbend}(x_b)}\, c_o \bar{w} \qquad (112)
\end{aligned}
$$

$$\mathcal{V}_{\text{vbend}} = \mathcal{V}_{\text{vbend}_c} + \mathcal{V}_{\text{vbend}_b} \tag{113}$$
$$W_{\text{vbend}} = \rho_{\text{bend}}\, g \mathcal{V}_{\text{vbend}} \tag{114}$$
$$x\!W_{\text{vbend}} = \tfrac{1}{3}(2x_{\text{wing}} + x_{\text{vbend}})W_{\text{vbend}} \tag{115}$$

For simplicity, the $W_{\text{hbend}}, W_{\text{vbend}}$ weights' contributions to $\mathcal{M}_{\text{h}}$ are excluded from (81) and the subsequent calculations. A practical reason is that the added material does not have a simple distribution, and hence would greatly complicate the $\mathcal{M}_{\text{h}(x)}$ function, thus preventing the analytic integration of the added material's weight. Fortunately, the added bending material is localized close to the wing centroid and hence its contribution to the overall bending moment is very small in any case, so neglecting its weight on the loading is well justified at this level of approximation.

2.4 Total Fuselage Weight

The total fuselage weight includes the shell with stiffeners, tailcone, floor beams, fixed weight, payload-proportional equipment and material, seats, and the added horizontal and vertical-axis bending material.

$$\begin{aligned} W_{\text{fuse}} = {} & W_{\text{fix}} + W_{\text{apu}} + W_{\text{padd}} + W_{\text{seat}} \\ & + W_{\text{shell}} + W_{\text{cone}} + W_{\text{window}} + W_{\text{insul}} + W_{\text{floor}} \\ & + W_{\text{hbend}} + W_{\text{vbend}} \end{aligned} \tag{116}$$

$$\begin{aligned} x\!W_{\text{fuse}} = {} & x\!W_{\text{fix}} + x\!W_{\text{apu}} + x\!W_{\text{padd}} + x\!W_{\text{seat}} \\ & + x\!W_{\text{shell}} + x\!W_{\text{cone}} + x\!W_{\text{window}} + x\!W_{\text{insul}} + x\!W_{\text{floor}} \\ & + x\!W_{\text{hbend}} + x\!W_{\text{vbend}} \end{aligned} \tag{117}$$

2.5 Wing or Tail Planform

The surface geometry relations derived below correspond to the wing. Most of these apply equally to the tails if the wing parameters are simply replaced with the tail counterparts. The exceptions which pertain to only the wing will be indicated with "(Wing only)" in the subsection title.

2.5.1 Chord distribution

The wing or tail surface is assumed to have a two-piece linear planform with constant sweep Λ, shown in Figure 7. The inner and outer surface planforms are defined in terms of the center chord c_o and the inner and outer taper ratios.

$$\lambda_s = c_s/c_o \tag{118}$$
$$\lambda_t = c_t/c_o \tag{119}$$

Similarly, the spanwise dimensions are defined in terms of the span b and the normalized spanwise coordinate η.

$$\eta = 2y/b \tag{120}$$

$$\eta_o = b_o/b \tag{121}$$
$$\eta_s = b_s/b \tag{122}$$

For generality, the wing center box width b_o is assumed to be different from the fuselage width to allow possibly strongly non-circular fuselage cross-sections. It will also be different for the tail surfaces. A planform break inner span b_s is defined, where possibly also a strut or engine is attached. Setting $b_s = b_o$ and $c_s = c_o$ will recover a single-taper surface.

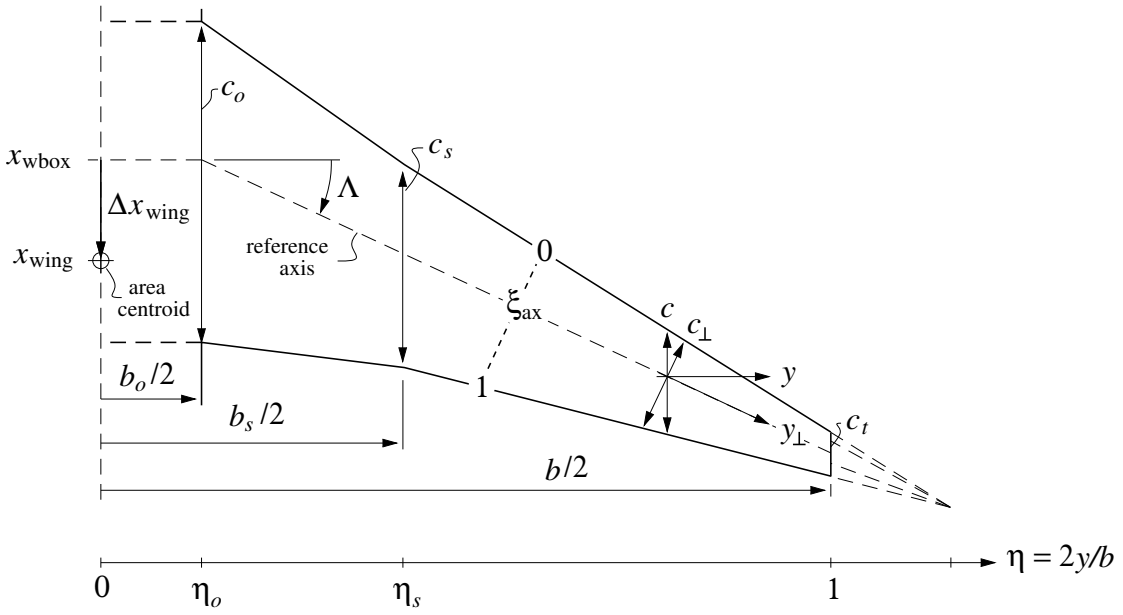

Figure 7: Piecewise-linear wing or tail surface planform, with break at η_s.

It's convenient to define the piecewise-linear normalized chord function $C_{(\eta)}$.

$$\frac{c(\eta)}{c_o} \equiv C_{(\eta;\eta_o,\eta_s,\lambda_s,\lambda_t)} = \begin{cases} 1 & , \quad 0 < \eta < \eta_o \\ 1 + (\lambda_s - 1)\dfrac{\eta-\eta_o}{\eta_s-\eta_o} & , \quad \eta_o < \eta < \eta_s \\ \lambda_s + (\lambda_t - \lambda_s)\dfrac{\eta-\eta_s}{1-\eta_s} & , \quad \eta_s < \eta < 1 \end{cases} \tag{123}$$

The following integrals will be useful for area, volume, shear, and moment calculations.

$$\int_0^{\eta_o} C \; \mathrm{d}\eta = \eta_o \tag{124}$$
$$\int_{\eta_o}^{\eta_s} C \; \mathrm{d}\eta = \frac{1}{2}(1+\lambda_s)(\eta_s-\eta_o) \tag{125}$$
$$\int_{\eta_s}^{1} C \; \mathrm{d}\eta = \frac{1}{2}(\lambda_s+\lambda_t)(1-\eta_s) \tag{126}$$
$$\int_0^{\eta_o} C^2 \; \mathrm{d}\eta = \eta_o \tag{127}$$
$$\int_{\eta_o}^{\eta_s} C^2 \; \mathrm{d}\eta = \frac{1}{3}(1+\lambda_s+\lambda_s^2)(\eta_s-\eta_o) \tag{128}$$

$$\int_{\eta_s}^{1} C^2 \, \mathrm{d}\eta \;=\; \frac{1}{3}(\lambda_s^2+\lambda_s\lambda_t+\lambda_t^2)(1-\eta_s) \tag{129}$$

$$\int_{\eta_o}^{\eta_s} C\,(\eta-\eta_o) \, \mathrm{d}\eta \;=\; \frac{1}{6}(1+2\lambda_s)(\eta_s-\eta_o)^2 \tag{130}$$

$$\int_{\eta_s}^{1} C\,(\eta-\eta_s) \, \mathrm{d}\eta \;=\; \frac{1}{6}(\lambda_s+2\lambda_t)(1-\eta_s)^2 \tag{131}$$

$$\int_{\eta_o}^{\eta_s} C^2\,(\eta-\eta_o) \, \mathrm{d}\eta \;=\; \frac{1}{12}(1+2\lambda_s+3\lambda_s^2)(\eta_s-\eta_o)^2 \tag{132}$$

$$\int_{\eta_s}^{1} C^2\,(\eta-\eta_s) \, \mathrm{d}\eta \;=\; \frac{1}{12}(\lambda_s^2+2\lambda_s\lambda_t+3\lambda_t^2)(1-\eta_s)^2 \tag{133}$$

2.5.2 Surface area and aspect ratio

The surface area S is defined as the exposed surface area plus the fuselage carryover area.

$$S \;=\; 2\int_0^{b/2} c \, \mathrm{d}y \;=\; c_o \, b \, K_c \tag{134}$$

$$\text{where} \qquad K_c \;=\; \int_0^1 C \, \mathrm{d}\eta \;=\; \eta_o + \tfrac{1}{2}(1+\lambda_s)(\eta_s-\eta_o) + \tfrac{1}{2}(\lambda_s+\lambda_t)(1-\eta_s) \tag{135}$$

The aspect ratio is then defined in the usual way. This will also allow relating the root chord to the span and the taper ratios.

$$AR \;=\; \frac{b^2}{S} \tag{136}$$

It is also useful to define the wing's mean aerodynamic chord c_{ma} and area-centroid offset Δx_{wing} from the center axis.

$$\frac{c_{\mathrm{ma}}}{c_o} \;=\; \frac{2}{S}\int_0^{b/2} c^2 \, \mathrm{d}y \;=\; \frac{K_{cc}}{K_c} \tag{137}$$

$$\Delta x_{\mathrm{wing}} \;=\; \frac{2}{S}\int_{b_o/2}^{b/2} c\,(y-y_o)\tan\Lambda \, \mathrm{d}y \;=\; \frac{K_{cx}}{K_c}\, b \, \tan\Lambda \tag{138}$$

$$x_{\mathrm{wing}} \;=\; x_{\mathrm{wbox}} \,+\, \Delta x_{\mathrm{wing}} \tag{139}$$

$$\text{where} \quad K_{cc} \;=\; \int_0^1 C^2 \, \mathrm{d}\eta$$

$$=\; \eta_o + \frac{1}{3}(1+\lambda_s+\lambda_s^2)(\eta_s-\eta_o) + \frac{1}{3}(\lambda_s^2+\lambda_s\lambda_t+\lambda_t^2)(1-\eta_s) \tag{140}$$

$$K_{cx} \;=\; \int_{\eta_o}^1 C\,(\eta-\eta_o) \, \mathrm{d}\eta$$

$$=\; \frac{1}{12}(1+2\lambda_s)(\eta_s-\eta_o)^2 + \frac{1}{12}(\lambda_s+2\lambda_t)(1-\eta_s)^2 + \frac{1}{4}(\lambda_s+\lambda_t)(1-\eta_s)(\eta_s-\eta_o) \tag{141}$$

The wing area centroid is used in the fuselage bending load calculations as described earlier.

2.5.3 Reference quantities

The aircraft reference quantities are chosen to be simply the values for the wing.

$$b_{\mathrm{ref}} \;=\; (b)_{\mathrm{wing}} \tag{142}$$

$$S_{\text{ref}} = (S)_{\text{wing}} \tag{143}$$
$$AR_{\text{ref}} = (AR)_{\text{wing}} \tag{144}$$
$$c_{\text{ref}} = (c_{\text{ma}})_{\text{wing}} \tag{145}$$

2.6 Surface Airloads

2.6.1 Lift distribution

The surface lift distribution $\tilde{p}$ is defined in terms of a baseline piecewise-linear distribution $p_{(\eta)}$ defined like the chord planform, but with its own taper ratios γ_s and γ_t. These are actually defined using local section c_ℓ factors $r_{c_{\ell s}}$ and $r_{c_{\ell t}}$.

$$\gamma_s = r_{c_{\ell s}}\,\lambda_s \tag{146}$$
$$\gamma_t = r_{c_{\ell t}}\,\lambda_t \tag{147}$$
$$\frac{p(\eta)}{p_o} \equiv P_{(\eta\,;\,\eta_o,\eta_s,\gamma_s,\gamma_t)} = \begin{cases} 1 & , \quad 0 < \eta < \eta_o \\ 1 + (\gamma_s - 1)\dfrac{\eta-\eta_o}{\eta_s-\eta_o} & , \quad \eta_o < \eta < \eta_s \\ \gamma_s + (\gamma_t - \gamma_s)\dfrac{\eta-\eta_s}{1-\eta_s} & , \quad \eta_s < \eta < 1 \end{cases} \tag{148}$$

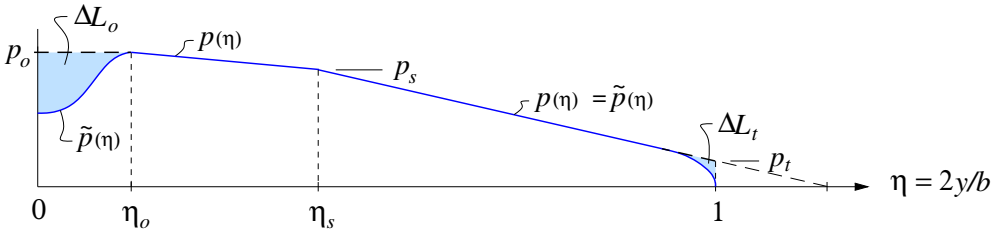

Figure 8: Piecewise-linear aerodynamic load $\tilde{p}_{(\eta)}$, with modifications at center and tip.

To get the actual aerodynamic load $\tilde{p}$, lift corrections ΔL_o and ΔL_t are applied to account for the fuselage carryover and tip lift rolloff, as sketched in Figure 8. The detailed shapes of these modifications are not specified, but instead only their integrated loads are defined by the following integral relation.

$$\frac{L_{\text{wing}}}{2} = \int_0^{b/2} \tilde{p}\ \mathrm{d}y = \int_0^{b/2} p\ \mathrm{d}y + \Delta L_o + \Delta L_t \tag{149}$$

The corrections are specified in terms of the center load magnitude p_o and the f_{L_o}, f_{L_t} adjustment factors.

$$\Delta L_o = f_{L_o}\,p_o\,\frac{b_o}{2} = f_{L_o}\,p_o\,\frac{b}{2}\,\eta_o \tag{150}$$
$$\Delta L_t = f_{L_t}\,p_t\,c_t = f_{L_t}\,p_o\,c_o\,\gamma_t\,\lambda_t \tag{151}$$
$$f_{L_o} \simeq -0.5 \tag{152}$$
$$f_{L_t} \simeq -0.05 \tag{153}$$

2.6.2 Lift load magnitude (Wing only)

The wing's p_o center loading magnitude is determined by requiring that the aerodynamic loading integrated over the whole span is equal to the total weight times the load factor, minus the tail lift.

$$2\int_0^{b/2} \tilde{p}_{(\eta)}\ \mathrm{d}y \ = \ p_o\, b \int_0^1 P_{(\eta)}\ \mathrm{d}\eta \ + \ 2\Delta L_o \ + \ 2\Delta L_t \ = \ NW \ - \ (L_{\mathrm{htail}})_N \tag{154}$$

For structural sizing calculations $N = N_{\mathrm{lift}}$ is chosen, and the appropriate value of $(L_{\mathrm{htail}})_N$ is the worst-case (most negative) tail lift expected in the critical sizing case. One possible choice is the trimmed tail load at dive speed, where N_{lift} is most likely to occur.

The wing area (134) and aspect ratio (136) definitions allow the root chord and the tip lift drop (151) to be expressed as

$$c_o \ = \ b\, K_o \tag{155}$$

$$\Delta L_t \ = \ f_{L_t}\, p_o\, b\, K_o\, \gamma_t\, \lambda_t \tag{156}$$

$$\text{where} \qquad K_o \ = \ \frac{1}{K_c\, AR} \tag{157}$$

so that (154) can be evaluated to the following. The $P_{(\eta)}$ integrals have the form as for $C_{(\eta)}$, given by (124)–(133), but with the λ's replaced by γ's.

$$p_o\, b\, K_p \ = \ NW - (L_{\mathrm{htail}})_N \tag{158}$$

$$\begin{aligned} \text{where} \qquad K_p \ &= \ \eta_o + \tfrac{1}{2}(1+\gamma_s)(\eta_s - \eta_o) + \tfrac{1}{2}(\gamma_s + \gamma_t)(1-\eta_s) \\ &+ \ f_{Lo}\eta_o \ + \ 2 f_{Lt} K_o \gamma_t \lambda_t \end{aligned} \tag{159}$$

The root and planform-break loadings can then be explicitly determined.

$$p_o \ = \ \frac{NW - (L_{\mathrm{htail}})_N}{K_p\, b} \tag{160}$$

$$p_s \ = \ p_o\, \gamma_s \tag{161}$$

$$p_t \ = \ p_o\, \gamma_t \tag{162}$$

2.6.3 Surface pitching moment

The surface's reference axis is at some specified chordwise fractional location ξ_{ax}, as shown in Figure 7. The profile pitching moment acts along the span-axis coordinate $y_\perp$, and scales with the normal-plane chord $c_\perp$. These are shown in Figure 7, and related to the spanwise and streamwise quantities via the sweep angle.

$$y_\perp \ = \ y / \cos\Lambda \tag{163}$$

$$c_\perp \ = \ c\, \cos\Lambda \tag{164}$$

$$V_\perp \ = \ V_\infty\, \cos\Lambda \tag{165}$$

The airfoil's pitching moment contribution shown in Figure 9 is

$$dM_{y_\perp} \;=\; \frac{1}{2}\rho V_\perp^2\, c_\perp^2\, c_m\; \mathrm{d}y_\perp \tag{166}$$

$$c_{m(\eta)} \;=\; \begin{cases} c_{m_o} & , \quad 0<\eta<\eta_o \\ c_{m_o} + (c_{m_s}-c_{m_o})\dfrac{\eta-\eta_o}{\eta_s-\eta_o} & , \quad \eta_o<\eta<\eta_s \\ c_{m_s} + (c_{m_t}-c_{m_s})\dfrac{\eta-\eta_s}{1-\eta_s} & , \quad \eta_s<\eta<1 \end{cases} \tag{167}$$

and including the contribution of the lift load $\tilde{p}$ with its moment arm gives the following overall wing pitching moment ΔM_{wing} increment about the axis center location.

$$\mathrm{d}\Delta M_{\text{wing}} \;=\; \tilde{p}\left[c_\perp\left(\xi_{\text{ax}}-\tfrac{1}{4}\right)\cos\Lambda \;-\; (y-y_o)\tan\Lambda\right]\mathrm{d}y \;+\; \mathrm{d}M_{y_\perp}\,\cos\Lambda \tag{168}$$

Integrating this along the whole span then gives the total surface pitching moment about its root axis.

$$\begin{aligned}
\Delta M_{\text{wing}} \;&=\; (p_o\, b_o + 2\Delta L_o)\, c_o\left(\xi_{\text{ax}}-\tfrac{1}{4}\right) \\
&+\; \cos^2\Lambda\; b\int_{\eta_o}^{1} p_{(\eta)}\, c_{(\eta)}\left(\xi_{\text{ax}}-\tfrac{1}{4}\right)\,\mathrm{d}\eta \\
&-\; \frac{b}{2}\,\tan\Lambda\, b\int_{\eta_o}^{1} p_{(\eta)}(\eta-\eta_o)\,\mathrm{d}\eta \\
&+\; 2\Delta L_t\left[c_o\lambda_t\left(\xi_{\text{ax}}-\tfrac{1}{4}\right)\cos^2\Lambda \;-\; \frac{b}{2}(1-\eta_o)\,\tan\Lambda\right] \\
&+\; \frac{1}{2}\rho V_\infty^2\,\cos^4\Lambda\, b\int_{\eta_o}^{1} c_{m(\eta)}\, c_{(\eta)}^2\,\mathrm{d}\eta
\end{aligned} \tag{169}$$

$$\begin{aligned}
\Delta M_{\text{wing}} \;&=\; p_o\, b\, c_o\, \eta_o\,(1+f_{L_o})\left(\xi_{\text{ax}}-\tfrac{1}{4}\right) \\
&+\; p_o\, b\, c_o\left(\xi_{\text{ax}}-\tfrac{1}{4}\right)\cos^2\Lambda\,\frac{1}{3}\Big[\left(1+\tfrac{1}{2}\,(\lambda_s+\gamma_s)+\lambda_s\gamma_s\right)(\eta_s-\eta_o) \\
&\qquad\qquad +\left(\lambda_s\gamma_s+\tfrac{1}{2}\,(\lambda_s\gamma_t+\gamma_s\lambda_t)+\lambda_t\gamma_t\right)(1-\eta_s)\Big] \\
&-\; p_o\, b\, c_o\,\frac{\tan\Lambda}{K_o}\,\frac{1}{12}\Big[\,(1+2\gamma_s)\,(\eta_s-\eta_o)^2 \;+\; (\gamma_s+2\gamma_t)\,(1-\eta_s)^2 \;+\; 3\,(\gamma_s+\gamma_t)\,(\eta_s-\eta_o)(1-\eta_s)\,\Big] \\
&+\; 2\,p_o\, b\, c_o\, f_{L_t}\,\lambda_t\,\gamma_t\left[K_o\lambda_t\left(\xi_{\text{ax}}-\tfrac{1}{4}\right)\cos^2\Lambda \;-\; \tfrac{1}{2}(1-\eta_o)\,\tan\Lambda\right] \\
&+\; \frac{1}{2}\rho V_\infty^2\, S\, c_o\,\frac{\cos^4\Lambda}{K_c}\,\frac{1}{12}\Big[\left(c_{m_o}(3+2\lambda_s+\lambda_s^2)+c_{m_s}(3\lambda_s^2+2\lambda_s+1)\right)(\eta_s-\eta_o) \\
&\qquad\qquad +\left(c_{m_s}(3\lambda_s^2+2\lambda_s\lambda_t+\lambda_t^2)+c_{m_t}(3\lambda_t^2+2\lambda_s\lambda_t+\lambda_s^2)\right)(1-\eta_s)\Big]
\end{aligned} \tag{170}$$

By using the relation

$$p_o\, b \;=\; \frac{1}{2}\rho V_\infty^2\, S\,\frac{1}{K_p}\left(C_L-\frac{S_{\text{h}}}{S}C_{L_{\text{h}}}\right) \tag{171}$$

equation (170) gives the equivalent pitching moment coefficient constant and C_L derivative.

$$\Delta C_{M_{\text{wing}}} \;\equiv\; \frac{\Delta M_{\text{wing}}}{\frac{1}{2}\rho V_\infty^2 S c_o} \;=\; \Delta C_{m_0} \;+\; \frac{\mathrm{d}C_m}{\mathrm{d}C_L}\left(C_L-\frac{S_{\text{h}}}{S}C_{L_{\text{h}}}\right) \tag{172}$$

$$
\begin{aligned}
\frac{\mathrm{d}C_m}{\mathrm{d}C_L} \;=\; & \frac{1}{K_p}\Bigg\{ \eta_o\,(1+f_{Lo})\Big(\xi_{\mathrm{ax}}-\tfrac{1}{4}\Big) \\
& + \Big(\xi_{\mathrm{ax}}-\tfrac{1}{4}\Big)\cos^2\Lambda\;\frac{1}{3}\Big[\,\Big(1+\tfrac{1}{2}\,(\lambda_s+\gamma_s)+\lambda_s\gamma_s\Big)\,(\eta_s-\eta_o) \\
& \qquad\qquad + \Big(\lambda_s\gamma_s+\tfrac{1}{2}\,(\lambda_s\gamma_t+\gamma_s\lambda_t)+\lambda_t\gamma_t\Big)\,(1-\eta_s)\,\Big] \\
& - \frac{\tan\Lambda}{K_o}\,\frac{1}{12}\Big[\,(1+2\gamma_s)\,(\eta_s-\eta_o)^2 \;+\; (\gamma_s+2\gamma_t)\,(1-\eta_s)^2 \\
& \qquad\qquad + 3\,(\gamma_s+\gamma_t)\,(\eta_s-\eta_o)(1-\eta_s)\,\Big] \\
& + 2\,f_{Lt}\,\lambda_t\,\gamma_t\Big[K_o\lambda_t\Big(\xi_{\mathrm{ax}}-\tfrac{1}{4}\Big)\cos^2\Lambda \;-\; \tfrac{1}{2}(1-\eta_o)\,\tan\Lambda\Big]\Bigg\} \qquad (173)
\end{aligned}
$$

$$
\begin{aligned}
\Delta C_{m_0} \;=\; & \frac{\cos^4\Lambda}{K_c}\,\frac{1}{12}\Big[\Big(c_{m_o}(3+2\lambda_s+\lambda_s^2)+c_{m_s}(3\lambda_s^2+2\lambda_s+1)\Big)\,(\eta_s-\eta_o) \\
& + \Big(c_{m_s}(3\lambda_s^2+2\lambda_s\lambda_t+\lambda_t^2)+c_{m_t}(3\lambda_t^2+2\lambda_s\lambda_t+\lambda_s^2)\Big)\,(1-\eta_s)\Big] \qquad (174)
\end{aligned}
$$

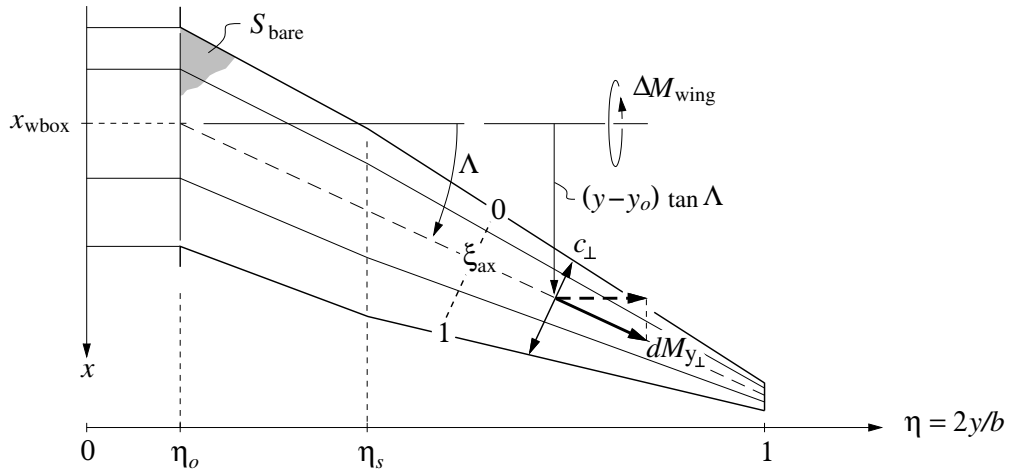

Figure 9: Wing pitching moment quantities.

2.7 Wing or Tail Structural Loads

Figure 10 shows the airload $\tilde{p}$ again, partly offset by weight load distributions of the structure and fuel, producing shear and bending moment distributions.

2.7.1 Shear and bending moment magnitudes

The $\mathcal{S}_s$, $\mathcal{M}_s$ magnitudes at η_s are set by integration of the assumed $p_{(\eta)}$ defined by (148), with the tip lift drop ΔL_t included as a point load at the tip station. The weight loading $w_{(\eta)}$ is also included via its overall outer panel weight W_{out} and weight moment $\Delta y W_{\mathrm{out}}$, which

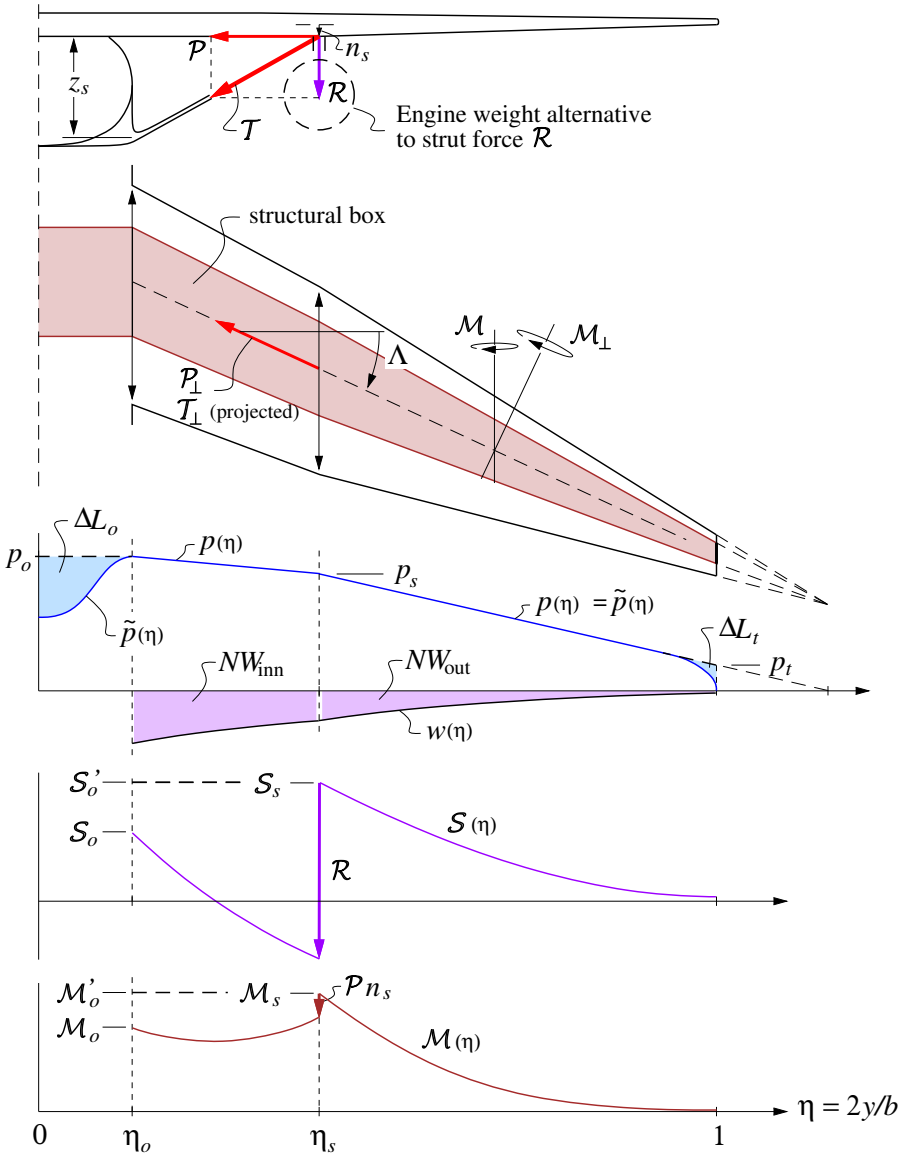

Figure 10: Aerodynamic load $\tilde{p}_{(\eta)}$ and weight load $w_{(\eta)}$, with resulting shear and bending moments. An optional strut modifies the shear and bending moment as indicated.

are typically taken from a previous weight iteration.

$$\begin{aligned} \mathcal{S}_s &= \frac{b}{2}\int_{\eta_s}^{1} p_{(\eta)}\ \mathrm{d}\eta \ +\ \Delta L_t \ -\ NW_{\text{out}} \\ &= \frac{p_o\, b}{4}(\gamma_s{+}\gamma_t)(1{-}\eta_s) \ +\ \Delta L_t \ -\ NW_{\text{out}} \end{aligned} \tag{175}$$

$$\begin{aligned} \mathcal{M}_s &= \frac{b^2}{4}\int_{\eta_s}^{1} p_{(\eta)}\,(\eta{-}\eta_s)\ \mathrm{d}\eta \ +\ \Delta L_t \frac{b}{2}(1{-}\eta_s) \ -\ N\,\Delta y W_{\text{out}} \\ &= \frac{p_o\, b^2}{24}(\gamma_s{+}2\gamma_t)(1{-}\eta_s)^2 \ +\ \Delta L_t \frac{b}{2}(1{-}\eta_s) \ -\ N\,\Delta y W_{\text{out}} \end{aligned} \tag{176}$$

Similarly, the $\mathcal{S}_o$ and $\mathcal{M}_o$ magnitudes at η_o are obtained by integrating the inner loading $p_{(\eta)}$, and adding the contributions of the strut load vertical component $\mathcal{R}$ and the spar

compression component $\mathcal{P}$. The latter is applied at the strut attachment point, at a normal-offset distance n_s, as shown in Figure 10.

$$\begin{aligned}
\mathcal{S}_o &= \mathcal{S}_s - \mathcal{R} + \frac{b}{2}\int_{\eta_o}^{\eta_s} p_{(\eta)}\,\mathrm{d}\eta - NW_{\text{inn}} \\
&= \mathcal{S}_s - \mathcal{R} + \frac{p_o\, b}{4}(1+\gamma_s)(\eta_s-\eta_o) - NW_{\text{inn}} \qquad (177)
\end{aligned}$$

$$\begin{aligned}
\mathcal{M}_o &= \mathcal{M}_s - \mathcal{P}n_s + (\mathcal{S}_s-\mathcal{R})\frac{b}{2}(\eta_s-\eta_o) + \frac{b^2}{4}\int_{\eta_o}^{\eta_s} p_{(\eta)}\,(\eta-\eta_o)\,\mathrm{d}\eta - N\,\Delta y W_{\text{inn}} \\
&= \mathcal{M}_s - \mathcal{P}n_s + (\mathcal{S}_s-\mathcal{R})\frac{b}{2}(\eta_s-\eta_o) + \frac{p_o\, b^2}{24}(1+2\gamma_s)(\eta_s-\eta_o)^2 - N\,\Delta y W_{\text{inn}} \qquad (178)
\end{aligned}$$

2.7.2 Outer surface shear and bending moment distributions

Rather than obtain the exact $\mathcal{S}_{(\eta)}$ and $\mathcal{M}_{(\eta)}$ distributions by integration of the assumed $p_{(\eta)}$, $\mathcal{S}_s$ and $\mathcal{M}_s$ are simply scaled with the appropriate power of the local chord.

$$\mathcal{S}_{(\eta)} = \mathcal{S}_s \left(\frac{c}{c_s}\right)^2 \quad , \qquad (\eta_s \le \eta \le 1) \qquad (179)$$

$$\mathcal{M}_{(\eta)} = \mathcal{M}_s \left(\frac{c}{c_s}\right)^3 \quad , \qquad (\eta_s \le \eta \le 1) \qquad (180)$$

These approximations are exact in the sharp-taper limit $\lambda_t, \gamma_t \to 0$, and are quite accurate for the small λ_t values typical of transport aircraft. Their main error is to slightly overpredict the loads near the tip where minimum-gauge constraints are most likely be needed anyway, so the approximation is deemed to be justified. Their great benefit is that they give a self-similar structural cross section for the entire cantilevered surface portion, and thus give simple explicit relations for the cross-section dimensions and the surface weight.

2.7.3 Strut or engine loads

The vertical load $\mathcal{R}$ applied at location η_s can represent either a strut load, or an engine weight. The two cases are described separately below.

2.7.4 Inner surface shear and moment — strut load case

In principle, both the strut anchor position η_s and the vertical strut load $\mathcal{R}$ can be optimized so as to achieve some best overall aircraft performance objective. A complication here is that multiple load conditions would need to be considered during the optimization, since a strut-braced wing optimized for a straight pullup case may not be able to withstand significant downloads, or may be too flexible in torsion and be susceptible to flutter. To avoid these great complications, it is assumed here that the strut is prestressed so as to give equal bending moments at the ends of the inner panel in level flight. The particular $\mathcal{R}$ which is then required in level flight is determined from (178).

$$\mathcal{M}_o = \mathcal{M}_s - \mathcal{P}n_s \qquad \text{(assumed)} \qquad (181)$$

$$\mathcal{R} = \frac{p_o\, b}{12}(1+2\gamma_s)(\eta_s-\eta_o) + \mathcal{S}_s \qquad (182)$$

Referring to Figure 10, this required $\mathcal{R}$ then gives the projected strut tension $\mathcal{T}$ and the inner-wing projected compression $\mathcal{P}$ loads from the strut front-view geometry.

$$\ell_s = \sqrt{z_s^2 + \frac{b^2}{4}(\eta_s - \eta_o)^2} \tag{183}$$

$$\mathcal{T} = \mathcal{R}\,\frac{\ell_s}{z_s} \tag{184}$$

$$\mathcal{P} = \mathcal{R}\,\frac{b/2}{z_s}(\eta_s - \eta_o) \tag{185}$$

The applied vertical load (182) implicitly contains the strut's own weight, although this is immaterial in the present formulation. The associated strut tension force (184) which will be used to size the strut cross-section will still correctly give the maximum strut tension at the wing strut-attach location.

Although the inner shear and moment distributions can be obtained by integrating the inner loading $p_{(\eta)}$ and including the contribution of the strut tension, these inner $\mathcal{S}_{(\eta)}$ and $\mathcal{M}_{(\eta)}$ are not appropriate for sizing the inner wing structure at each spanwise location, since buckling, torsional stiffness, etc. typically come into play here. Instead, the inner wing structure will be sized to match the $\mathcal{S}_s$ and $\mathcal{M}_s$ values.

2.7.5 Inner surface shear and moment — engine load case

For the case of an engine attached at location η_s, the vertical load $\mathcal{R}$ is simply the engine weight times the load factor N. The new inner wing compression load is zero in this case.

$$\mathcal{R} = N\,W_{\text{eng}}/n_{\text{eng}} \tag{186}$$

$$\mathcal{T} = 0 \tag{187}$$

$$\mathcal{P} = 0 \tag{188}$$

The wing root shear and bending moment $\mathcal{S}_o$ and $\mathcal{M}_o$ are then obtained immediately from (177) and (178). Unlike in the strut case, these root loads will in general be greater than $\mathcal{S}_s$ and $\mathcal{M}_s$, so the inner wing panel structural elements need to be sized accordingly.

2.8 Wing or Tail Stresses

2.8.1 Normal-plane quantities

The wing and tail surface stress and weight analyses are performed in the cross-sectional plane, normal to the spanwise axis $y_\perp$ running along the wing box sketched in Figures 7 and 10. Together with the normal-plane coordinate and chord relations (163) and (164), the shear and bending moment are related to the corresponding airplane-axes quantities and to the sweep angle Λ as follows.

$$\mathcal{S}_\perp = \mathcal{S} \tag{189}$$

$$\mathcal{M}_\perp = \mathcal{M}/\cos\Lambda \tag{190}$$

2.8.2 Wing or tail section

The assumed wing or tail airfoil and structural box cross-section is shown in Figure 11. The box is assumed to be the only structurally-significant element, with the slats, flaps, and spoilers (if any), represented only by added weight. It is convenient to define all dimensions as ratios with the local normal-plane chord $c_\perp$.

$$\bar{h} = \frac{h_{\text{wbox}}}{c_\perp} \tag{191}$$

$$\bar{w} = \frac{w_{\text{wbox}}}{c_\perp} \tag{192}$$

$$\bar{t}_{\text{cap}} = \frac{t_{\text{cap}}}{c_\perp} \tag{193}$$

$$\bar{t}_{\text{web}} = \frac{t_{\text{web}}}{c_\perp} \tag{194}$$

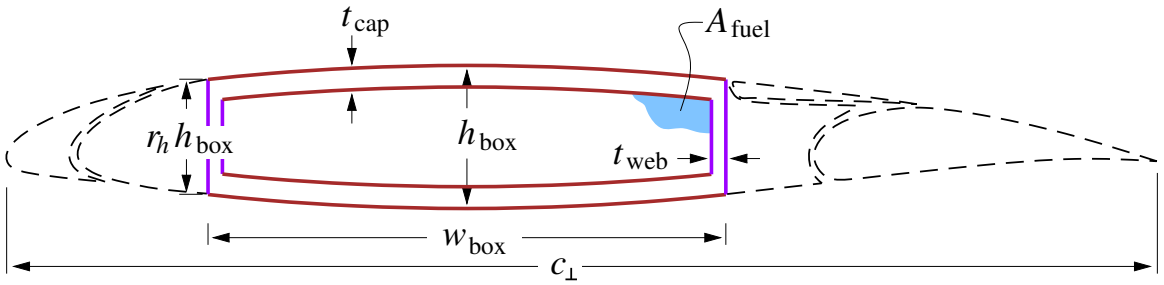

Figure 11: Wing or tail airfoil and structure cross-section, shown perpendicular to spar axis. Leading edges, fairings, slats, flaps, and spoilers contribute to weight but not to the primary structure.

The maximum height h_{wbox} at the box center corresponds to the airfoil thickness, so that $\bar{h}$ is the usual "t/c" airfoil thickness ratio. The height is assumed to taper off quadratically to a fraction r_h at the webs, so that the local height $h_{(\xi)}$ is

$$h_{(\xi)} = h_{\text{wbox}} \left[1 - (1-r_h)\xi^2 \right] \tag{195}$$

where $\xi = -1 \ldots 1$ runs chordwise over the sparbox extent. Typical metal wings and airfoils have $\bar{w} \simeq 0.5$, $r_h \simeq 0.75$, although these are left as input parameters. For evaluating areas and approximating the bending inertia, it's useful to define the simple average and r.m.s. average normalized box heights.

$$\bar{h}_{\text{avg}} = \frac{1}{c_\perp} \int_0^1 h_{(\xi)} \, \mathrm{d}\xi = \bar{h} \left[1 - \frac{1}{3}(1-r_h) \right] \tag{196}$$

$$\bar{h}^2_{\text{rms}} = \frac{1}{c_\perp^2} \int_0^1 h^2_{(\xi)} \, \mathrm{d}\xi = \bar{h}^2 \left[1 - \frac{2}{3}(1-r_h) + \frac{1}{5}(1-r_h)^2 \right] \tag{197}$$

The areas and the bending and torsion inertias, all normalized by the normal chord, can now be determined.

$$\bar{A}_{\text{fuel}} = \frac{A_{\text{fuel}}}{c_\perp^2} = (\bar{w} - 2\bar{t}_{\text{web}})(\bar{h}_{\text{avg}} - 2\bar{t}_{\text{cap}}) \tag{198}$$

$$\bar{A}_{\rm cap} \;=\; \frac{A_{\rm cap}}{c_\perp^2} \;=\; 2\,\bar{t}_{\rm cap}\bar{w} \tag{199}$$

$$\bar{A}_{\rm web} \;=\; \frac{A_{\rm web}}{c_\perp^2} \;=\; 2\,\bar{t}_{\rm web}\,r_h\,\bar{h} \tag{200}$$

$$\bar{I}_{\rm cap} \;\simeq\; \frac{I_{\rm cap}}{c_\perp^4} \;=\; \frac{\bar{w}}{12}\left[\bar{h}_{\rm rms}^3 - (\bar{h}_{\rm rms}{-}2\bar{t}_{\rm cap})^3\right] \tag{201}$$

$$\bar{I}_{\rm web} \;=\; \frac{I_{\rm web}}{c_\perp^4} \;=\; \frac{\bar{t}_{\rm web}\,r_h^3\,\bar{h}^3}{6} \;\ll\; \bar{I}_{\rm cap} \qquad \text{(typically)} \tag{202}$$

$$G\bar{J} \;=\; \frac{4(\bar{w}-\bar{t}_{\rm web})^2(\bar{h}_{\rm avg}-\bar{t}_{\rm cap})^2}{2\dfrac{r_h\bar{h}-\bar{t}_{\rm cap}}{G_{\rm web}\bar{t}_{\rm web}} \;+\; 2\dfrac{\bar{w}-\bar{t}_{\rm web}}{G_{\rm cap}\bar{t}_{\rm cap}}} \tag{203}$$

2.8.3 Outboard surface stresses

The wing or tail surface outboard of the strut-attach location η_s is a simple cantilever, whose local shear and bending stresses can be obtained explicitly.

$$\tau_{\rm web} \;=\; \frac{\mathcal{S}_\perp}{A_{\rm web}} \;=\; \frac{\mathcal{S}_\perp}{c_\perp^2}\,\frac{1}{2\,\bar{t}_{{\rm web}_s}\bar{h}} \tag{204}$$

$$\sigma_{\rm cap} \;=\; \frac{\mathcal{M}_\perp h_{\rm wbox}/2}{I_{\rm cap}+r_{\scriptscriptstyle E}I_{\rm web}} \;\simeq\; \frac{\mathcal{M}_\perp h_{\rm wbox}/2}{I_{\rm cap}} \;=\; \frac{\mathcal{M}_\perp}{c_\perp^3}\,\frac{6\bar{h}}{\bar{w}}\,\frac{1}{\bar{h}_{\rm rms}^3 - (\bar{h}_{\rm rms}{-}2\bar{t}_{{\rm cap}_s})^3} \tag{205}$$

$$r_{\scriptscriptstyle E} \;=\; \frac{E_{\rm web}}{E_{\rm cap}} \tag{206}$$

With the assumed triangular chord distribution (123), and the simplified shear and bending moment distributions (179) and (180), the shear and bending stresses become

$$\tau_{\rm web} \;=\; \frac{\mathcal{S}_s}{c_s^2}\,\frac{1}{2\,\bar{t}_{{\rm web}_s}\,r_h\,\bar{h}}\,\frac{1}{\cos^2\Lambda} \tag{207}$$

$$\sigma_{\rm cap} \;=\; \frac{\mathcal{M}_s}{c_s^3}\,\frac{6\bar{h}}{\bar{w}}\,\frac{1}{\bar{h}_{\rm rms}^3 - (\bar{h}_{\rm rms}{-}2\bar{t}_{{\rm cap}_s})^3}\,\frac{1}{\cos^4\Lambda} \tag{208}$$

which are spanwise constant across the outer wing. This great simplification was the major motivator behind assuming the simple triangular planform and loading and the chord-scaled shear and moment (179), (180) for the outer wing. The optimally-sized wing sections at all spanwise locations then become geometrically self-similar, and only one convenient characteristic cross-section, e.g. at the strut-attach location η_s, needs to be sized to fully define the outer wing's structural and weight characteristics.

For a wing or tail surface without a strut, the outer surface constitutes the entire surface. In this case, the strut and inner-surface sizing below is omitted.

2.8.4 Inboard surface — strut case

The inboard surface structure is defined by its two end locations η_o and η_s, with linear material-gauge variation in between. The shear webs of the inner surface are assumed to be

dominated by torsional requirements rather than bending-related shear requirements. Hence the inner panel is sized for the shear distribution shown dashed in Figure 10, defined by the strut-attach value $\mathcal{S}_s$.

$$\S_o' = \mathcal{S}_s \tag{209}$$

$$\tau_{\text{web}} = \frac{\S_o'}{c_o^2} \frac{1}{2\,\bar{t}_{\text{web}_o}\, r_h\, \bar{h}} \frac{1}{\cos^2\Lambda} \tag{210}$$

Similarly, the inner panel bending stiffness must not only withstand the normal-flight bending loads, but also landing downloads and buckling loads from the strut compression. Hence, the sparcaps are sized to the linear bending moment shown dashed in Figure 10, and defined by the end values $\mathcal{M}_s$ and $\mathcal{M}_o'$.

With the strut assumed to be attached to the bottom sparcap at $n_s = h/2$, the strut's compression load $\mathcal{P}$ cannot influence the compression stress on the top sparcap. An equivalent alternative view is that the offset-load bending moment reduction $-\mathcal{P}n_s$ is cancelled by $\mathcal{P}$'s own added compression stress. In any case, $\mathcal{P}$ does not explicitly enter into the sparcap sizing, provided $\mathcal{M}$ is positive everywhere on the inner panel, which is a reasonable assumption for a structurally-efficient wing. Hence, the strut-attach outer moment $\mathcal{M}_s$ is used for sizing the bending structure of the inner panel.

$$\mathcal{M}_o' = \mathcal{M}_s \tag{211}$$

$$\sigma_{\text{cap}} = \frac{\mathcal{M}_o'}{c_o^3} \frac{6\bar{h}}{\bar{w}} \frac{1}{\bar{h}_{\text{rms}}^3 - (\bar{h}_{\text{rms}} - 2\bar{t}_{\text{cap}_o})^3} \frac{1}{\cos^4\Lambda} \tag{212}$$

2.8.5 Inboard surface — engine case

In the case of an engine mounted at η_s, the root shear is simply offset by the single-engine weight, as shown in Figure 12.

$$\mathcal{R} = NW_{\text{eng}}/n_{\text{eng}} \tag{213}$$

$$\mathcal{P} = 0 \tag{214}$$

The root shear and moment $\mathcal{S}_o$ and $\mathcal{M}_o$ are then given immediately by (177) and (178). The root web and cap stresses are then obtained with the same relations (207) and (208) used for station η_s.

$$\tau_{\text{web}} = \frac{\mathcal{S}_o}{c_o^2} \frac{1}{2\,\bar{t}_{\text{web}_o}\, r_h\, \bar{h}} \frac{1}{\cos^2\Lambda} \tag{215}$$

$$\sigma_{\text{cap}} = \frac{\mathcal{M}_o}{c_o^3} \frac{6\bar{h}}{\bar{w}} \frac{1}{\bar{h}_{\text{rms}}^3 - (\bar{h}_{\text{rms}} - 2\bar{t}_{\text{cap}_o})^3} \frac{1}{\cos^4\Lambda} \tag{216}$$

2.8.6 Strut

The full strut length $\ell_{s_\perp}$ and full tension $\mathcal{T}_\perp$ are determined from the strut geometry.

$$\ell_{s_\perp} = \sqrt{z_s^2 + \frac{b^2}{4}\frac{(\eta_s - \eta_o)^2}{\cos^2\Lambda}} \tag{217}$$

$$\mathcal{T}_\perp = \mathcal{T}\,\frac{\ell_{s_\perp}}{\ell_s} \tag{218}$$

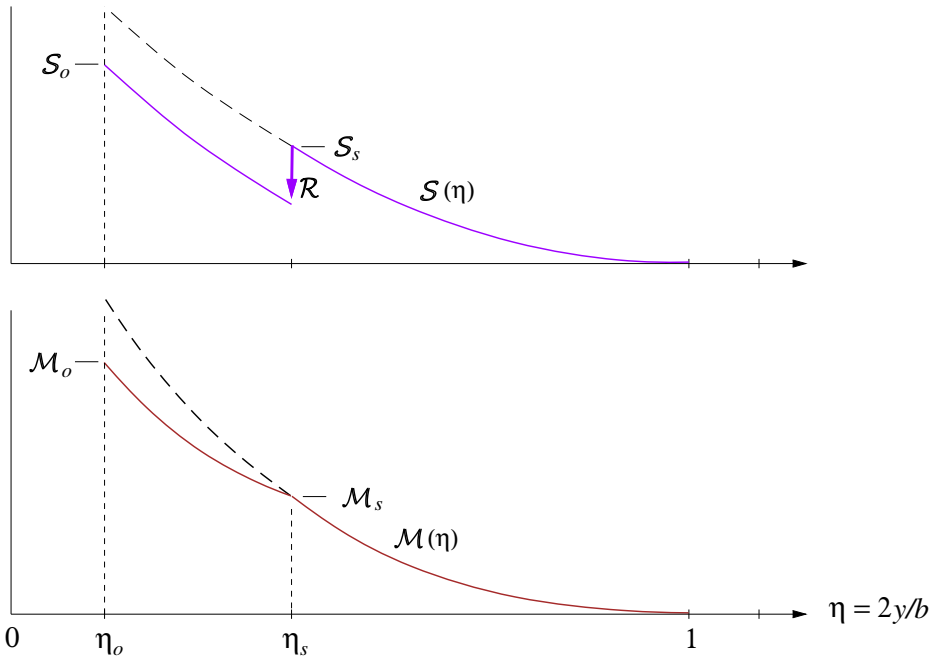

Figure 12: Surface loads modified by load $\mathcal{R}$ equal to engine weight attached at η_s.

The strut stress is then simply related to $\mathcal{T}_\perp$ and the strut cross-sectional area A_{strut}.

$$\sigma_{\text{strut}} \;=\; \frac{\mathcal{T}_\perp}{A_{\text{strut}}} \tag{219}$$

2.9 Surface Weights

2.9.1 Surface material volumes and volume moments

The surface structural weight is obtained directly from the total volume of the caps and webs, and the corresponding material densities. The volume $\mathcal{V}$ of any element of the swept surface is computed using the element's normalized cross sectional area $\bar{A}$, and the local streamwise chord $c_{(\eta)}$. The volume x-moment offsets $\Delta x\mathcal{V}$ from the center box are also computed for mass-centroid calculations. The volume y-moment offsets $\Delta y\mathcal{V}$ from y_o or y_s are computed for their contributions to the structural shear bending moment (175) and (176).

$$\mathrm{d}y_\perp \;=\; \frac{\mathrm{d}y}{\cos\Lambda} \;=\; \frac{b}{2}\frac{d\eta}{\cos\Lambda} \tag{220}$$

$$A \;=\; \bar{A}\,c_\perp^2 \;=\; \bar{A}\,c^2\,\cos^2\Lambda \tag{221}$$

$$\mathcal{V} \;=\; \int A\,\mathrm{d}y_\perp \;=\; \frac{b}{2}\int \bar{A}c^2\,\cos\Lambda\;\mathrm{d}\eta \tag{222}$$

$$\Delta x\mathcal{V} \;=\; \int A\,(x-x_{\text{wbox}})\,\mathrm{d}y_\perp \;=\; \frac{b^2}{4}\int \bar{A}c^2\,(\eta-\eta_o)\,\sin\Lambda\;\mathrm{d}\eta \tag{223}$$

$$\Delta y\mathcal{V} \;=\; \int A\,(y-y_o)\;\mathrm{d}y_\perp \;=\; \frac{b^2}{4}\int \bar{A}c^2\,(\eta-\eta_o)\,\cos\Lambda\;\mathrm{d}\eta \tag{224}$$

Using the assumed three-panel chord distribution (123), the unit-area ($\bar{A}=1$) volume and volume moments evaluate to the following for each of the three panels of one wing half.

$$\mathcal{V}_{\text{cen}} = \frac{b}{2}\int_0^{\eta_o} c^2 \, \mathrm{d}\eta = c_o^2 \frac{b}{2}\,\eta_o \tag{225}$$

$$\mathcal{V}_{\text{inn}} = \frac{b}{2}\int_{\eta_o}^{\eta_s} c^2 \cos\Lambda \, \mathrm{d}\eta = c_o^2 \frac{b}{6}\,(1+\lambda_s+\lambda_s^2)(\eta_s-\eta_o)\cos\Lambda \tag{226}$$

$$\mathcal{V}_{\text{out}} = \frac{b}{2}\int_{\eta_s}^{1} c^2 \cos\Lambda \, \mathrm{d}\eta = c_o^2 \frac{b}{6}\,(\lambda_s^2+\lambda_s\lambda_t+\lambda_t^2)(1-\eta_s)\cos\Lambda \tag{227}$$

$$\Delta x\mathcal{V}_{\text{inn}} = \frac{b^2}{4}\int_{\eta_o}^{\eta_s} c^2\,(\eta-\eta_o)\sin\Lambda \, \mathrm{d}\eta = c_o^2 \frac{b^2}{48}\,(1+2\lambda_s+3\lambda_s^2)(\eta_s-\eta_o)^2\sin\Lambda \tag{228}$$

$$\Delta x\mathcal{V}_{\text{out}} = \frac{b^2}{4}\int_{\eta_s}^{1} c^2\,(\eta-\eta_o)\sin\Lambda \, \mathrm{d}\eta = c_o^2 \frac{b^2}{48}\,(\lambda_s^2+2\lambda_s\lambda_t+3\lambda_t^2)(1-\eta_s)^2\sin\Lambda + c_o^2 \frac{b^2}{12}\,(\lambda_s^2+\lambda_s\lambda_t+\lambda_t^2)(\eta_s-\eta_o)(1-\eta_s)\sin\Lambda \tag{229}$$

$$\Delta y\mathcal{V}_{\text{inn}} = \frac{b^2}{4}\int_{\eta_o}^{\eta_s} c^2\,(\eta-\eta_o)\sin\Lambda \, \mathrm{d}\eta = c_o^2 \frac{b^2}{48}\,(1+2\lambda_s+3\lambda_s^2)(\eta_s-\eta_o)^2\cos\Lambda \tag{230}$$

$$\Delta y\mathcal{V}_{\text{out}} = \frac{b^2}{4}\int_{\eta_s}^{1} c^2\,(\eta-\eta_s)\sin\Lambda \, \mathrm{d}\eta = c_o^2 \frac{b^2}{48}\,(\lambda_s^2+2\lambda_s\lambda_t+3\lambda_t^2)(1-\eta_s)^2\cos\Lambda \tag{231}$$

2.9.2 Surface weights and weight moments

For the structural sizing calculations it's necessary to determine the contributions of the structure and fuel separately for the inner and outer panels. These are calculated by applying the material densities and actual area ratios to the unit-area volumes calculated previously.

$$\bar{A}_{\text{cap}_{\text{inn}}} = \frac{\bar{A}_{\text{cap}_o} + \bar{A}_{\text{cap}_s}\lambda_s^2}{1+\lambda_s^2} \tag{232}$$

$$\bar{A}_{\text{web}_{\text{inn}}} = \frac{\bar{A}_{\text{web}_o} + \bar{A}_{\text{web}_s}\lambda_s^2}{1+\lambda_s^2} \tag{233}$$

$$W_{\text{scen}} = \Big[\rho_{\text{cap}}\,\bar{A}_{\text{cap}_o} + \rho_{\text{web}}\,\bar{A}_{\text{web}_o}\Big]\, g\,\mathcal{V}_{\text{cen}} \tag{234}$$

$$W_{\text{sinn}} = \Big[\rho_{\text{cap}}\,\bar{A}_{\text{cap}_{\text{inn}}} + \rho_{\text{web}}\,\bar{A}_{\text{web}_{\text{inn}}}\Big]\, g\,\mathcal{V}_{\text{inn}} \tag{235}$$

$$\Delta x W_{\text{sinn}} = \Big[\rho_{\text{cap}}\,\bar{A}_{\text{cap}_{\text{inn}}} + \rho_{\text{web}}\,\bar{A}_{\text{web}_{\text{inn}}}\Big]\, g\,\Delta x\mathcal{V}_{\text{inn}} \tag{236}$$

$$\Delta y W_{\text{sinn}} = \Big[\rho_{\text{cap}}\,\bar{A}_{\text{cap}_{\text{inn}}} + \rho_{\text{web}}\,\bar{A}_{\text{web}_{\text{inn}}}\Big]\, g\,\Delta y\mathcal{V}_{\text{inn}} \tag{237}$$

$$W_{\text{sout}} = \Big[\rho_{\text{cap}}\,\bar{A}_{\text{cap}_s} + \rho_{\text{web}}\,\bar{A}_{\text{web}_s}\Big]\, g\,\mathcal{V}_{\text{out}} \tag{238}$$

$$\Delta x W_{\text{sout}} = \Big[\rho_{\text{cap}}\,\bar{A}_{\text{cap}_s} + \rho_{\text{web}}\,\bar{A}_{\text{web}_s}\Big]\, g\,\Delta x\mathcal{V}_{\text{out}} \tag{239}$$

$$\Delta y W_{\text{sout}} = \Big[\rho_{\text{cap}}\,\bar{A}_{\text{cap}_s} + \rho_{\text{web}}\,\bar{A}_{\text{web}_s}\Big]\, g\,\Delta y\mathcal{V}_{\text{out}} \tag{240}$$

$$W_{\text{fcen}} = \rho_{\text{fuel}}\,\bar{A}_{\text{fuel}_o}\, g\,\mathcal{V}_{\text{inn}} \tag{241}$$

$$\bar{A}_{\text{fuel}_{\text{inn}}} = \frac{\bar{A}_{\text{fuel}_o} + \bar{A}_{\text{fuel}_s}\lambda_s^2}{1+\lambda_s^2} \tag{242}$$

$$
\begin{aligned}
W_{\text{finn}} &= \rho_{\text{fuel}}\, \bar{A}_{\text{fuel}_{\text{inn}}}\, g\, \mathcal{V}_{\text{inn}} && (243)\\
\Delta x W_{\text{finn}} &= \rho_{\text{fuel}}\, \bar{A}_{\text{fuel}_{\text{inn}}}\, g\, \Delta x \mathcal{V}_{\text{inn}} && (244)\\
\Delta y W_{\text{finn}} &= \rho_{\text{fuel}}\, \bar{A}_{\text{fuel}_{\text{inn}}}\, g\, \Delta y \mathcal{V}_{\text{inn}} && (245)\\
W_{\text{fout}} &= \rho_{\text{fuel}}\, \bar{A}_{\text{fuel}_s}\, g\, \mathcal{V}_{\text{out}} && (246)\\
\Delta x W_{\text{fout}} &= \rho_{\text{fuel}}\, \bar{A}_{\text{fuel}_s}\, g\, \Delta x \mathcal{V}_{\text{out}} && (247)\\
\Delta y W_{\text{fout}} &= \rho_{\text{fuel}}\, \bar{A}_{\text{fuel}_s}\, g\, \Delta y \mathcal{V}_{\text{out}} && (248)
\end{aligned}
$$

Assuming chord^2-weighted average areas $\bar{A}_{\text{inn}}$ over the inner panel is deemed to be adequate for approximating the material and fuel volumes, since $\bar{A}_o$ and $\bar{A}_s$ will be very similar for any reasonable wing/strut configuration, and in fact are equal for the small taper ratio cantilevered wing case like for the outer panel.

The total structural wing weight and x-moment is obtained by summing the weights for all the panels for the two wing halves, with added wing weight accounted for by the f_{wadd} fraction components.

$$
\begin{aligned}
f_{\text{wadd}} &= f_{\text{flap}} + f_{\text{slat}} + f_{\text{aile}} + f_{\text{lete}} + f_{\text{ribs}} + f_{\text{spoi}} + f_{\text{watt}} && (249)\\
W_{\text{wing}} &= 2\,(W_{\text{scen}} + W_{\text{sinn}} + W_{\text{sout}})\,(1+f_{\text{wadd}}) && (250)\\
\Delta x W_{\text{wing}} &= 2\,(\Delta x W_{\text{sinn}} + \Delta x W_{\text{sout}})\,(1+f_{\text{wadd}}) && (251)
\end{aligned}
$$

The maximum (volume-limited) wing fuel weight and x-moment is computed the same way.

$$
\begin{aligned}
W_{\text{fmax}} &= 2\,(W_{\text{fcen}} + W_{\text{finn}} + W_{\text{fout}}) && (252)\\
\Delta x W_{\text{fmax}} &= 2\,(\Delta x W_{\text{finn}} + \Delta x W_{\text{fout}}) && (253)
\end{aligned}
$$

This can be modified if only some of the wingbox volume is chosen to hold fuel.

2.9.3 Total panel weights

The wing structural shear and bending moment relations (175) – (178) require the weights and weight y-moments of the individual wing panels. These are assembled by summing the structure's and maximum fuel's weight contributions derived previously, with the latter simply scaled by the max-fuel usage fraction r_{fmax}.

$$
\begin{aligned}
r_{\text{fmax}} &= \frac{W_{\text{fuel}}}{W_{\text{fmax}}} && (254)\\
W_{\text{inn}} &= W_{\text{sinn}}(1+f_{\text{wadd}}) + r_{\text{fmax}}\, W_{\text{finn}} && (255)\\
W_{\text{out}} &= W_{\text{sout}}(1+f_{\text{wadd}}) + r_{\text{fmax}}\, W_{\text{fout}} && (256)\\
\Delta y W_{\text{inn}} &= \Delta y W_{\text{sinn}}(1+f_{\text{wadd}}) + r_{\text{fmax}}\, \Delta y W_{\text{finn}} && (257)\\
\Delta y W_{\text{out}} &= \Delta y W_{\text{sout}}(1+f_{\text{wadd}}) + r_{\text{fmax}}\, \Delta y W_{\text{fout}} && (258)
\end{aligned}
$$

Using a single r_{fmax} value assumes the partial fuel load is uniformly distributed percentage-wise in all the available volume. Of course, r_{fmax} could be varied between the panels to reflect other fuel distributions.

2.9.4 Strut weight

The weight of the strut is computed directly from its cross-sectional area and total length for the two sides.

$$W_{\text{strut}} = \rho_{\text{strut}}\, g A_{\text{strut}}\, 2\ell_{s_\perp} \tag{259}$$

$$\Delta x W_{\text{strut}} = \frac{b}{4}\,(\eta_s - \eta_o)\,\tan\Lambda\, W_{\text{strut}} \tag{260}$$

2.9.5 Wingbox component weights

The overall sparcap and web weights for the entire wing can also be determined, although these are merely informative and are not needed for any other calculations.

$$W_{\text{cap}} = 2\rho_{\text{cap}}\, g\left[\bar{A}_{\text{cap}_o}\mathcal{V}_{\text{cen}} + \tfrac{1}{2}\Big(\bar{A}_{\text{cap}_o} + \bar{A}_{\text{cap}_s}\Big)\mathcal{V}_{\text{inn}} + \bar{A}_{\text{cap}_s}\mathcal{V}_{\text{out}}\right] \tag{261}$$

$$W_{\text{web}} = 2\rho_{\text{web}}\, g\left[\bar{A}_{\text{web}_o}\mathcal{V}_{\text{cen}} + \tfrac{1}{2}\Big(\bar{A}_{\text{web}_o} + \bar{A}_{\text{web}_s}\Big)\mathcal{V}_{\text{inn}} + \bar{A}_{\text{web}_s}\mathcal{V}_{\text{out}}\right] \tag{262}$$

2.9.6 Tail surface weight

All the wing wing stress and weight analyses above apply equally to the vertical and horizontal tail surfaces, with the appropriate span and load definitions. It is assumed that no strut is used, so that

$$c_{s_{\text{h}}} = c_{o_{\text{h}}} \tag{263}$$

$$b_{s_{\text{h}}} = b_{o_{\text{h}}} \tag{264}$$

and likewise for the vertical tail. The main difference is the derivation of the root loading magnitude p_o, which is set by the maximum design loads at q_{NE}, defined by (74) and (76). Specifically, we have

$$p_{o_{\text{h}}} = \frac{L_{\text{h}_{\max}}}{b_{\text{h}}}\,\frac{2}{1+\lambda_{\text{h}}} \tag{265}$$

where the $()_{\text{h}}$ subscript denotes the horizontal tail/ The same relation is used for the vertical tail. Gravity and inertial loads are neglected here, since for tails they are typically much smaller than the airloads at q_{NE}. Of course, they could be included as was done for the wing. With the tail p_o values defined, the structural-box sizing and weight estimation proceeds using the same relations as for the wing, starting with $\mathcal{S}_o$. The vertical tail is treated by assuming its mirror image exists, so that the b value in (175) and (176) is actually twice the actual vertical tail span. No other adjustments need to be made. The net result is the overall horizontal and vertical tail weights, and tail weight moments.

$$\rightarrow\ W_{\text{htail}} \tag{266}$$

$$\rightarrow\ W_{\text{vtail}} \tag{267}$$

$$\rightarrow\ \Delta x W_{\text{htail}} \tag{268}$$

$$\rightarrow\ \Delta x W_{\text{vtail}} \tag{269}$$

2.10 Engine System Weight

The bare engine weight W_{ebare} is calculated using an assumed dependence on the engine design core mass flow $\dot{m}_{\text{D}}$, overall design pressure ratio OPR_{D}, and the design bypass ratio BPR_{D}. The added weight W_{eadd}, specified via the empirical fraction f_{eadd}, accounts for the fuel system, accessories, and miscellaneous related equipment.

$$\begin{aligned} W_{\text{ebare}} &= n_{\text{eng}}\, W_{e_1}(\dot{m}_{\text{D}}, OPR_{\text{D}}, BPR_{\text{D}}) && (270)\\ W_{\text{eadd}} &= W_{\text{ebare}}\, f_{\text{eadd}} && (271) \end{aligned}$$

The bare weight function W_{e_1} has been calibrated with listed weights for existing turbofans, as described in the related document *Turbofan Weight Model from Historical Data*.

The nacelle plus thrust reverser weight is calculated using an assumed dependence on the engine fan diameter d_{f}, LPC diameter d_{lpc}, and the nacelle surface area S_{nace_1}, the latter being specified by the empirical area ratio r_{Snace} relative to the fan area.

$$\begin{aligned} S_{\text{nace}_1} &= r_{\text{Snace}}\, \frac{\pi}{4}\, d_{\text{f}}^2 && (272)\\ A_{\text{inlet}} &= 0.4\, S_{\text{nace}_1} && (273)\\ A_{\text{fan cowl}} &= 0.2\, S_{\text{nace}_1} && (274)\\ A_{\text{exh}} &= 0.4\, S_{\text{nace}_1} && (275)\\ A_{\text{core cowl}} &= 3.0\, \pi d_{\text{lpc}}^2 && (276)\\ W_{n_1} &= (2.5 + 0.0238\, d_{\text{f}}) A_{\text{inlet}} \;+\; 1.9 A_{\text{fan cowl}} \\ &+\; (2.5 + 0.0363\, d_{\text{f}}) A_{\text{exh}} \;+\; 1.9 A_{\text{core cowl}} && (277)\\ W_{\text{nace}} &= n_{\text{eng}}\, W_{n_1}(d_{\text{f}}, d_{\text{lpc}}, S_{\text{nace}_1}) && (278) \end{aligned}$$

The nacelle weight function (277), shown in Figure 13, was obtained from the historical data fit derived in reference [18], in which the areas are in square feet, d_{f} in inches, and the resulting W_{n_1} is in pounds. The 40/20/40 split of S_{nace_1} into the inlet, fan-cowl, and exhaust fractions is assumed here. Also assumed is that the core cowl length is 3.0 times the LPC diameter d_{lpc}.

The pylon weight W_{pylon}, specified via the empirical fraction f_{pylon}, accounts for the pylon and other mounting structure.

$$W_{\text{pylon}} = (W_{\text{ebare}} + W_{\text{eadd}} + W_{\text{nace}})\, f_{\text{pylon}} \qquad (279)$$

The total engine system weight and weight moment is then defined as follows. The engine weight fraction is also defined, and is used in the overall weight iteration procedure.

$$\begin{aligned} W_{\text{eng}} &= W_{\text{ebare}} + W_{\text{eadd}} + W_{\text{nace}} + W_{\text{pylon}} && (280)\\ xW_{\text{eng}} &= x_{\text{eng}}\, W_{\text{eng}} && (281)\\ f_{\text{eng}} &= \frac{W_{\text{eng}}}{W_{\text{MTO}}} && (282) \end{aligned}$$

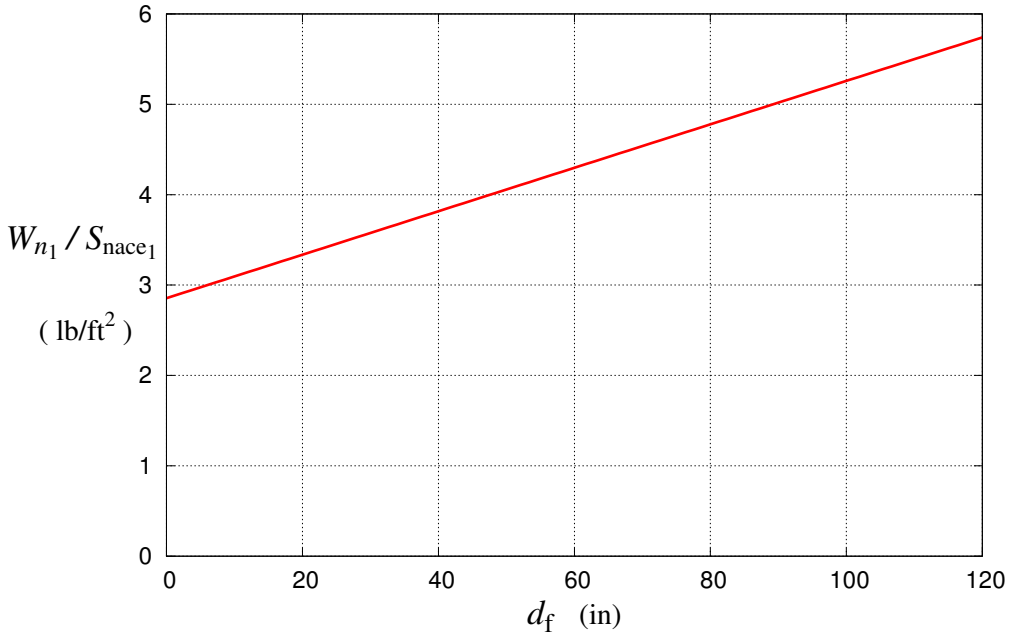

Figure 13: Nacelle weight per area versus fan diameter, as given by equations (272)–(277), with $A_{\text{core cowl}} = 0.25\, S_{\text{nace}_1}$ assumed here.

2.11 Moments and Balance

Weight moment and aerodynamic moment calculations are used to size the horizontal tail to meet stability or trim-limit requirements, to determine allowable CG limits, and to determine the required pitch-trim tail lift.

2.11.1 Overall weight moment

The overall flying weight is summed as follows. Partial payload and partial fuel are specified with the arbitrary r_{pay} and r_{fuel} ratios relative to maximum design values.

$$\begin{aligned} W &= r_{\text{pay}} W_{\text{pay}} + r_{\text{fuel}} W_{\text{fuel}} \\ &+ W_{\text{fuse}} + W_{\text{wing}} + W_{\text{strut}} + W_{\text{htail}} + W_{\text{vtail}} \\ &+ W_{\text{eng}} + W_{\text{hpesys}} + W_{\text{lgnose}} + W_{\text{lgmain}} \end{aligned} \tag{283}$$

The partial passenger payload distribution in the cabin is specified by the parameter ξ_{pay} which can take on any value $0 \ldots 1$. Specific instances are

$$\xi_{\text{pay}} = \begin{cases} 0.0 & , \text{ passengers packed towards the front} \\ 0.5 & , \text{ passengers centered in cabin} \\ 1.0 & , \text{ passengers packed towards the back} \end{cases} \tag{284}$$

This then determines the passenger payload weight centroid x_{pay}.

$$x_{\text{cabin}} = \tfrac{1}{2}(x_{\text{shell}\,1} + x_{\text{shell}\,2}) \tag{285}$$

$$l_{\text{cabin}} = x_{\text{shell}\,2} - x_{\text{shell}\,1} \tag{286}$$

$$x_{\text{pay}} = x_{\text{cabin}} + l_{\text{cabin}} \left(\xi_{\text{pay}} - \tfrac{1}{2}\right)(1 - r_{\text{pay}}) \tag{287}$$

Note that with a full passenger load, $r_{\rm pay}=1$, the mass centroid is always at the center point $x_{\rm cabin}$, regardless of $\xi_{\rm pay}$. The overall aircraft weight moment is then computed as follows.

$$\begin{aligned} xW &= r_{\rm pay}\, x_{\rm pay} W_{\rm pay} \\ &+ r_{\rm fuel}\,(x_{\rm wbox} W_{\rm fuel} + \Delta x W_{\rm fuel}) \\ &+ xW_{\rm fuse} \\ &+ x_{\rm wbox} W_{\rm wing} + \Delta x W_{\rm wing} \\ &+ x_{\rm wbox} W_{\rm strut} + \Delta x W_{\rm strut} \\ &+ x_{\rm htail} W_{\rm htail} + \Delta x W_{\rm htail} \\ &+ x_{\rm vtail} W_{\rm vtail} + \Delta x W_{\rm vtail} \\ &+ xW_{\rm eng} \\ &+ x_{\rm hpesys} W_{\rm hpesys} \\ &+ x_{\rm lgnose} W_{\rm lgnose} \\ &+ x_{\rm lgmain} W_{\rm lgmain} \end{aligned} \tag{288}$$

The aircraft CG location then follows.

$$x_{CG} = \frac{xW}{W} \tag{289}$$

2.11.2 Overall aerodynamic moment

The overall aerodynamic pitching moment about the origin comes from the wing, the horizontal tail, and the fuselage. For simplicity, the wing root chord c_o is used here as the arbitrary reference moment arm. The more traditional m.a.c. will be used to define the static margin.

$$\begin{aligned} C_m \equiv \frac{M}{\frac{1}{2}\rho V_\infty^2 S c_o} &= C_{m{\rm w}_0} + \left(C_{m{\rm w}_1} - \frac{x_{\rm wbox}}{c_o}\right)\left(C_L - \frac{S_{\rm h}}{S} C_{L_{\rm h}}\right) \\ &+ \frac{S_{\rm h}\, c_{o{\rm h}}}{S\, c_o}\, C_{m{\rm h}_0} + \left(\frac{c_{o{\rm h}}}{c_o}\, C_{m{\rm h}_1} - \frac{x_{\rm hbox}}{c_o}\right)\frac{S_{\rm h}}{S}\, C_{L_{\rm h}} \\ &+ \frac{CMV_{{\rm f}_1}}{S c_o}\,(C_L - C_{L_{Mf\,0}}) \end{aligned} \tag{290}$$

and $CMV_{{\rm f}_1}$ and $C_{L_{Mf\,0}}$ give the fuselage's pitching moment volume dependence on aircraft C_L.

$$\frac{M_{\rm fuse}}{\frac{1}{2}\rho V_\infty^2} \equiv CMV_{\rm f} = CMV_{{\rm f}_1}\,(C_L - C_{L_{Mf\,0}}) \tag{291}$$

From slender body theory, a fuselage of volume $\mathcal{V}_{\rm f}$ isolated from the wing has

$$CMV_{\rm f} \equiv \frac{M_{\rm f}}{q_\infty S c_o} \simeq 2\mathcal{V}_{\rm f}\,(\alpha - \alpha_{Mf\,0}) \tag{292}$$

$$CMV_{{\rm f}_1} \equiv \frac{\partial M_{\rm f}/\partial C_L}{q_\infty S c_o} \simeq \frac{2\mathcal{V}_{\rm f}}{{\rm d}C_L/{\rm d}\alpha} \tag{293}$$

but this will typically be considerably modified by the interaction with the wing. Regardless, the aircraft center of pressure (or lift centroid) is given as follows.

$$x_{CP} \;=\; -\frac{c_o\, C_m}{C_L} \tag{294}$$

2.11.3 Neutral point

The neutral point is estimated by first translating the aerodynamic pitching moment (290) to some arbitrary reference x location.

$$C_m(x) \;=\; C_m(0) \;+\; \frac{x}{c_o}\, C_L \tag{295}$$

The neutral point is the x location which makes (295) stationary with respect to C_L, or

$$\frac{\partial C_m(x_{NP})}{\partial C_L} \;=\; \frac{\partial C_m}{\partial C_L} \;+\; \frac{x_{NP}}{c_o} \;=\; 0 \tag{296}$$

$$x_{NP} \;=\; -c_o\, \frac{\partial C_m}{\partial C_L} \tag{297}$$

$$\begin{aligned} \text{where} \qquad c_o\, \frac{\partial C_m}{\partial C_L} \;&=\; (c_o C_{m\mathrm{w_1}} \;-\; x_{\mathrm{wbox}}) \left(1 \;-\; \frac{S_\mathrm{h}}{S}\, \frac{\partial C_{L_\mathrm{h}}}{\partial C_L}\right) \\ &+\; (c_{o\mathrm{h}} C_{m\mathrm{h_1}} \;-\; x_{\mathrm{hbox}})\, \frac{S_\mathrm{h}}{S}\, \frac{\partial C_{L_\mathrm{h}}}{\partial C_L} \\ &+\; \frac{C M V_{\mathrm{f_1}}}{S} \end{aligned} \tag{298}$$

The tail lift-curve slope is based on the combination of finite-wing theory using the surface aspect ratios, infinite swept-wing theory using the wing and tail surface sweep angles Λ and Λ_h, and a specified downwash derivative $\mathrm{d}\varepsilon/\mathrm{d}\alpha$ at the tail, all corrected for compressibility using the Prandtl-Glauert factor $\sqrt{1-M_\infty^2}$.

$$\frac{\partial C_{L_\mathrm{h}}}{\partial C_L} \;=\; \frac{\sqrt{1-M_\infty^2} + 2/AR}{\sqrt{1-M_\infty^2} + 2/AR_\mathrm{h}}\, \frac{\sqrt{(1-M_\infty^2) + \tan^2\Lambda}}{\sqrt{(1-M_\infty^2) + \tan^2\Lambda_h}} \left(1 - \frac{\mathrm{d}\varepsilon}{\mathrm{d}\alpha}\right) \tag{299}$$

2.11.4 Pitch trim requirement

Every operating point must meet the requirement of pitch trim, which is equivalent to the centers of weight and pressure coinciding. This is enforced by requiring that the following total-moment residual is zero.

$$\mathcal{R}_M(x_{\mathrm{wbox}}, S_\mathrm{h}, C_{L\mathrm{h}}, C_L, r_{\mathrm{fuel}}, r_{\mathrm{pay}}, \xi_{\mathrm{pay}}) \;\equiv\; x_{CG} \;-\; x_{CP} \;=\; \frac{\partial W}{W} + \frac{c_o\, C_m}{C_L} \;=\; 0 \tag{300}$$

The argument list of the residual indicates the variables which have the strongest influence on pitch trim.

2.11.5 Pitch stability requirement

An aircraft must also have some minimum amount of static pitch stability, which means that the rearmost center of gravity must be ahead of the neutral point by the static margin fraction f_{SM} of the mean aerodynamic chord. This is met when the following stability residual is zero.

$$\mathcal{R}_{S_\mathrm{h}}(x_\mathrm{wbox}, S_\mathrm{h}, r_\mathrm{fuel}, r_\mathrm{pay}, \xi_\mathrm{pay}) \;\equiv\; x_{CG} \,-\, x_{NP} \,+\, f_{SM}\, c_{MA} \;=\; 0 \tag{301}$$

The argument list indicates the variables which have the strongest influence on pitch stability.

2.12 Horizontal Tail Sizing

The horizontal tail area can be sized by a number of alternative requirements, described below.

2.12.1 Specified horizontal tail volume

This is the simplest approach. The pitch stability margin or pitch damping requirements are assumed to be quantified by the horizontal tail volume,

$$l_\mathrm{h} \;=\; x_\mathrm{htail} \,-\, x_\mathrm{wing} \tag{302}$$

$$V_\mathrm{h} \;=\; \frac{S_\mathrm{h}}{S}\,\frac{l_\mathrm{h}}{c_\mathrm{mac}} \tag{303}$$

which when specified gives the necessary S_h. Defining the tail arm from the center of wing centroid is simpler than using the wing's aerodynamic center, and is reasonable for these rather simple sizing relations.

2.12.2 Design-case: Horizontal tail sizing and wing positioning

For the design case, both S_h and x_wbox are determined so as to drive the pitch trim and stability residuals (300) and (301) to zero simultaneously. Their remaining arguments are set for the appropriate worst-case situations:

$$\mathcal{R}_M(x_\mathrm{wbox}, S_\mathrm{h}\,;\, (C_{L\mathrm{h}})_\mathrm{min}, (C_L)_\mathrm{max}, (r_\mathrm{fuel})_\mathrm{fwd}, (r_\mathrm{pay})_\mathrm{fwd}, 0) \;=\; 0 \tag{304}$$

$$\mathcal{R}_{S_\mathrm{h}}(x_\mathrm{wbox}, S_\mathrm{h}\,;\, (r_\mathrm{fuel})_\mathrm{aft}, (r_\mathrm{pay})_\mathrm{aft}, 1) \;=\; 0 \tag{305}$$

Specifically, for the pitch trim residual (304) the most-forward CG and most-negative flaps-down wing airfoil c_m, at maximum flight C_L are assumed. For the stability residual (305) the most-aft CG is assumed. The r_pay values which give the extreme forward and aft CG locations are obtained by solving the extremizing relation

$$\frac{\partial \mathcal{R}_M}{\partial r_\mathrm{pay}} \;=\; 0 \tag{306}$$

which is a quadratic for r_pay. It is solved twice, with $\xi_\mathrm{pay} = 0$ chosen to give $(r_\mathrm{pay})_\mathrm{fwd}$, and then $\xi_\mathrm{pay} = 1$ chosen to give $(r_\mathrm{pay})_\mathrm{aft}$. Zero fuel, or $r_\mathrm{fuel} = 0$ is assumed for both cases, as

this typically gives the most extreme CG locations together with the worst-case payload distributions.

The two residuals (304) and (305) are simultaneously driven to zero by varying the wing position $x_{\rm wbox}$ and the horizontal tail area $S_{\rm h}$, by solving the 2×2 Newton system. The four Jacobian elements are readily calculated.

$$\begin{bmatrix} \frac{\partial \mathcal{R}_M}{\partial S_{\rm h}} & \frac{\partial \mathcal{R}_M}{\partial x_{\rm wbox}} \\ \frac{\partial \mathcal{R}_{S_{\rm h}}}{\partial S_{\rm h}} & \frac{\partial \mathcal{R}_{S_{\rm h}}}{\partial x_{\rm wbox}} \end{bmatrix} \begin{Bmatrix} \delta S_{\rm h} \\ \delta x_{\rm wbox} \end{Bmatrix} = - \begin{Bmatrix} \mathcal{R}_M \\ \mathcal{R}_{S_{\rm h}} \end{Bmatrix} \tag{307}$$

This system is converged in every cycle of the overall aircraft weight iteration, so that the final aircraft is trimmed and stable to within the specified limits.

2.12.3 Off-design case: Horizontal tail lift setting

For off-design calculations where the wing location and horizontal tail area are fixed, pitch trim is achieved by adjusting $C_{L_{\rm h}}$. The pitch-trim residual (300) is therefore again driven to zero, but this time with a Newton step on $C_{L_{\rm h}}$.

$$\frac{\partial \mathcal{R}_M}{\partial C_{L_{\rm h}}} = \frac{1}{C_L}\left[-(c_o C_{m_1} - x_{\rm wbox})\frac{S_{\rm h}}{S} + (c_{o{\rm h}} C_{m{\rm h}_1} - x_{\rm hbox})\frac{S_{\rm h}}{S}\right] \tag{308}$$

$$(C_{L_{\rm h}})_{\rm new} = C_{L_{\rm h}} - \frac{\mathcal{R}_M}{\partial \mathcal{R}_M / \partial C_{L_{\rm h}}} \tag{309}$$

2.13 Vertical Tail Sizing

The vertical tail area can be sized by four alternative requirements, described below. In practice, any or the maximum value could be chosen.

2.13.1 Specified tail volume

This is the simplest approach. The yaw stability or yaw damping requirements are assumed to be quantified by the vertical tail volume,

$$l_{\rm v} = x_{\rm vtail} - x_{\rm wing} \tag{310}$$

$$V_{\rm v} = \frac{S_{\rm v}}{S}\frac{l_{\rm v}}{b} \tag{311}$$

which when specified gives the necessary $S_{\rm v}$.

2.13.2 Vertical tail sizing via engine-out yaw power

An alternative is to size the vertical tail area $S_{\rm v}$ so that it can achieve yaw trim with one engine out. The requirement is

$$q_{\rm min}\, S_{\rm v}\, l_{\rm v}\, C_{L{\rm v}_{\rm eng\,out}} = (F_{\rm eng} + q_{\rm min} C_{D{\rm eng}} A_{\rm eng})\, y_{\rm eng} \tag{312}$$

where $q_{\min}$ is the minimum takeoff dynamic pressure, $C_{L\mathrm{v}_{\mathrm{eng\,out}}}$ is the maximum lift coefficient of the vertical tail with some yaw control margin, F_{eng} is the thrust of one engine, $C_{D\mathrm{eng}}$ is the drag coefficient of a windmilling engine with reference area A_{eng}, and y_{eng} is the lateral distance of the outermost engine from the centerline.

2.13.3 Vertical tail sizing via yaw acceleration authority

Another alternative is the requirement of obtaining a required yaw acceleration $\dot{r}_{\mathrm{req}}$, which for example might be needed to align the aircraft with the runway just before touchdown in a crosswind landing. The requirement is

$$q_{\min}\, S_{\mathrm{v}}\, l_{\mathrm{v}}\, C_{L\mathrm{v}_{\mathrm{yaw}}} \;=\; \frac{\dot{r}_{\mathrm{req}}}{I_z} \tag{313}$$

where I_z is the aircraft yaw inertia. The specified vertical tail lift coefficient $C_{L\mathrm{v}_{\mathrm{yaw}}}$ for this maneuver would be close to the maximum stall value with some reasonable safety margin from stall.

2.13.4 Vertical tail sizing via sideslip trim authority

Yet another alternative is the requirement of maintaining yaw trim at some maximum sideslip angle $\beta_{\max}$ which the aircraft is to be able to safely sustain. This requirement is

$$S_{\mathrm{v}}\, l_{\mathrm{v}}\, C_{L\mathrm{v}_{\mathrm{sideslip}}} \;=\; -\frac{CNV_{\mathrm{f}}}{\partial\beta}\,\beta_{\max} \tag{314}$$

$$\frac{CNV_{\mathrm{f}}}{\partial\beta} \;\simeq\; -2\mathcal{V}_{\mathrm{f}} \tag{315}$$

where $CNV_{\mathrm{f}} \equiv N_{\mathrm{f}}/q_\infty$ is the yaw moment volume, in which N_{f} is the (destabilizing) fuselage yaw moment. In the estimate (315), which follows from slender-body theory, $\mathcal{V}_{\mathrm{f}}$ is the fuselage volume.

The sideslip vertical tail lift coefficient in (314) must allow for some margin $\Delta(C_{L_{\mathrm{v}}})_{\max}$ from the maximum value,

$$C_{L\mathrm{v}_{\mathrm{sideslip}}} \;=\; (C_{L_{\mathrm{v}}})_{\max} \;-\; \Delta(C_{L_{\mathrm{v}}})_{\max} \tag{316}$$

so that there will still be sufficient residual yaw stability. Here we must further recognize that the vertical tail in the sideslip condition will have some negative (opposing the steady lift) rudder deflection, which in general will reduce maximum lift. This can be estimated from the linearized relation

$$(C_{L_{\mathrm{v}}})_{\max} \;=\; (C_{L_{\mathrm{v}}})_{\max_0} \;+\; (C_{L_{\mathrm{v}}})_{\max_\delta}\,\delta_r \tag{317}$$

where, for example, for the representative NACA 0012 jet transport tail airfoil at $Re = 10^7$, $M_\infty = 0.3$, $N_{\mathrm{crit}} = 1$ we have the following estimates from XFOIL.

$$(C_{L_{\mathrm{v}}})_{\max_0} \;\simeq\; 1.7 \tag{318}$$

$$(C_{L_{\mathrm{v}}})_{\max_\delta} \;\simeq\; 0.03\,\mathrm{deg}^{-1} \tag{319}$$

The rudder deflection itself can be estimated from

$$C_{L_{\mathrm{v}_{\mathrm{sideslip}}}} \;=\; \frac{\partial C_{L_{\mathrm{v}}}}{\partial \beta}\,\beta_{\max} \;+\; \frac{\partial C_{L_{\mathrm{v}}}}{\partial \delta_r}\,\delta_r \tag{320}$$

where we further estimate the stability and control derivatives from 2D airfoil coefficients with compressibility and sweep corrections.

$$\frac{\partial C_{L_{\mathrm{v}}}}{\partial \beta} \;=\; \frac{\partial c_{\ell_{\mathrm{v}}}}{\partial \alpha}\,\frac{1}{\sqrt{1-M_\infty^2}+2/AR_{\mathrm{v}}}\,\frac{1}{\sqrt{(1-M_\infty^2)+\tan^2\Lambda_{\mathrm{v}}}} \tag{321}$$

$$\frac{\partial C_{L_{\mathrm{v}}}}{\partial \beta} \;=\; \frac{\partial c_{\ell_{\mathrm{v}}}}{\partial \delta}\,\frac{1}{\sqrt{1-M_\infty^2}+2/AR_{\mathrm{v}}}\,\frac{1}{\sqrt{(1-M_\infty^2)+\tan^2\Lambda_{\mathrm{v}}}} \tag{322}$$

Typical values for the incompressible 2D coefficients are

$$\frac{\partial c_{\ell_{\mathrm{v}}}}{\partial \alpha} \;\simeq\; 0.11\,\mathrm{deg}^{-1} \tag{323}$$

$$\frac{\partial c_{\ell_{\mathrm{v}}}}{\partial \delta} \;\simeq\; 0.07\,\mathrm{deg}^{-1} \tag{324}$$

which were also obtained from XFOIL.

It's useful to note that for a yaw-stable airplane we must have $\partial(N_{\mathrm{v}}+N_{\mathrm{f}})/\partial\beta > 0$, or more specifically the vertical tail's positive (stable) yaw derivative must overpower the fuselage's negative (unstable) yaw derivative. In this case a positive $\beta_{\max}$ must produce a negative δ_r in equation (320), which will decrease $(C_{L_{\mathrm{v}}})_{\max}$ as given by (317).

In a typical sizing case, the procedurally simplest approach is to simultaneously solve equations (314) and (320) for the two unknowns S_{v} and δ_r, using the other equations to replace the various other unknowns ultimately in terms of the specified $\beta_{\max}$ and $\Delta(C_{L_{\mathrm{v}}})_{\max}$, and the various known airfoil coefficients.

2.14 Dissipation (Drag) Calculation

2.14.1 Power-based formulation

The performance calculations used here are based on the power balance and dissipation analysis of Drela [12]. In brief, the usual streamwise force balance equation in constant-velocity flight is replaced with the power balance relation

$$FV_\infty \;=\; DV_\infty \;+\; W\dot{h} \tag{325}$$

where $\dot{h}$ is the climb rate, F is an effective thrust, and D is an effective drag. These two effective forces are actually defined in terms of the net propulsive power and the net dissipation and vortex kinetic energy loss rate.

$$FV_\infty \;\equiv\; P_{K_{\mathrm{inl}}} + P_{V_{\mathrm{inl}}} + P_{K_{\mathrm{out}}} \;-\; \Phi_{\mathrm{jet}} \;+\; \dot{m}_{\mathrm{fuel}}V_\infty^2 \tag{326}$$

$$DV_\infty \;\equiv\; \Phi_{\mathrm{surf}} - P_{V_{\mathrm{surf}}} \;+\; \Phi_{\mathrm{wake}} - P_{V_{\mathrm{wake}}} \;+\; \Phi_{\mathrm{vortex}} \tag{327}$$

The advantage of this power-balance approach is that it naturally handles the presence of boundary layer ingestion (BLI) without the ambiguities or complications which arise with a force-balance approach. If no BLI is present then the two approaches become entirely equivalent, and F, D become the conventional thrust and drag. The BLI accounting is described in more detail in the separate document "Power Accounting with Boundary Layer Ingestion". Only the relevant results will be used here.

The disspation and power loss terms in the above power equations are used to define the following convenient coefficients.

$$C_{D_p} \equiv \frac{\Phi_{\text{surf}} - P_{V_{\text{surf}}} + \Phi_{\text{wake}} - P_{V_{\text{wake}}}}{\frac{1}{2}\rho_\infty V_\infty^3 S} \tag{328}$$

$$C_{D_i} \equiv \frac{\Phi_{\text{vortex}}}{\frac{1}{2}\rho_\infty V_\infty^3 S} = C_{D_i} \tag{329}$$

$$C_D \equiv \frac{DV_\infty}{\frac{1}{2}\rho_\infty V_\infty^3 S} = C_{D_p} + C_{D_i} \tag{330}$$

As with "F" and "D", the "C_D" notation is used as a reminder that if there is no BLI, the above definitions reduce to the conventional drag coefficients and the primes can be simply dropped in that case.

In the following subsections, the various contributions to the overall power-loss coefficient C_D' will be computed. Most of these rely on traditional drag models and terminology, hence the "Drag" label will be used in the sections titles, mostly out of habit. As a useful indicator, the prime $()'$ will be retained only for those contributions which are potentially influenced by BLI. Unprimed contributions will thus also correspond to the conventional drag coefficients.

2.14.2 Fuselage Profile Drag

The fuselage profile drag is determined by an pseudo-axisymmetric viscous/inviscid calculation method, which is described in the separate document "Simplified Viscous/Inviscid Calculation for Nearly-Axisymmetric Bodies". This gives reliable viscous flow and fuselage drag predictions for any reasonable fuselage shape, without the need to rely on effective wetted area or fineness-ratio correlations.

The method requires the geometry to be specified in the form of a cross-sectional area distribution $A_{(x)}$ and also a perimeter distribution $b_{0(x)}$, shown in Figure 14. For a round cross-section these are of course related, but to allow treating more general fuselage cross-sections, they are assumed to be specified separately. The cross section sizes and shapes can vary along the body, provided the variation is reasonably smooth.

The cross-sectional area over the center cylindrical portion is A_{fuse}, which has already been defined by (6). This also defines the radius of the equivalent round cylinder.

$$R_{\text{cyl}} = \sqrt{\frac{A_{\text{fuse}}}{\pi}} \tag{331}$$

The equivalent radii over the tapering nose and radius are then defined via the following

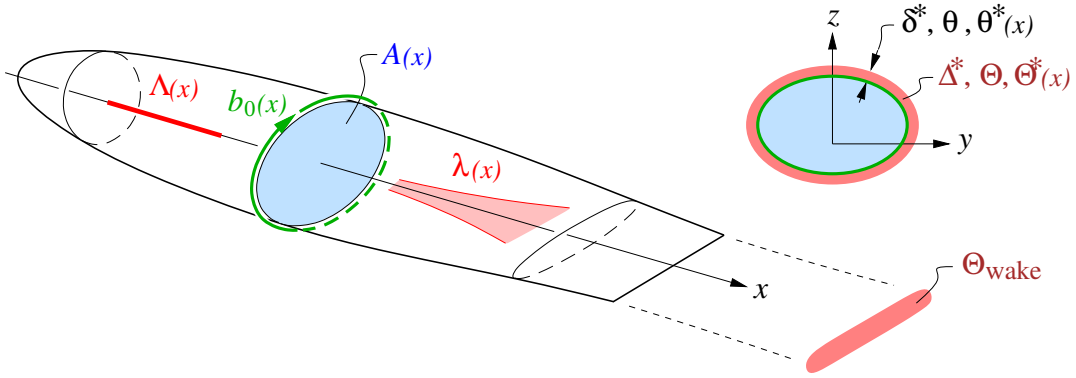

Figure 14: Fuselage defined by cross-sectional area $A_{(x)}$ and perimeter $b_{0(x)}$ distributions. Viscous calculation produces displacement, momentum, and kinetic energy areas $\Delta^*, \Theta, \Theta^*_{(x)}$.

convenient functions.

$$R_{(x)} = \begin{cases} R_{\rm cyl}\left[\,1-\left(\dfrac{x_{\rm blend_1}-x}{x_{\rm blend_1}-x_{\rm nose}}\right)^a\,\right]^{1/a} & , \quad x_{\rm nose} < x < x_{\rm blend_1} \\ R_{\rm cyl} & , \quad x_{\rm blend_1} < x < x_{\rm blend\,2} \\ R_{\rm cyl}\left[\,1-\left(\dfrac{x-x_{\rm blend\,2}}{x_{\rm end}-x_{\rm blend\,2}}\right)^b\,\right] & , \quad x_{\rm blend\,2} < x < x_{\rm tail} \end{cases} \tag{332}$$

$$a \simeq 1.6 \tag{333}$$

$$b \simeq 2.0 \tag{334}$$

The $x_{\rm blend_1}$ and $x_{\rm blend\,2}$ locations are the nose and tailcone blend points, and do not necessarily have to be exactly the same as the $x_{\rm shell_1}$ and $x_{\rm shell\,2}$ locations which define the loaded pressure shell. Likewise, $x_{\rm end}$ is the aerodynamic endpoint of the tailcone, and is distinct from its structural endpoint $x_{\rm conend}$. The a and b constant values above give reasonable typical fuselage shapes.

If the fuselage is nearly round, the necessary area and perimeter distributions follow immediately.

$$A_{(x)} = \pi\, R_{(x)}^2 \tag{335}$$

$$b_{0(x)} = 2\pi R_{(x)} \tag{336}$$

This would be suitably modified for non-circular cross-sections.

With this geometry definition, the viscous/inviscid calculation procedure provides the momentum and kinetic energy area distributions along the body and wake,

$$\{\Theta_{(s)}\,,\ \Theta^*_{(s)}\} = f_{\rm f_{excr}}\,\mathcal{F}(M_\infty, Re_\ell\,;\, A_{(x)}, b_{0(x)}) \tag{337}$$

where $\mathcal{F}$ denotes the overall viscous/inviscid calculation procedure, and $f_{\rm f_{excr}} \geq 1$ is an empirical factor to allow for fuselage excrescence drag sources.

Specific values of interest are the momentum area $\Theta_{\rm wake}$ at the wake numerical endpoint $s_{\rm wake}$, the far-downstream momentum area Θ_∞, and the kinetic energy area Θ_{TE} at the body

endpoint or trailing edge.

$$\Theta_{\rm wake} = \Theta(s_{\rm wake}) \tag{338}$$

$$H_{\rm avg} = \tfrac{1}{2}\left[H(s_{\rm wake}) + 1 + (\gamma-1)M_\infty^2\right] \tag{339}$$

$$\Theta_\infty = \Theta_{\rm wake}\left(\frac{u_e(s_{\rm wake})}{V_\infty}\right)^{H_{\rm avg}} \tag{340}$$

$$\Theta^*_{TE} = \Theta^*(s_{TE}) \tag{341}$$

Equation (340) is the Squire-Young formula, with $H_{\rm avg}$ being the average shape parameter between the end of the wake and far downstream.

The fuselage surface + wake dissipated power in the absence of BLI is then evaluated as follows, consistent with the usual wake momentum defect relations.

$$C'_{D_{\rm fuse}} \equiv \frac{\Phi_{\rm surf} - P_{V_{\rm surf}} + \Phi_{\rm wake} - P_{V_{\rm wake}}}{\frac{1}{2}\rho_\infty V_\infty^3 S} \qquad \text{(without BLI)} \tag{342}$$

$$C'_{D_{\rm fuse}} = \frac{D_{\rm fuse}}{\frac{1}{2}\rho_\infty V_\infty^2 S} = \frac{2\Theta_\infty}{S} \qquad \text{(without BLI)} \tag{343}$$

If BLI is present at or near the trailing edge, the upstream boundary layer and corresponding surface dissipation $\Phi_{\rm surf}$ will be mostly unaffected. But the viscous fluid flowing into the wake is now reduced by the ingestion fraction $f_{\rm BLI\,f}$, so that the wake dissipation $\Phi_{\rm wake}$ will be reduced by the same fraction. This then gives the following overall fuselage dissipation coefficient for the BLI case.

$$C_{D_{\rm fuse}} = \frac{\Phi_{\rm surf} - P_{V_{\rm surf}} + (\Phi_{\rm wake} - P_{V_{\rm wake}})(1-f_{\rm BLI\,f})}{\frac{1}{2}\rho_\infty V_\infty^3 S} \qquad \text{(with BLI)} \tag{344}$$

$$C_{D_{\rm fuse}} \simeq C_{D_{\rm fuse}} - C_{\Phi_{\rm wake}} f_{\rm BLI\,f} \qquad \text{(with BLI)} \tag{345}$$

$$\text{where} \quad C_{\Phi_{\rm wake}} = \frac{2\Theta_\infty}{S} - \frac{\Theta^*_{TE}}{S} \tag{346}$$

2.14.3 Wing Profile Drag

The power dissipated in the wing's surface and wake for the non-ingesting case defines the wing's profile drag coefficient.

$$C'_{D_{\rm wing}} = \frac{\Phi_{\rm surf} - P_{V_{\rm surf}} + \Phi_{\rm wake} - P_{V_{\rm wake}}}{\frac{1}{2}\rho_\infty V_\infty^3 S} \qquad \text{(without BLI)} \tag{347}$$

Any ingestion of the wing boundary layer is captured by the ingestion fraction $f_{\rm BLI\,w}$, in the same manner as for the fuselage.

$$C_{D_{\rm wing}} = C_{D_{\rm wing}} - C_{\Phi_{\rm wake}} f_{\rm BLI\,w} \qquad \text{(with BLI)} \tag{348}$$

$$\text{where} \quad C_{\Phi_{\rm wake}} \simeq r_{\Phi_{\rm wake}}\, C_{D_{\rm wing}} \tag{349}$$

$$r_{\Phi_{\rm wake}} \simeq 0.15 \tag{350}$$

The wake dissipation is assumed here to be $r_{\Phi_{\text{wake}}} = 15\%$ of the total airfoil dissipation, which is typical of optimized modern transonic airfoils.

The actual calculation of $C_{D_{\text{wing}}}$ is via the drag using infinite swept wing theory, which also gives the lift in term of the perpendicular-plane velocity $V_\perp$ and lift coefficient $c_{\ell_\perp}$. Figure 15 shows the relations. These quantities are related to the local loading via

$$V_\perp = V_\infty \cos\Lambda \tag{351}$$

$$\mathrm{d}L = \tilde{p}\,\mathrm{d}y = \tfrac{1}{2}\rho_\infty V_\perp^2\, c_\perp\, c_{\ell_\perp}\,\mathrm{d}y_\perp \tag{352}$$

$$p_o\, P_{(\eta)} = \tfrac{1}{2}\rho_\infty V_\infty^2\, c_o\, C_{(\eta)}\, c_{\ell_\perp(\eta)}\, \cos^2\Lambda \tag{353}$$

excluding the wing center and extreme tip where the lift adjustments ΔL_o and ΔL_t are located. The loading scale p_o in level flight is obtained from (160) with $N=1$ as follows.

$$W = L = \tfrac{1}{2}\rho_\infty V_\infty^2\, S\, C_L \tag{354}$$

$$L_{\text{htail}} = \tfrac{1}{2}\rho_\infty V_\infty^2\, S_{\text{h}}\, C_{L_{\text{h}}} \tag{355}$$

$$p_o = \frac{1}{K_p\, b}\,(L - L_{\text{htail}}) \tag{356}$$

Using (356) to substitute for p_o in (353) and rearranging gives an explicit expression for the local section lift coefficient.

$$C_{L_{\text{htail}}} = \frac{S_{\text{h}}}{S}\, C_{L_{\text{h}}} \tag{357}$$

$$c_{\ell_\perp(\eta)} = \frac{C_L - C_{L_{\text{htail}}}}{\cos^2\Lambda}\,\frac{S}{K_p\, b\, c_o}\,\frac{P_{(\eta)}}{C_{(\eta)}} \tag{358}$$

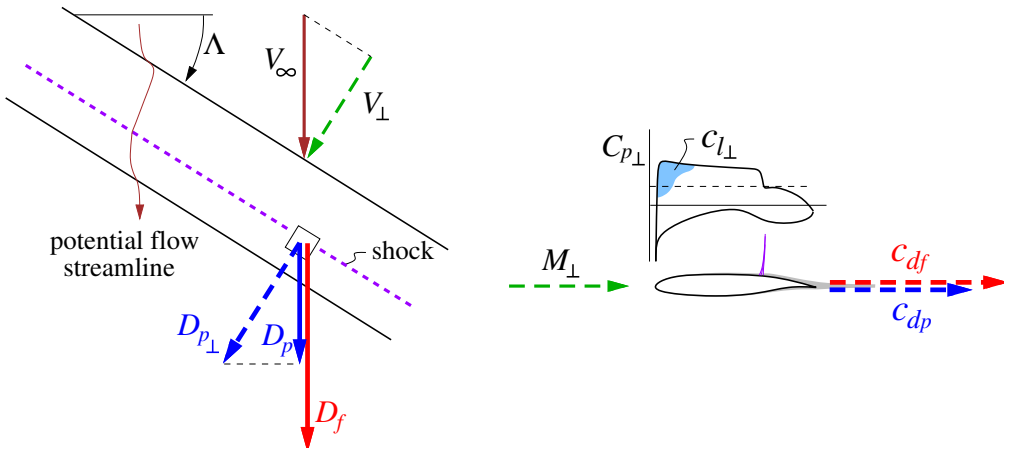

Figure 15: Friction and pressure drag forces on infinite swept wing

Using this $c_{\ell_\perp}$ and also $M_\perp$, the perpendicular-plane friction and pressure drag coefficients are then obtained from a 2D airfoil drag database having the form

$$c_{d_f} = f_{\text{wexcr}}\, \bar{c}_{d_f}(c_{\ell_\perp}, M_\perp, \tfrac{t}{c}) \left(\frac{Re_c}{Re_{\text{ref}}}\right)^{a_{Re}} \tag{359}$$

$$c_{d_p} = f_{\text{wexcr}}\, \bar{c}_{d_p}(c_{\ell_\perp}, M_\perp, \tfrac{t}{c}) \left(\frac{Re_c}{Re_{\text{ref}}}\right)^{a_{Re}} \tag{360}$$

$$\text{where} \qquad M_\perp = M_\infty \cos\Lambda \tag{361}$$

$$\frac{t}{c} = \bar{h} \tag{362}$$

$$Re_c = \frac{\rho_\infty V_\infty c}{\mu_\infty} \tag{363}$$

$$a_{Re} \simeq -0.15 \tag{364}$$

and $f_{\text{wexcr}} \geq 1$ is an empirical specified factor to account for wing excrescence drag sources, and Re_{ref} is a reference Reynolds number at which the database functions $\bar{c}_{d_f}, \bar{c}_{d_p}$ were computed. The chord Reynolds number Re_c could of course be treated as an additional parameter in the database, but at a considerable increase in the size of the database and the computational effort needed to construct it. The value of the Re-scaling exponent $a_{Re} \simeq -0.15$ is appropriate for fully-turbulent flow.

Note that the database includes the airfoil thickness/chord ratio $\frac{t}{c} = \bar{h}$, which is crucial for obtaining a realistic wing thickness/sweep/C_L/Mach tradeoff. The thickness dependence is determined by viscous MSES [19] calculations on a number of transonic airfoils or varying thickness, such as the ones shown in Figure 16. Each airfoil has been designed independently for a well-behaved transonic drag rise, so that the database returns c_{d_f} and c_{d_p} values representative of the best transonic airfoil technology. A piecewise-linear airfoil thickness distribution is assumed, defined by the three values $\bar{h}_o, \bar{h}_s, \bar{h}_t$.

$$\bar{h}_{(\eta)} = \begin{cases} \bar{h}_o & , \quad 0<\eta<\eta_o \\ \bar{h}_o + (\bar{h}_s - \bar{h}_o)\dfrac{\eta-\eta_o}{\eta_s-\eta_o} & , \quad \eta_o<\eta<\eta_s \\ \bar{h}_s + (\bar{h}_t - \bar{h}_s)\dfrac{\eta-\eta_s}{1-\eta_s} & , \quad \eta_o<\eta<\eta_s \end{cases} \tag{365}$$

On typical transport wings most of the thickness/chord variation occurs inboard, so in that case, only $\bar{h}_o$ and $\bar{h}_s$ would be considered as design variables, and $\bar{h}_t = \bar{h}_s$ would be assumed.

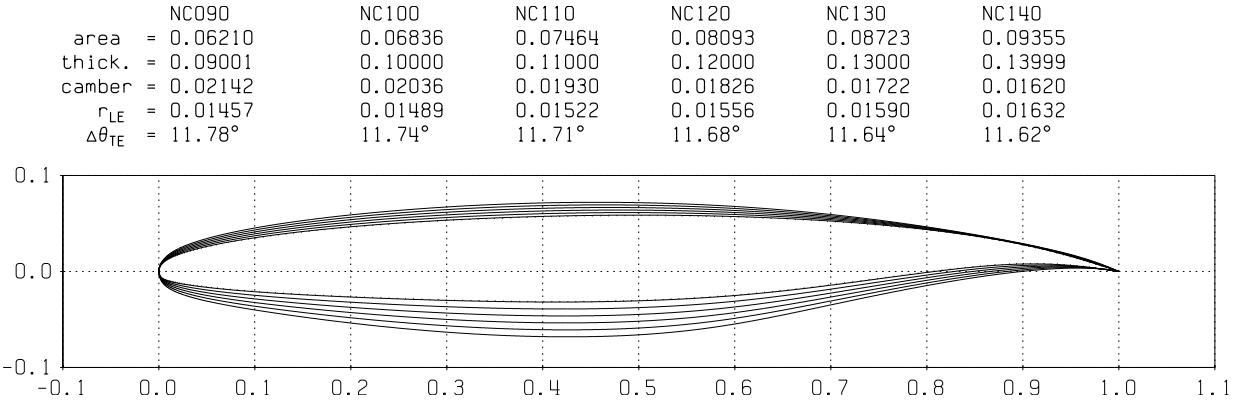

Figure 16: Airfoil family used to generate airfoil-performance database.

The 2D profile drag coefficients are applied to the swept wing using infinite swept-wing theory, illustrated in Figure 15. This treatment is exact for laminar flow on untapered wings, and quite accurate for turbulent flow. The friction drag is assumed to scale with

freestream dynamic pressure and to act mostly along the freestream flow direction, while the pressure drag from the shock and viscous displacement is assumed to scale with the wing-normal dynamic pressure and to act normal to the wing-spanwise axis. The total local streamwise drag element is then given as follows.

$$\begin{aligned} \mathrm{d}D_{\text{wing}} &= \mathrm{d}D_f + \mathrm{d}D_p = \mathrm{d}D_f + \mathrm{d}D_{p_\perp}\cos\Lambda \\ &= \tfrac{1}{2}\rho_\infty V_\infty^2\, c\, c_d\ \mathrm{d}y \qquad (366) \\ c_d &= c_{d_f} + c_{d_p}\cos^3\Lambda \qquad \text{(infinite swept wing)} \qquad (367) \end{aligned}$$

However, this relation is not realistic near the fuselage. Here the potential flow is forced parallel to the freestream direction which causes the wing shock to become locally unswept, as shown in Figure 17. Also, the full streamwise dynamic pressure (as opposed to the wing-normal dynamic pressure) acts at the trailing edge where most of the displacement-effect pressure drag occurs. Hence, the sweep correction is dropped off towards the fuselage via the heuristic "unsweep" function $f_{\text{Suns}(\eta)}$.

$$c_{d(\eta)} = \left\{c_{d_f} + c_{d_p}\left[f_{\text{Suns}} + (1-f_{\text{Suns}})\cos^2\Lambda\right]\cos\Lambda\right\} \qquad \text{(actual swept wing)} \qquad (368)$$

$$f_{\text{Suns}(\eta)} = \exp\left(-\frac{1}{k_{\text{Suns}}}\frac{y-y_o}{c}\right) = \exp\left(-\frac{1}{k_{\text{Suns}}}\frac{\eta-\eta_o}{C_{(\eta)}}\frac{b}{2c_o}\right) \qquad (369)$$

$$k_{\text{Suns}} \simeq 0.5 \qquad (370)$$

The k_{Suns} decay constant controls the area of the wing most influenced by the shock unsweep correction, as shown in Figure 17.

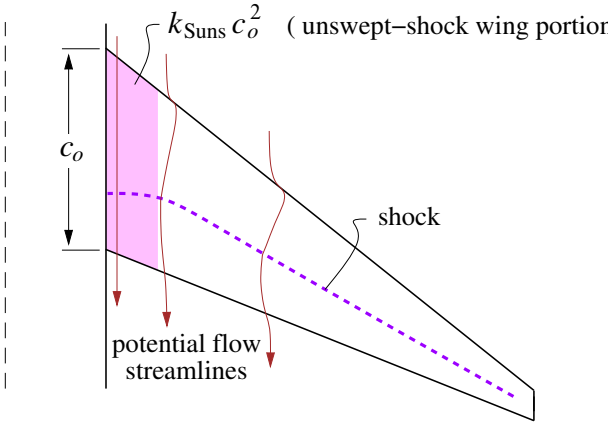

Figure 17: Wing shock unsweeps near the fuselage, roughly over the area $k_{\text{uns}}c_o^2$.

The overall wing profile drag is then obtained by numerical integration of (366), using (368) for the $c_{d(\eta)}$ function and (123) for the chord $c_{(\eta)}$ function.

$$C_{D_{\text{wing}}} \equiv \frac{D_{\text{wing}}}{\frac{1}{2}\rho_\infty V_\infty^2\, S} = \frac{bc_o}{S}\int_{\eta_o}^{1} c_{d(\eta)}\, C_{(\eta)}\ \mathrm{d}\eta \qquad (371)$$

2.14.4 Tail Profile Drag

The viscous dissipation of the tail surfaces is computed using the same relations as for the wing, giving the equivalent tail drag coefficients $C_{D_{\text{htail}}}$ and $C_{D_{\text{vtail}}}$. No BLI is assumed, but

could be included in the same manner as for the wing. Because tail surfaces typically do not have significant shock waves, the shock-unsweep correction (368) is inappropriate. Instead, the 2D friction and pressure drag coefficients c_{d_f} and c_{d_p} are specified directly and are used in the infinite-wing relation (367), and are assumed constant over the surface so that numerical spanwise integration is unnecessary.

$$C_{D_{\text{htail}}} = \frac{S_{\text{h}}}{S}\left(c_{d_{f\text{h}}} + c_{d_{p\text{h}}}\cos^3\Lambda_{\text{h}}\right) \tag{372}$$

$$C_{D_{\text{vtail}}} = \frac{S_{\text{v}}}{S}\left(c_{d_{f\text{v}}} + c_{d_{p\text{v}}}\cos^3\Lambda_{\text{v}}\right) \tag{373}$$

2.14.5 Strut Profile Drag

In the absence of any BLI on the strut, its dissipation is fully captured by its conventional drag coefficient, scaled by the local mean-cube-average velocity ratio $r_{V_{\text{strut}}}$ to allow for the fact that a strut is typically in the decreased flow velocity below a lifting wing. Simple sweep corrections are also used as for the wing.

$$c_{\text{strut}} = \sqrt{\frac{A_{\text{strut}}}{k_A\,\bar{h}_{\text{strut}}}} \quad , \qquad k_A \simeq 0.65 \tag{374}$$

$$S_{\text{strut}} = 2c_{\text{strut}}\,\ell_{s_\perp} \tag{375}$$

$$\cos\Lambda_s = \frac{\ell_s}{\ell_{s_\perp}} \tag{376}$$

$$C_{D_{\text{strut}}} = \frac{S_{\text{strut}}}{S}\left(c_{d_{f\text{s}}} + c_{d_{p\text{s}}}\cos^3\Lambda_{\text{s}}\right) r^3_{V_{\text{strut}}} \tag{377}$$

Picking a strut thickness/chord ratio $\bar{h}_{\text{strut}} \simeq 0.15\ldots0.20$ typically gives the minimum overall drag for a given strut cross-sectional area A_{strut}. The k_A area factor of 0.65 is typical of most symmetric airfoils.

2.14.6 Engine Nacelle Profile Drag

The nacelle viscous dissipation accounts for the external nacelle flow only, since the internal flow is represented by the engine diffuser and nozzle losses. The external wetted area and corresponding area fraction is determined as an assumed fraction r_{Snace} of the engine fan area.

$$S_{\text{nace}} = n_{\text{eng}}\, r_{\text{Snace}}\,\frac{\pi}{4}\,d^2_{\text{fan}} \tag{378}$$

$$f_{\text{Snace}} = \frac{S_{\text{nace}}}{S} \tag{379}$$

The skin friction coefficient can also be calculated based on the nacelle-length Reynolds number and a standard turbulent skin-friction law, with an excrescence factor $f_{\text{n}_{\text{excr}}} \geq 1$ included as for the fuselage and wing.

$$\ell_{\text{nace}} = 0.15\, r_{\text{Snace}}\, d_{\text{fan}} \tag{380}$$

$$Re_{\text{nace}} = \frac{\rho_\infty V_\infty \ell_{\text{nace}}}{\mu_\infty} \tag{381}$$

$$C_{f_{\text{nace}}} = f_{\text{n}_{\text{excr}}}\, C_{f_{\text{turb}}}(Re_{\text{nace}}) \tag{382}$$

The nacelle is assumed to be immersed in the potential nearfield of a nearby wing or fuselage, with a local effective freestream $V_{\rm nace}$ which differs somewhat from the true freestream V_∞, and is specified via the ratio $V_{\rm nace}/V_\infty$. Depending on the flight condition and engine power, the fan-face Mach number M_2 will in general differ considerably from the corresponding local M'_∞, The nacelle is therefore effectively a loaded ring airfoil, which can be represented by a ring vortex sheet whose resulting external nacelle-surface velocity is approximately

$$V_{{\rm n}_{LE}} \;\simeq\; 2V_{\rm nace} \;-\; V_2 \tag{383}$$

$$\frac{V_{\rm nace}}{V_\infty} \;=\; r_{V_{\rm nace}} \tag{384}$$

$$\frac{V_{{\rm n}_{LE}}}{V_\infty} \;=\; 2\frac{V_{\rm nace}}{V_\infty} - \frac{V_2}{V_\infty} \;\simeq\; \max\!\left(2r_{V_{\rm nace}} - \frac{M_2}{M_\infty}\;,\;0\right) \tag{385}$$

at the lip, as sketched in Figure 18. Limiting $V_{{\rm n}_{LE}}$ above zero avoids unrealistic results for low airspeed, high-power operation situations, where the external nacelle drag is minor in any case.

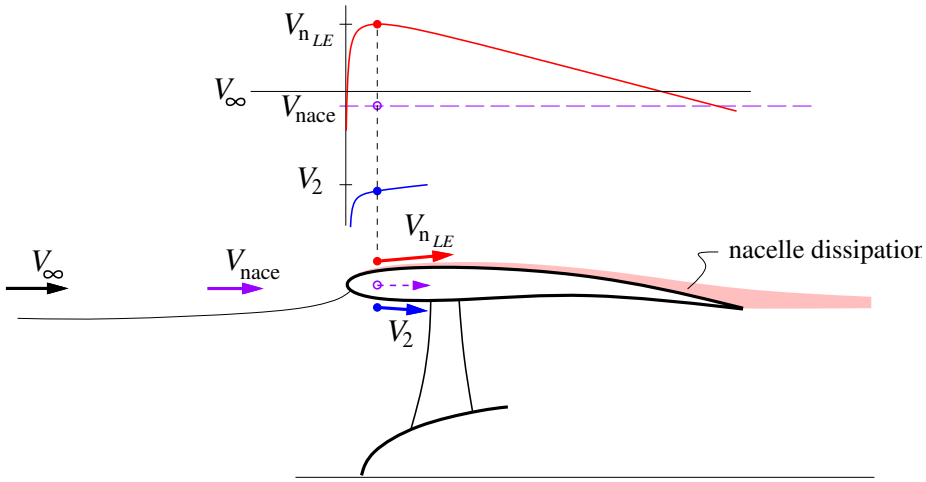

Figure 18: Velocity distribution on inside and outside of engine nacelle. Outside velocity determines nacelle dissipation and implied nacelle drag. The $V_{{\rm n}_{LE}} > V_2$ case shown is for a typical cruise condition, while $V_{{\rm n}_{LE}} < V_2$ will occur at low speeds and high power.

Assuming a linear acceleration or deceleration from $V_{{\rm n}_{LE}}$ to $V_{\rm nace}$ at the nacelle nozzle gives the following mean-cube velocity ratio on the nacelle surface.

$$r^3_{V_{\rm nsurf}} \;\equiv\; \int_0^1 \left(\frac{V(\xi)}{V_\infty}\right)^3 {\rm d}\xi \;=\; \frac{1}{V_\infty^3}\int_0^1 \Big[V_{\rm nace} \,+\, (V_{{\rm n}_{LE}} - V_{\rm nace})\,(1-\xi)\Big]^3\,{\rm d}\xi \tag{386}$$

$$=\; \frac{1}{4}\left[\frac{V_{{\rm n}_{LE}}}{V_\infty} \,+\, r_{V_{\rm nace}}\right]\left[\left(\frac{V_{{\rm n}_{LE}}}{V_\infty}\right)^2 + r^2_{V_{\rm nace}}\right] \tag{387}$$

The nacelle-surface dissipation, expressed as the equivalent nacelle drag coefficient, is now estimated using a turbulent wetted-area skin-friction coefficient, so that $r^3_{V_{\rm nsurf}}$ in effect becomes the conventional drag form factor.

$$C_{D_{\rm nace}} \;\equiv\; \frac{D_{\rm nace}}{\frac{1}{2}\rho_\infty V_\infty^2\, S} \;=\; f_{\rm Snace}\, C_{f_{\rm nace}}\, r^3_{V_{\rm nsurf}} \tag{388}$$

Figure 19 shows the nacelle profile drag form factor $r^3_{V_{\text{nsurf}}} = D_{\text{nace}}/\frac{1}{2}\rho_\infty V_\infty^2 C_{f_{\text{nace}}} S_{\text{nace}}$ versus fan-face Mach number and local velocity ratio V_{nace}/V_∞.

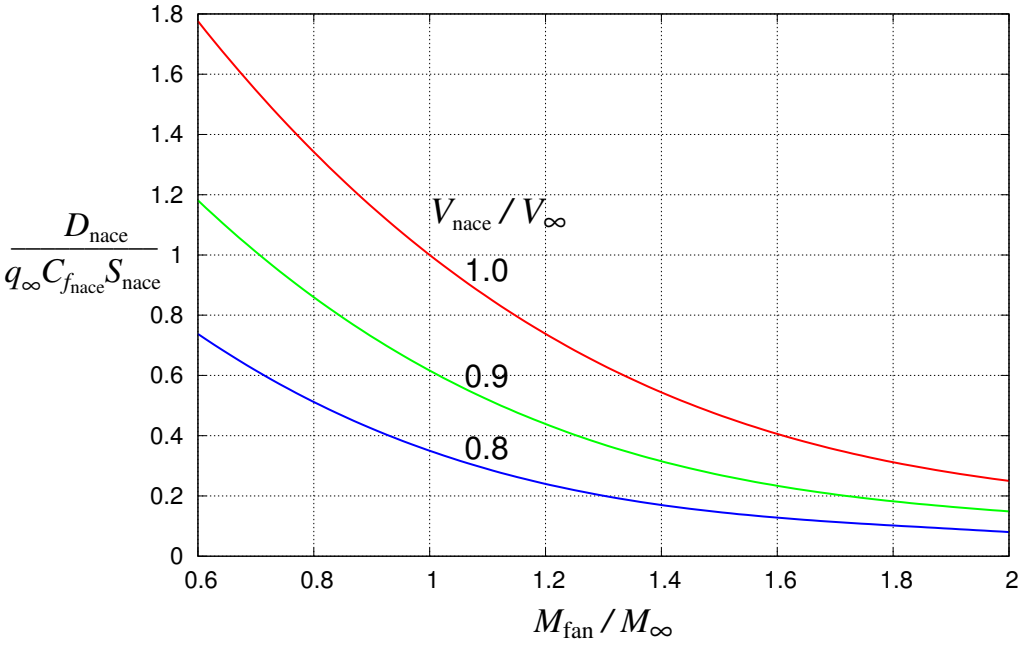

Figure 19: Nacelle profile drag factor versus fan-face Mach number and local velocity ratio.

2.14.7 Induced Drag

The induced drag is calculated using a discrete vortex Trefftz-Plane analysis. The circulation of the wing wake immediately behind the trailing edge is

$$\Gamma_{\text{wing}(\eta)} = \frac{\tilde{p}(\eta)}{\rho_\infty V_\infty} \simeq \frac{p(\eta)}{\rho_\infty V_\infty}\sqrt{1-\eta^{k_t}} \tag{389}$$

$$k_t \simeq 16 \tag{390}$$

where the approximation realistically represents the tip lift rolloff for typical taper ratios, and is consistent with the assumed $f_{L_t} \simeq -0.05$ value for the tip lift loss factor. This circulation is convected into the wake along streamlines which will typically constrict behind the fuselage by continuity. Figure 20 shows two possible aft fuselage taper shapes, giving two different wake constrictions.

An annular streamtube at the wing contracts to another annular streamtube in the wake with the same cross-sectional area. The y and y' locations on the wing and wake which are connected by a streamline are therefore related by the correspondence function.

$$y'_{(y)} = \sqrt{y^2 - y_o^2 + {y'_o}^2} \tag{391}$$

The Trefftz Plane circulation $\Gamma_{(y')}$ is then given by the coordinate shift. The mapping function $y'_{(y)}$ is not defined for $y < y_o$, so the circulation there is simply set from the y_o value.

$$\Gamma_{\text{wake}(y')} = \begin{cases} \Gamma_{\text{wing}}\left(y_{(y')}\right) & , \quad y > y_o \\ \Gamma_{\text{wing}}\left(y_o\right) \end{cases} \tag{392}$$

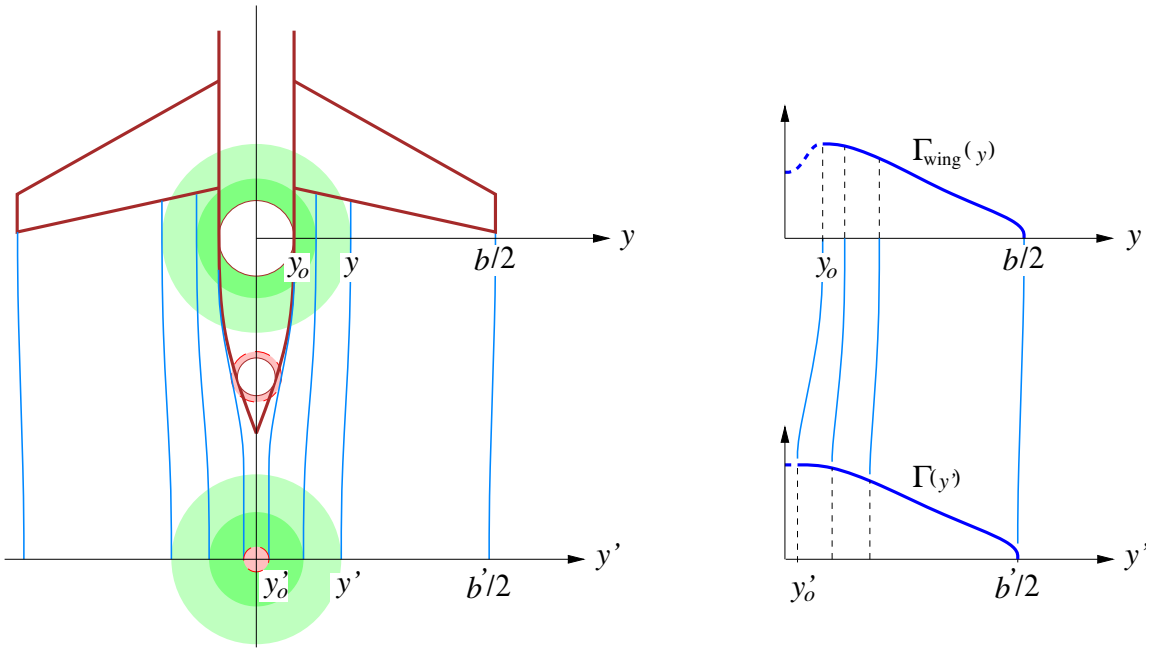

Figure 20: Wake streamline contraction due to fuselage thickness, carrying wing circulation into the wake. Two shaded streamtubes are shown. Wake center radius y_o' is nonzero due to the fuselage viscous wake displacement area.

The Trefftz Plane analysis uses point vortices. The circulation (392) is evaluated at the midpoints of n intervals along the wake trace, spaced more or less evenly in the Glauert angle to give a cosine distribution in physical space. The wake's vertical z positions are simply taken directly from the wing.

$$\theta_{i+1/2} = \frac{\pi}{2}\frac{i-1/2}{n} \quad , \quad i = 1 \ldots n \tag{393}$$

$$y_{i+1/2} = \frac{b}{2}\cos\theta_{i+1/2} \tag{394}$$

$$y'_{i+1/2} = \sqrt{y_{i+1/2}^2 - y_o^2 + {y'_o}^2} \tag{395}$$

$$z'_{i+1/2} = z_{i+1/2} \tag{396}$$

$$\Gamma_{i+1/2} = \Gamma_{\text{wing}}(y_{i+1/2}) \tag{397}$$

The locations of $n+1$ trailing vortices are computed similarly.

$$\theta_i = \frac{\pi}{2}\frac{i-1}{n} \quad , \quad i = 1 \ldots n+1 \tag{398}$$

$$y_i = \frac{b}{2}\cos\theta_i \tag{399}$$

$$y'_i = \sqrt{y_i^2 - y_o^2 + {y'_o}^2} \tag{400}$$

$$z'_i = z_i \tag{401}$$

The circulations of these trailing vortices are the differences of the adjacent bound circula-

tions, with the circulation beyond the tips effectively zero.

$$\bar{\Gamma}_i \;=\; \begin{cases} -\Gamma_{i-1/2} & , \quad i=1 \qquad\quad \text{(left tip)} \\ \Gamma_{i+1/2} - \Gamma_{i-1/2} & , \quad i=2\ldots n \\ \Gamma_{i+1/2} & , \quad i=n+1 \qquad \text{(right tip)} \end{cases} \tag{402}$$

The above definitions are also applied to the horizontal tail, with its discrete points simply appended to the list and n increased accordingly.

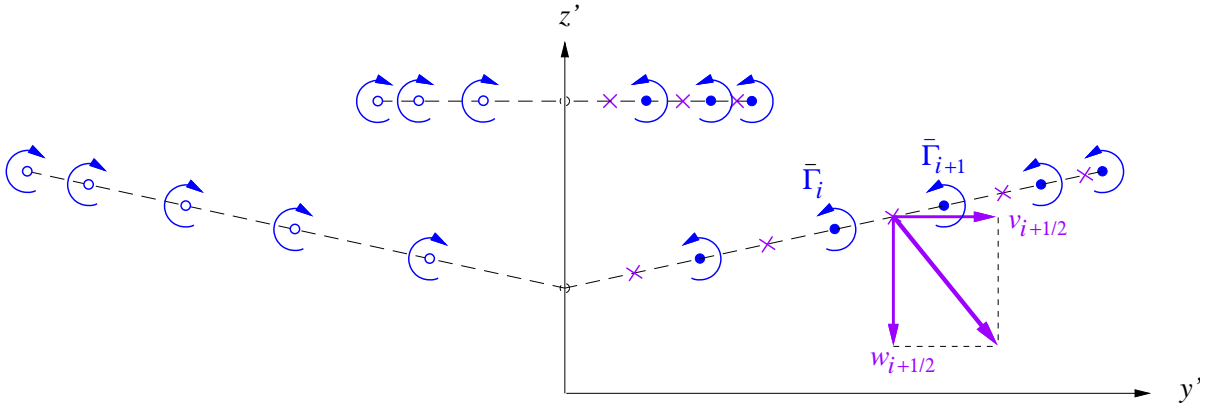

Figure 21: Trefftz Plane vortices $i, i+1\ldots$ and collocation points $i+1/2$ used for velocity, impulse, and kinetic energy calculations. Left/right symmetry is exploited.

The Trefftz plane calculation proceeds by first calculating the y-z wake velocity components at the $y'_{i+1/2}, z'_{i+1/2}$ interval midpoints, induced by all the trailing vortices and their left-side images.

$$v_{i+1/2} \;=\; \sum_{j=1}^{n+1} \frac{\bar{\Gamma}_j}{2\pi} \left[\frac{-(z'_{i+1/2}-z'_j)}{(y'_{i+1/2}-y'_j)^2 + (z'_{i+1/2}-z'_j)^2} - \frac{-(z'_{i+1/2}-z'_j)}{(y'_{i+1/2}+y'_j)^2 + (z'_{i+1/2}-z'_j)^2} \right] \tag{403}$$

$$w_{i+1/2} \;=\; \sum_{j=1}^{n+1} \frac{\bar{\Gamma}_j}{2\pi} \left[\frac{y'_{i+1/2}-y'_j}{(y'_{i+1/2}-y'_j)^2 + (z'_{i+1/2}-z'_j)^2} - \frac{y'_{i+1/2}+y'_j}{(y'_{i+1/2}+y'_j)^2 + (z'_{i+1/2}-z'_j)^2} \right] \tag{404}$$

The overall lift and induced drag are then computed using the Trefftz Plane vertical impulse and kinetic energy. The sums are doubled to account for the left side image.

$$C_{L_{TP}} \;=\; \frac{2}{\frac{1}{2}\rho_\infty V_\infty^2 S} \sum_{i=1}^{n} \rho_\infty V_\infty \, \Gamma_{i+1/2} \, (y'_{i+1} - y'_i) \tag{405}$$

$$C_{D_{TP}} \;=\; \frac{2}{\frac{1}{2}\rho_\infty V_\infty^2 S} \sum_{i=1}^{n} -\frac{\rho_\infty}{2} \, \Gamma_{i+1/2} \left[w_{i+1/2} \, (y'_{i+1} - y'_i) \;-\; v_{i+1/2} \, (z'_{i+1} - z'_i) \right] \tag{406}$$

To minimize any modeling and numerical errors incurred in the wake contraction model and the point-vortex summations, the final induced drag value is scaled by the square of the surface-integral and Trefftz-Plane drag values.

$$C_{D_i} \;=\; C_{D_{TP}} \left(\frac{C_L}{C_{L_{TP}}} \right)^2 \tag{407}$$

This is equivalent to using the Trefftz Plane analysis to calculate the span efficiency rather than the actual induced drag coefficient.

2.14.8 Total Drag

The total effective aircraft dissipation coefficient is obtained by summing all the contributions.

$$C'_D \;=\; C_{D_i} + C'_{D_{\rm fuse}} + C'_{D_{\rm wing}} + C_{D_{\rm htail}} + C_{D_{\rm vtail}} + C_{D_{\rm strut}} + C_{D_{\rm nace}} \tag{408}$$

2.15 Engine Performance Model and Sizing

2.15.1 Engine model summary

The extensive details of the engine calculations are given in the separate documents "Turbofan Sizing and Analysis with Variable $c_{p(T)}$" and "Film Cooling Flow Loss Model". The treatment of the inlet kinetic energy defect $K_{\rm inl}$ is described in the document "Power Accounting with Boundary Layer Ingestion". In brief, $K_{\rm inl}$ reduces the fan inlet total pressure, and also adds to the net effective thrust by the amount $K_{\rm inl}/V_\infty$, which in engine parlance can be interpreted as a reduction in inlet "ram drag".

The engine model can be run in one of three modes:

1) Design sizing mode. The net effective thrust $F'_{\rm e}$ and combustor exit temperature $T_{t\,4}$ are specified along with a number of other component and operating parameters, and the engine flow areas $A_2, A_5 \ldots$ are computed.

2) Off-design analysis mode. The areas and $T_{t\,4}$ are prescribed, and thrust $F'_{\rm e}$ is computed.

3) Off-design analysis mode. The areas and $F'_{\rm e}$ are prescribed, and $T_{t\,4}$ is computed.

For all three modes, the specific fuel consumption $TSFC'$ and all other engine operating parameters which are not specified are also computed.

$$\{A_2, A_{5\cdots}\,;\, TSFC'_{\cdots}\} \;=\; \mathcal{F}_{\rm eng_1}(F'_{\rm e}, T_{t_4}, OPR_{\rm D}, BPR_{\rm D\cdots}\,;\, M_\infty, p_\infty, T_\infty, \mathcal{K}_{\rm inl\cdots}) \tag{409}$$

$$\{F'_{\rm e}\,;\, TSFC', OPR, BPR_{\cdots}\} \;=\; \mathcal{F}_{\rm eng_2}(T_{t_4}, A_2, A_{5\cdots}\,;\, M_\infty, p_\infty, T_\infty, \mathcal{K}_{\rm inl\cdots}) \tag{410}$$

$$\{T_{t_4}\,;\, TSFC', OPR, BPR_{\cdots}\} \;=\; \mathcal{F}_{\rm eng_3}(F'_{\rm e}, A_2, A_{5\cdots}\,;\, M_\infty, p_\infty, T_\infty, \mathcal{K}_{\rm inl\cdots}) \tag{411}$$

$$\text{where} \qquad TSFC' \;\equiv\; \frac{F'_{\rm e}}{\dot m_{\rm fuel}\, g} \tag{412}$$

$$\mathcal{K}_{\rm inl} \;\equiv\; \left(\tfrac{1}{2}\rho_e V_e^3 \Theta^*\right)_{\rm inl} \;=\; \frac{f_{\rm BLI\,f}}{n_{\rm eng}} \left(\tfrac{1}{2}\rho_e V_e^3 \Theta^*\right)_{TE} \tag{413}$$

In these calculations, the fan inlet total pressure $p_{t\,2}$ is reduced as a result of the BLI, via the mass-averaged inlet entropy which is quantified by $\mathcal{K}_{\rm inl}$.

$$\bar s \;=\; \frac{\mathcal{K}_{\rm inl}}{\dot m_{\rm inl}} \frac{\gamma}{a_2^2} \tag{414}$$

$$p_{t\,2} \;=\; p_{t\,\infty}\, \exp(-\bar s) \tag{415}$$

where a_e is the local speed of sound outside the viscous layer, and $\dot m_{\rm inl}$ is the mass flow of the fluid with which the viscous defect mixes. The latter can be either the fan flow or the entire fan plus core flow.

2.15.2 Engine Sizing

In the design mode 1), the specified thrust is obtained is determined from the start-of-cruise weight W_c, lift/drag ratio, and the slight cruise-climb angle $\gamma_{\rm CR}$.

$$F'_{\rm D} = r_{B_c} W_c \left(\frac{C'_D}{C_L} + \gamma_{\rm CR} \right)_c \tag{416}$$

$$F'_{\rm e_D} = \frac{F'_{\rm D}}{n_{\rm eng}} \tag{417}$$

The engine calculations determine the specific thrust

$$F_{\rm sp_D} \equiv \frac{F'_{\rm e_D}}{a_\infty \dot{m}_{\rm core}(1+BPR_{\rm D})} \tag{418}$$

which then determines the core mass flow $\dot{m}_{\rm core}$ and the associated fan flow area A_2 and fan diameter $d_{\rm f}$.

$$A_2 = \frac{\dot{m}_{\rm core}(1+BPR_{\rm D})}{\rho_2 u_2} = \frac{1}{F_{\rm sp_D}} \frac{F'_{\rm e_D}}{\gamma p_\infty} \frac{1}{M_{2_{\rm D}}} \left(\frac{1+\frac{\gamma-1}{2} M^2_{2_{\rm D}}}{1+\frac{\gamma-1}{2} M^2_\infty} \right)^{\frac{\gamma+1}{2(\gamma-1)}} \tag{419}$$

$$d_{\rm f} = \sqrt{\frac{4A_2}{\pi(1-HTR^2_{\rm f})}} \tag{420}$$

Similar calculations are used for the other component and nozzle areas.

2.16 Mission Performance and Fuel Burn Analysis

2.16.1 Mission profiles

The altitude, weight, and thrust profiles versus range are schematically shown in Figure 22.

At any profile point these are related via the following normal force and axial force relations.

$$W \sin\gamma = F' - D' - \frac{W}{g} \frac{{\rm d}V}{{\rm d}t} \tag{421}$$

$$W \cos\gamma = L \tag{422}$$

Equation (421) is merely a recast form of the power-balance equation (325), with the added last acceleration term. The subscript has also been dropped from V_∞ and ρ_∞ for convenience.

The flight speed at any profile point is obtained from a specified C_L and ambient density using equation (422).

$$V = \sqrt{\frac{2W\cos\gamma}{\rho S C_L}} \tag{423}$$

Some iteration is required with the thrust/drag relations below to determine the climb angle γ needed in (423).

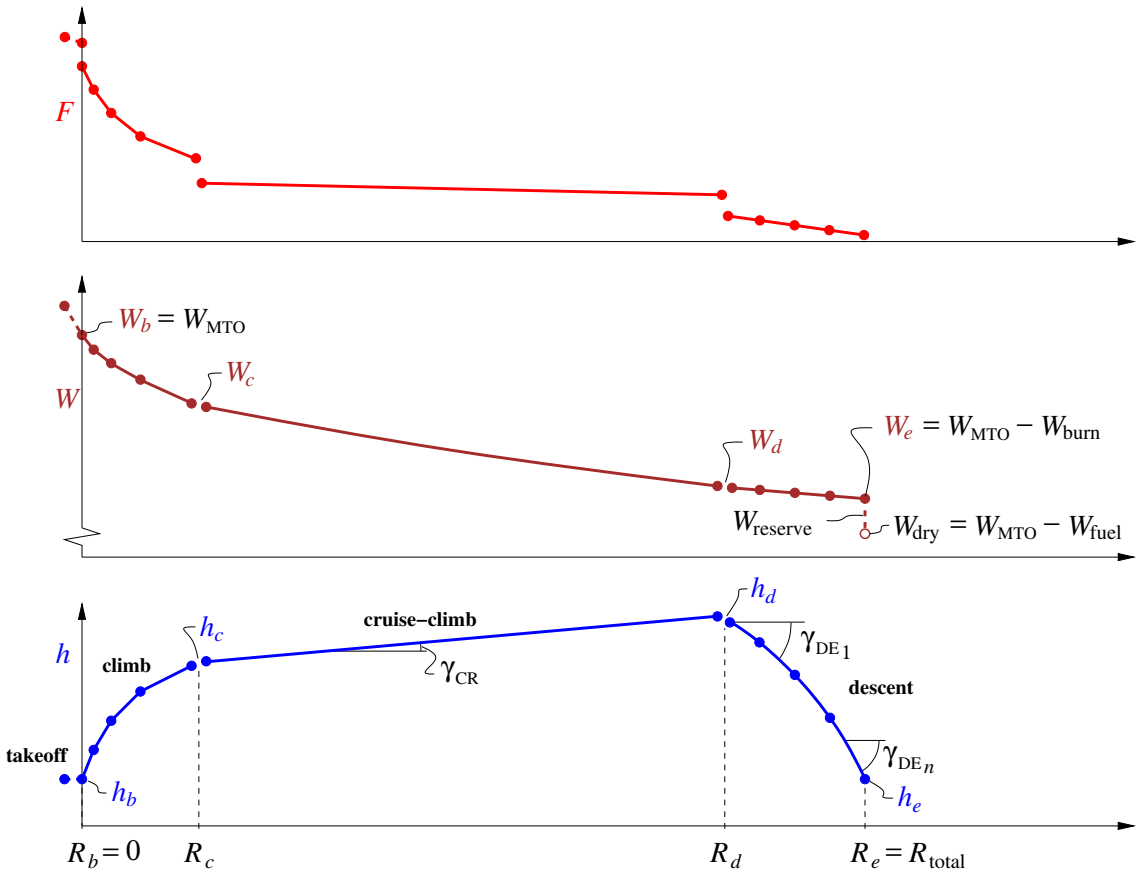

Figure 22: Design-mission profiles of altitude, weight, thrust, versus range.

Dividing (421) by (422), and using the kinematic ground-speed relation

$$\frac{\mathrm{d}R}{\mathrm{d}t} \;=\; V\cos\gamma \tag{424}$$

together with the fuel-burn to thrust relation

$$\frac{\mathrm{d}W}{\mathrm{d}t} \;=\; -\dot{m}_{\mathrm{fuel}}\, g \;=\; -F'\, TSFC' \tag{425}$$

gives an expression for the climb angle γ or the equivalent climb gradient $\mathrm{d}h/\mathrm{d}R$, and also the weight-loss gradient $\mathrm{d}W/\mathrm{d}R$.

$$\tan\gamma \;=\; \frac{\mathrm{d}h}{\mathrm{d}R} \;=\; \frac{F'}{W}\frac{1}{\cos\gamma} \;-\; \frac{D'}{L} \;-\; \frac{1}{2g}\frac{\mathrm{d}(V^2)}{\mathrm{d}R} \tag{426}$$

$$\frac{\mathrm{d}W}{\mathrm{d}R} \;=\; -F'\,\frac{TSFC'}{V\cos\gamma} \tag{427}$$

These will be suitably integrated over the mission segments to obtain the altitude and weight profiles $h_{(R)}$ and $W_{(R)}$.

The instantaneous climb or descent angle γ in the above expressions can be computed by combining (421) and (422), and solving for the resulting quadratic equation for $\sin\gamma$.

$$\phi \;=\; \frac{F'}{W} - \frac{\dot{V}}{g} \tag{428}$$

$$\epsilon = \frac{C'_D}{C_L} \tag{429}$$

$$\sin\gamma = \frac{\phi - \epsilon\sqrt{1-\phi^2+\epsilon^2}}{1+\epsilon^2} \tag{430}$$

The $\dot{V}$ acceleration term in the excess thrust-to-weight ratio ϕ can be neglected for most transport aircraft. The corresponding integrated $\mathrm{d}(V^2)$ differential in (426) is also typically small, but there's little reason to exclude it in calculations.

2.16.2 Mission profile integration

The fuel weight required for a given mission range is determined by integration of the trajectory equations (426) and (427), which are first put in the following equivalent differential forms.

$$\mathrm{d}R = \left(\mathrm{d}h + \frac{\mathrm{d}(V^2)}{2g}\right)\left(\frac{F'}{W}\frac{1}{\cos\gamma} - \frac{C'_D}{C_L}\right)^{-1} \tag{431}$$

$$\mathrm{d}(\ln W) = -\frac{F'}{W}\frac{TSFC'}{V\cos\gamma}\,\mathrm{d}R \tag{432}$$

The various terms are then approximated with 2-point finite differences or averages, and marched forward using a predictor/corrector scheme, over the climb, cruise, and descent segments of the mission. The details will be given in the Calculation Procedures section.

The following segment endpoint values are inputs to the integration, and are either specified externally, or obtained from the weight-sizing calculations:

W_b	takeoff weight
C_L	lift coefficient for all points
M_{CR}	cruise Mach number
h_b	takeoff altitude
h_c	start-of-cruise altitude
h_e	landing altitude

2.16.3 Climb distance

The climb-segment range R_c is computed by integrating equations (431) and (432) from the takeoff range $R_b = 0$, over the prescribed climb altitude change $h_b \ldots h_c$. The start-of-cruise weight W_c is computed in the process.

2.16.4 Cruise and descent angles, distances

Before the cruise and descent segments are integrated, it is first necessary to determine the end-of-cruise range R_d and altitude h_d.

The first step is to calculate the slight cruise-climb angle γ_{CR}, so as to preserve a constant flight Mach number M and flight C_L as the aircraft loses weight from fuel burn. These are related to the current weight W at any point in the cruise by the lift equation.

$$\frac{1}{2}\rho V^2 = \frac{\gamma}{2}pM^2 = \frac{W}{SC_L} \tag{433}$$

This assumes that $\cos\gamma \simeq 1$ which is appropriate for the extremely small climb angles occurring during a typical cruise-climb segment. With M and C_L held at their prescribed cruise values, this then gives the atmospheric pressure as a function of weight.

$$p = \frac{2}{\gamma M^2 S C_L} W \tag{434}$$

$$\frac{\mathrm{d}p}{\mathrm{d}W} = \frac{p}{W} \tag{435}$$

The very small change in W_{buoy} over the cruise-climb is neglected here. Using the atmospheric hydrostatic pressure gradient $\mathrm{d}p/\mathrm{d}h = -\rho g$, and the fuel-burn weight gradient (427), equation (435) is used to explicitly obtain the small climb angle during the cruise.

$$\gamma \simeq \tan\gamma = \frac{\mathrm{d}h}{\mathrm{d}R} = \frac{\mathrm{d}h}{\mathrm{d}p}\frac{\mathrm{d}p}{\mathrm{d}W}\frac{\mathrm{d}W}{\mathrm{d}R} \tag{436}$$

$$= \left[-\frac{1}{\rho g}\right]\left[\frac{p}{W}\right]\left[-W\frac{TSFC'}{V}\left(\frac{C_D'}{C_L}+\gamma\right)\right] \tag{437}$$

$$\gamma_{\text{CR}} = \left(\frac{C_D'}{C_L}\frac{p\,TSFC'}{\rho g V - p\,TSFC'}\right)_c \tag{438}$$

With the calculated cruise-climb angle γ_{CR}, the prescribed initial and final descent angles $\gamma_{\text{DE}_1}, \gamma_{\text{DE}_n}$, and the total cruise+descent remaining range $R_{\text{total}} - R_c$, the end-of-cruise range and altitude is the geometric intersection of the straight cruise-climb path and the straight or parabolic descent path, calculated as follows.

$$\gamma_{\text{DE}_{\text{avg}}} = \frac{1}{2}\left(\gamma_{\text{DE}_1} + \gamma_{\text{DE}_n}\right) \tag{439}$$

$$R_d = R_c + \frac{h_e - h_c - \gamma_{\text{DE}_{\text{avg}}}(R_{\text{total}} - R_c)}{\gamma_{\text{CR}} - \gamma_{\text{DE}_{\text{avg}}}} \tag{440}$$

$$h_d = h_c + \gamma_{\text{CR}}(R_d - R_c) \tag{441}$$

2.16.5 Cruise-Climb

Because the cruise-climb segment proceeds at a fixed Mach number, the integrand in equation (432) can be assumed to be constant and equal to its value at start of cruise, so that an analytic integration is possible. The result is of course a form of the Breguet equation.

$$\frac{W_d}{W_c} = \exp\left[-\left(\frac{F'}{W}\frac{TSFC'}{V}\right)_c (R_d - R_c)\right] \tag{442}$$

$$t_d = t_c + \frac{R_d - R_c}{V} \tag{443}$$

2.16.6 Descent

The descent integration proceeds in much the same way as the climb, except that the descent angle is now prescribed, and the necessary thrust at each integration point i is computed

from equation (431). The corresponding $T_{t\,4}$ and all the other engine operating variables are the calculated via the engine model run in prescribed-thrust off-design mode 3.

$$F'_{\rm e} = \frac{W}{n_{\rm eng}}\left(\sin\gamma_{\rm DE} + \frac{C'_D}{C_L}\cos\gamma_{\rm DE}\right) \tag{444}$$

$$\{T_{t_4}\,;\,TSFC', OPR, BPR...\} = \mathcal{F}_{\rm eng_3}(F'_{\rm e}, A_2, A_{5...}\,;\,M_\infty, p_\infty, T_\infty, \mathcal{K}_{\rm inl...}) \tag{445}$$

The end result of the integration is the final weight W_e and flight time t_e.

2.17 Mission fuel

From the final landing weight W_e, the fuel burn and takeoff fuel weight can then be obtained.

$$W_{\rm burn} = W_b - W_e \tag{446}$$

$$W_{\rm fuel} = W_{\rm burn}\,(1+f_{\rm reserve}) \tag{447}$$

$$f_{\rm fuel} = \frac{W_{\rm fuel}}{W_{\rm MTO}} \tag{448}$$

3 Calculation Procedures

Note:
This section is not currently up to date with the previous model-development sections

This relations developed in the previous Model Derivation section will now be recast and sequenced into sizing and weight formulas, together with drag, engine performance, mission trajectory, and fuel burn formulas. These are organized such that most sections can each be naturally implemented as a subroutine.

The overall calculation is iterative, and the calculation sequence presented here must be repeated until the design parameters, in particular the maximum takeoff weight W_{MTO}, stop changing to within a convergence tolerance.

This section gives the calculations for the design mission, where the airframe is updated along with the mission flight profiles and performance. The off-design mission case is a subset of this procedure, in that the mission flight profiles and performance are calculated in the same way, but the airframe updates are skipped so that the airframe is in effect held frozen. Each subsection which is skipped or irrelevant for the off-design case will be indicated with "(Design only)" in the subsection title.

3.1 Input Parameters

3.1.1 Operating and mission parameters

h_{TO} takeoff altitude
h_{LA} landing altitude
M_{CR} cruise flight Mach number
C_L aircraft lift coefficient, one for each mission point
R_{total} mission range

3.1.2 Operating and load parameters (Design only)

h_{CR} start-of-cruise altitude
q_{NE} never-exceed dynamic pressure (for sizing tail structure)
N_{lift} maximum lift load factor (scales wing loads)
N_{land} maximum landing load factor (scales fuselage loads)

3.1.3 Payload weight

W_{pay} payload weight

3.1.4 Other weights and weight fractions (Design only)

W_{fix} all fixed weight, accounting for ...
- pilots
- cockpit windows
- cockpit seats, furnishings, mechanisms
- flight instrumentation

navigation and communication equipment, antennas, etc.
cockpit power-related weight (power generation, wiring)

f_{padd} max-payload-proportional weight fraction, accounting for ...
flight attendants
food and water
galleys
toilets
doors and emergency exits
in-flight entertainment systems
overhead luggage compartments
interior furnishings, lighting
ventilation and air conditioning system
emergency oxygen system
other emergency equipment (floatation vests, slides, lifeboats ...)
cabin power-related weight (power regulation, wiring)

f_{seat} seat weight / payload weight fraction

f_{eadd} bare-engine/added-weight fraction accounting for ...
engine accessories
fuel system

f_{pylon} pylon weight fraction accounting for ...
pylon
other mounting structure

f_{reserve} fuel burn-proportional weight fraction, accounting for ...
fuel reserve
oil and other fluids

f_{apu} auxiliary power unit weight faction
f_{hpesys} hydraulic, pneumatic, electrical system weight fraction
f_{lgnose} nose landing gear weight fraction
f_{lgmain} main landing gear weight fraction

3.1.5 Fuselage geometry and structure (Design only)

x_{nose} location of front tip of fuselage
x_{end} location of rear tip of fuselage
$x_{\text{blend}\,1}$ location of nose ellipsoid blend point
$x_{\text{blend}\,2}$ location of tail taper blend point
$x_{\text{shell}\,1}$ pressurized fuselage-shell cylinder start
$x_{\text{shell}\,2}$ pressurized fuselage-shell cylinder end
x_{conend} endpoint of tailcone's primary structure
R_{fuse} fuselage radius
ΔR_{fuse} bottom-bubble downward extension
w_{fb} fuselage double-bubble half-width (= 0 for circular fuselage)
w_{floor} floor half-width
h_{floor} floor beam height
x_{htail} location of horizontal tail

x_{vtail}	location of vertical tail
x_{wing}	location of wing's center of lift
λ_{cone}	tailcone radius taper ratio from x_{shell_2} to x_{tail}
p_{cabin}	minimum cabin pressure (sets maximum pressurization Δp)
r_{Mh}	inertial-relief factor for horizontal-tail load on fuselage
r_{Mv}	inertial-relief factor for vertical-tail load on fuselage
f_{string}	fuselage stringer/skin weight fraction
f_{frame}	fuselage frame/skin weight fraction
f_{fadd}	other skin-proportional weight fraction, accounting for ...
	local stiffeners
	hard points and reinforcements
	fasteners
W'_{window}	weight/cabin-length of windows, discounted for skin cutouts
W''_{insul}	weight/area of cabin insulation and padding
W''_{floor}	floor decking and carpeting (does not include floor beams)

3.1.6 Wing geometry and structure parameters (Design only)

AR	aspect ratio ($= b^2/S$)
b_o	wing center section span (typ. fuselage span at wing root)
η_s	strut-attach fractional span (b_s/b if no strut is present)
λ_s	inner taper ratio
λ_t	outer taper ratio
Λ	sweep angle
$\bar{w}$	wing box width/chord ratio
$\bar{h}$	wing box height/chord ratio (airfoil t/c)
r_h	wing box chordwise taper ratio
f_{flap}	flaps, flap mounts and actuators weight fraction
f_{slat}	slats, slat mounts and actuators weight fraction
f_{aile}	ailerons, aileron mounts and actuators weight fraction
f_{lete}	leading and trailing edge weight fraction
f_{ribs}	ribs, local stiffeners and reinforcements
f_{spoi}	spoilers, spoiler mounts and actuators
f_{watt}	wing attachment hardware weight fraction
z_s	strut vertical height component
$\bar{h}_{\text{strut}}$	strut thickness/chord ratio (if strut is present)

3.1.7 Wing aerodynamic parameters

$r_{c_{\ell s}}$	local section c_l scale at η_s location
$r_{c_{\ell t}}$	local section c_l scale at tip (excluding local lift roll-off)
c_{m_o}	wing profile c_m at η_o wing root location
c_{m_s}	wing profile c_m at η_s wing break location
c_{m_t}	wing profile c_m at η_t tip location

3.1.8 Tail parameters (Design only)

V_{h}	HT volume coefficient
V_{v}	VT volume coefficient
AR_{h}	HT aspect ratio
AR_{v}	VT aspect ratio
λ_{h}	HT taper ratio
λ_{v}	VT taper ratio
Λ_{h}	HT sweep angle
Λ_{v}	VT sweep angle
$\bar{w}_{\mathrm{h}}$	HT box width/chord ratio
$\bar{w}_{\mathrm{v}}$	VT box width/chord ratio
$\bar{h}_{\mathrm{h}}$	HT box height/chord ratio (airfoil t/c)
$\bar{h}_{\mathrm{v}}$	VT box height/chord ratio (airfoil t/c)
$r_{h_{\mathrm{h}}}$	HT box chordwise taper ratio
$r_{h_{\mathrm{v}}}$	VT box chordwise taper ratio
$C_{L\mathrm{h}_{\mathrm{max}}}$	max HT lift coefficient at q_{NE}
$C_{L\mathrm{v}_{\mathrm{max}}}$	max VT lift coefficient at q_{NE}
f_{hadd}	HT box-proportional added-weight fraction
f_{vadd}	VT box-proportional added-weight fraction

3.1.9 Material properties (Design only)

The stresses derived in the previous section corresponds to an idealized structure which is not attainable in reality. Hence, the specified stress allowables must be reduced from the listed material properties by some usual factor of safety, and also by the expected max/average stress within the associated structural component. The latter is due to stress concentrations from holes and cutouts, and also due to non-ideal shape from approximate design or cost or manufacturing constraints. For example, if the sparcap material's maximum (yield or ultimate) strength is 50 000 psi, the required factor of safety is 1.5, and the expected max/average stress is 1.1, then the specified sparcap stress would be

$$\sigma_{\mathrm{cap}} \;=\; \frac{50\,000\,\mathrm{psi}}{1.5 \times 1.1} \;=\; 30\,300\,\mathrm{psi}$$

σ_{skin}	max allowable fuselage skin pressurization stress
σ_{bend}	max allowable fuselage shell bending stress
σ_{cap}	max allowable wing spar cap stress
τ_{web}	max allowable wing spar web shear stress
σ_{strut}	max allowable strut stress
ρ_{skin}	fuselage pressure-skin density
ρ_{bend}	fuselage bending-material density
ρ_{web}	wing box web material density
ρ_{cap}	wing box cap material density
ρ_{strut}	strut material density
ρ_{fuel}	fuel density

3.1.10 Drag build-up parameters

c_{d_f}	wing profile friction-drag coefficient function $\bar{c}_{d_f}(c_{\ell_\perp}, M_\perp, \tau, Re_c)$
c_{d_p}	wing profile pressure-drag coefficient function $\bar{c}_{d_p}(c_{\ell_\perp}, M_\perp, \tau, Re_c)$
Re_{ref}	reference Reynolds number for c_{d_f}, c_{d_p} functions
a_{Re}	Reynolds-scaling exponent for c_{d_f}, c_{d_p} functions
$C_{f_{\text{wet}}}$	skin friction function $C_f(Re_l)$
$A_{(x)}$	fuselage cross-sectional area distribution
$b_{0(x)}$	fuselage cross-sectional perimeter distribution
$f_{\text{BLI f}}$	fuselage boundary layer ingestion fraction
$f_{\text{BLI w}}$	wing boundary layer ingestion fraction
$r_{V_{\text{nace}}}$	nacelle velocity ratio V'_∞/V_∞
$r_{V_{\text{strut}}}$	strut velocity ratio V'_∞/V_∞
k_{Suns}	shock-unsweep wing root area factor
e	span efficiency, one for each mission point
$c_{\ell\text{max}_{\text{TO}}}$	max section lift coefficient at takeoff

3.1.11 Standard Atmosphere functions

$p_{\text{atm}(h)}$	pressure
$T_{\text{atm}(h)}$	temperature
$a_{\text{atm}(h)}$	speed of sound ($= \sqrt{\gamma R T_{\text{atm}}}$)
$\rho_{\text{atm}(h)}$	density ($= p_{\text{atm}}/RT_{\text{atm}}$))

3.1.12 Air and Fuel properties

R_i	gas constant for constituent i
$c_{p_{i(T)}}$	specific heat for constituent i
$h_{i(T)}$	complete enthalpy for constituent i ($= \int^T c_{p_i}\,\mathrm{d}T \;+\; \Delta h_{\text{f}}$)
$\sigma_{i(T)}$	entropy complement for constituent i ($= \int^T c_{p_i}/T\,\mathrm{d}T$)

3.1.13 Engine sizing and performance parameters

$(T_{t\,4})_{\text{TO}}$	turbine inlet total temperature for takeoff
$f_{T_{\text{CL}_1}}$	turbine inlet total temperature fraction for initial climb
$f_{T_{\text{CL}_n}}$	turbine inlet total temperature fraction for final climb
$(T_{t\,4})_{\text{CR}}$	turbine inlet total temperature for cruise

The climb-segment temperatures are set via linear interpolation in altitude over the climb points $i = 1 \ldots n$ using the fractions.

$$f_i \;=\; \frac{n-i}{n-1}\, f_{T_{\text{CL}_1}} \;+\; \frac{i-1}{n-1}\, f_{T_{\text{CL}_n}} \tag{449}$$

$$T_{\text{CL}_i} \;=\; (T_{t\,4})_{\text{TO}}\,(1-f_i) \;+\; (T_{t\,4})_{\text{CR}}\, f_i \tag{450}$$

This conveniently ensures that the climb temperatures always automatically fall between the takeoff and cruise values, even when the latter are varied in a parameter sweep or in optimization.

3.1.14 Engine sizing and performance parameters (Design only)

n_{eng} number of engines
M_{2_D} design fan-face Mach number
BPR_{D} design bypass ratio
$\pi_{\text{f}_{\text{D}}}$ design fan pressure ratio
$\pi_{\text{lc}_{\text{D}}}$ design low-pressure compressor pressure ratio
$\pi_{\text{hc}_{\text{D}}}$ design high-pressure compressor pressure ratio
π_{d} diffuser pressure ratio
π_{b} burner pressure ratio
$\eta_{\text{pol}_{\text{f}}}$ max fan polytropic efficiency
$\eta_{\text{pol}_{\text{c}}}$ max compressor polytropic efficiency
$\eta_{\text{pol}_{\text{t}}}$ max turbine polytropic efficiency (does not include cooling-flow losses)

3.1.15 Engine turbine-cooling mass flow and loss parameters (Design only)

T_{metal} turbine metal temperature
ΔT_{streak} hot-streak temperature increment
M_{exit} turbine blade row exit Mach number
St_h turbine area-weighted Stanton number
M_{4a} representative turbine Mach at start of mixing zone
r_{u_c} cooling-flow exit velocity ratio (u_c/u_{4a})

3.2 Initial Guesses to Start Iteration

3.2.1 Initial fuel fraction

f_{fuel} fuel weight fraction (e.g. from rough Breguet estimate)

3.2.2 Initial weights, loads, fractions (Design only)

W_{htail} h. tail weight (e.g. some fraction of W_{pay})
W_{vtail} v. tail weight (e.g. some fraction of W_{pay})
W_{wing} wing weight (e.g. some fraction of W_{pay})
W_{eng} engine weight (e.g. some fraction of W_{pay})
$L_{\text{h}_{\text{max}}}$ max horizontal tail down lift (e.g. some fraction of W_{pay})
$L_{\text{v}_{\text{max}}}$ max vertical tail side lift (e.g. some fraction of W_{pay})
b_{v} vertical tail span (e.g. some fraction of l_{shell})
f_{Snace} engine nacelle wetted area/wing area ratio
f_{eng} engine weight fraction

3.3 Fuselage Sizing and Weight (Design only)

3.3.1 Pressure shell

$$\Delta p = p_{\text{cabin}} - p_{\text{eoc}} \tag{451}$$
$$\theta_{\text{fb}} = \arcsin(w_{\text{fb}}/R_{\text{fuse}}) \tag{452}$$

$$h_{\rm fb} = \sqrt{R_{\rm fuse}^2 - w_{\rm fb}^2} \tag{453}$$

$$t_{\rm skin} = \frac{\Delta p\, R_{\rm fuse}}{\sigma_{\rm skin}} \tag{454}$$

$$t_{\rm fb} = 2\frac{\Delta p\, w_{\rm fb}}{\sigma_{\rm skin}} \tag{455}$$

$$A_{\rm skin} = (2\pi + 4\theta_{\rm fb}) R_{\rm fuse}\, t_{\rm skin} \; + \; 2\Delta R_{\rm fuse} t_{\rm skin} \tag{456}$$

$$A_{\rm fb} = (2h_{\rm fb} + \Delta R_{\rm fuse}) t_{\rm fb} \tag{457}$$

$$S_{\rm end} = (2\pi + 4\theta_{\rm fb}) R_{\rm fuse}^2 \left\{ 1 \; + \; \left[\frac{1}{3} + \frac{2}{3} \left(\frac{l_{\rm nose}}{R_{\rm fuse}} \right)^{8/5} \right]^{5/8} \right\} \tag{458}$$

$$l_{\rm shell} = x_{\rm shell\,2} \; - \; x_{\rm shell\,1} \tag{459}$$

$$\mathcal{V}_{\rm skin} = A_{\rm skin}\, l_{\rm shell} \; + \; S_{\rm end}\, t_{\rm skin} \tag{460}$$

$$\mathcal{V}_{\rm fb} = A_{\rm fb}\, l_{\rm shell} \tag{461}$$

$$W_{\rm skin} = \rho_{\rm skin}\, g\, \mathcal{V}_{\rm skin} (1 + f_{\rm string} + f_{\rm frame} + f_{\rm fadd}) \tag{462}$$

$$W_{\rm fweb} = \rho_{\rm skin}\, g\, \mathcal{V}_{\rm fb} \tag{463}$$

$$W_{\rm shell} = W_{\rm skin} \; + \; W_{\rm fweb} \tag{464}$$

3.3.2 Cabin volume

$$\mathcal{V}_{\rm cabin} = A_{\rm fuse}\, (l_{\rm shell} \; + \; 0.67\, l_{\rm nose} \; + \; 0.67\, R_{\rm fuse}) \tag{465}$$

3.3.3 Windows and Insulation

$$W_{\rm window} = W'_{\rm window}\, l_{\rm shell} \tag{466}$$

$$W_{\rm insul} = W''_{\rm insul}\, [(1.1\pi + 2\theta_{\rm fb}) R_{\rm fuse}\, l_{\rm shell} \; + \; 0.55\, S_{\rm end}] \tag{467}$$

3.3.4 Floor

$$\sigma_{\rm floor} = \sigma_{\rm bend} \qquad \text{(assumed same for convenience)} \tag{468}$$

$$\tau_{\rm floor} = \tau_{\rm web} \qquad \text{(assumed same for convenience)} \tag{469}$$

$$\rho_{\rm floor} = \rho_{\rm bend} \qquad \text{(assumed same for convenience)} \tag{470}$$

$$\mathcal{S}_{\rm floor} = \begin{cases} \frac{1}{2}\, \mathcal{P}_{\rm floor} & , \quad \text{(w/o support)} \\ \frac{5}{16}\, \mathcal{P}_{\rm floor} & , \quad \text{(with support)} \end{cases} \tag{471}$$

$$\mathcal{M}_{\rm floor} = \begin{cases} \frac{1}{4}\, \mathcal{P}_{\rm floor}\, w_{\rm floor} & , \quad \text{(w/o support)} \\ \frac{9}{256}\, \mathcal{P}_{\rm floor}\, w_{\rm floor} & , \quad \text{(with support)} \end{cases} \tag{472}$$

$$w_{\rm floor} = w_{\rm fb} + R_{\rm fuse} \tag{473}$$

$$A_{\rm floor} = \frac{2.0\, \mathcal{M}_{\rm floor}}{\sigma_{\rm floor}\, h_{\rm floor}} \; + \; \frac{1.5\, \mathcal{S}_{\rm floor}}{\tau_{\rm floor}} \tag{474}$$

$$\mathcal{V}_{\rm floor} = 2 w_{\rm floor}\, A_{\rm floor} \tag{475}$$

$$W_{\rm floor} = \rho_{\rm floor}\, g\, \mathcal{V}_{\rm floor} \; + \; 2\, w_{\rm floor}\, l_{\rm shell}\, W''_{\rm floor} \tag{476}$$

3.3.5 Tail cone

$$\mathcal{Q}_{\rm v} = \frac{L_{\rm v}\, b_{\rm v}}{3} \frac{1+2\lambda_{\rm v}}{1+\lambda_{\rm v}} \tag{477}$$

$$\mathcal{V}_{\rm cone} = \frac{\mathcal{Q}_{\rm v}}{\tau_{\rm cone}} \frac{\pi+2\theta_{\rm fb}}{\pi+2\theta_{\rm fb}+\sin 2\theta_{\rm fb}} \frac{x_{\rm conend}-x_{\rm shell\,2}}{R_{\rm fuse}} \frac{2}{1+\lambda_{\rm cone}} \tag{478}$$

$$W_{\rm cone} = \rho_{\rm fuse}\, g\, \mathcal{V}_{\rm cone} \tag{479}$$

3.3.6 Lumped tail weight and location

$$W_{\rm tail} = \begin{cases} W_{\rm htail} + W_{\rm vtail} + W_{\rm cone} + W_{\rm eng} & , \quad \text{fuse engines} \\ W_{\rm htail} + W_{\rm vtail} + W_{\rm cone} & , \quad \text{wing engines} \end{cases} \tag{480}$$

$$x_{\rm cone} = \tfrac{1}{2}(x_{\rm shell\,2}+x_{\rm conend}) \tag{481}$$

$$x_{\rm tail} = \begin{cases} \dfrac{x_{\rm htail}W_{\rm htail} + x_{\rm vtail}W_{\rm vtail} + x_{\rm cone}W_{\rm cone} + x_{\rm eng}W_{\rm eng}}{W_{\rm tail}} & , \quad \text{fuse engines} \\ \dfrac{x_{\rm htail}W_{\rm htail} + x_{\rm vtail}W_{\rm vtail} + x_{\rm cone}W_{\rm cone}}{W_{\rm tail}} & , \quad \text{wing engines} \end{cases} \tag{482}$$

3.3.7 Fuselage shell matching stress for bending

$$r_E = \frac{E_{\rm bend}}{E_{\rm skin}} \tag{483}$$

$$t_{\rm shell} = t_{\rm skin}\left(1 + r_E\, f_{\rm string}\frac{\rho_{\rm skin}}{\rho_{\rm bend}}\right) \tag{484}$$

$$\sigma_{\rm Mh} = \sigma_{\rm bend} - r_E\,\frac{\Delta p}{2}\,\frac{R_{\rm fuse}}{t_{\rm shell}} \tag{485}$$

$$\sigma_{\rm Mv} = \sigma_{\rm bend} - r_E\,\frac{\Delta p}{2}\,\frac{R_{\rm fuse}}{t_{\rm shell}} \tag{486}$$

Note: $\sigma_{\rm Mh}$ and $\sigma_{\rm Mv}$ are the same here, but could be different with more detailed structural models.

3.3.8 Horizontal-axis bending material

$$\begin{aligned} I_{\rm hshell} = {} & \Big[(\pi + 2\theta_{\rm fb}+\sin 2\theta_{\rm fb})\, R_{\rm fuse}^2 \\ & + 8\cos\theta_{\rm fb}\,(\Delta R_{\rm fuse}/2)\, R_{\rm fuse} \\ & + (2\pi+4\theta_{\rm fb})\,(\Delta R_{\rm fuse}/2)^2 \Big]\, R_{\rm fuse}\, t_{\rm shell} \\ & + \frac{2}{3}(h_{\rm fb} + \Delta R_{\rm fuse}/2)^3 t_{\rm fb} \end{aligned} \tag{487}$$

$$h_{\rm fuse} = R_{\rm fuse} + \frac{1}{2}\Delta R_{\rm fuse} \tag{488}$$

$$A_2 = \frac{1}{h_{\rm fuse}\,\sigma_{\rm Mh}}\,\frac{N(W_{\rm pay}+W_{\rm padd}+W_{\rm shell}+W_{\rm window}+W_{\rm insul}+W_{\rm floor})}{2\,l_{\rm shell}} \tag{489}$$

$$
\begin{aligned}
A_1 &= \frac{1}{h_{\text{fuse}}\,\sigma_{\text{Mh}}}\left(NW_{\text{tail}} + r_{\text{Mh}} L_{\text{h}_{\max}}\right) && (490)\\
A_0 &= -\frac{I_{\text{hshell}}}{r_E\, h_{\text{fuse}}^2} && (491)\\
\bar{A}_2 &= A_2 && (492)\\
\bar{A}_1 &= 2A_2\, x_{\text{shell}\,2} + A_1 && (493)\\
\bar{A}_0 &= A_2\, x_{\text{shell}\,2}^2 + A_1 x_{\text{tail}} + A_0 && (494)\\
x_{\text{hbend}} &= \frac{1}{2\bar{A}_2}\left[\bar{A}_1 - \sqrt{\bar{A}_1^2 - 4\bar{A}_0\bar{A}_2}\right] && (495)\\
x_f &= x_{\text{wing}} + \Delta x_{\text{wing}} + \tfrac{1}{2} c_o \bar{w} && (496)\\
x_b &= x_{\text{wing}} - \Delta x_{\text{wing}} + \tfrac{1}{2} c_o \bar{w} && (497)\\
\mathcal{V}_{\text{hbend}_f} &= A_2\,\frac{(x_{\text{shell}\,2} - x_f)^3 - (x_{\text{shell}\,2} - x_{\text{hbend}})^3}{3}\\
&+ A_1\,\frac{(x_{\text{tail}} - x_f)^2 - (x_{\text{tail}} - x_{\text{hbend}})^2}{2}\\
&+ A_0\,(x_{\text{hbend}} - x_f) && (498)\\
\mathcal{V}_{\text{hbend}_b} &= A_2\,\frac{(x_{\text{shell}\,2} - x_b)^3 - (x_{\text{shell}\,2} - x_{\text{hbend}})^3}{3}\\
&+ A_1\,\frac{(x_{\text{tail}} - x_b)^2 - (x_{\text{tail}} - x_{\text{hbend}})^2}{2}\\
&+ A_0\,(x_{\text{hbend}} - x_b) && (499)\\
\mathcal{V}_{\text{hbend}_c} &= \frac{1}{2}\left[A_{\text{hbend}(x_b)} + A_{\text{hbend}(x_f)}\right] c_o \bar{w} && (500)\\
\mathcal{V}_{\text{hbend}} &= \mathcal{V}_{\text{hbend}_f} + \mathcal{V}_{\text{hbend}_c} + \mathcal{V}_{\text{hbend}_b} && (501)\\
W_{\text{hbend}} &= \rho_{\text{fuse}}\, g \mathcal{V}_{\text{hbend}} && (502)
\end{aligned}
$$

3.3.9 Vertical-axis bending material

$$
\begin{aligned}
I_{\text{vshell}} &= \Big[\,(\pi + 2\theta_{\text{fb}} - \sin 2\theta_{\text{fb}})\, R_{\text{fuse}}^2\\
&\quad + 8\cos\theta_{\text{fb}}\, w_{\text{fb}}\, R_{\text{fuse}}\\
&\quad + (2\pi + 4\theta_{\text{fb}})\, w_{\text{fb}}^2\,\Big]\, R_{\text{fuse}}\, t_{\text{shell}} && (503)\\
w_{\text{fuse}} &= R_{\text{fuse}} + w_{\text{fb}} && (504)\\
B_1 &= \frac{r_{\text{Mv}} L_{\text{v}}}{w_{\text{fuse}}\,\sigma_{\text{Mv}}} && (505)\\
B_0 &= -\frac{I_{\text{vshell}}}{r_E\, w_{\text{fuse}}^2} && (506)\\
x_{\text{vbend}} &= x_{\text{tail}} + \frac{B_0}{B_1} && (507)\\
\mathcal{V}_{\text{vbend}_b} &= B_1\,\frac{(x_{\text{tail}} - x_b)^2 - (x_{\text{tail}} - x_{\text{vbend}})^2}{2} + B_0\,(x_{\text{vbend}} - x_b) && (508)\\
\mathcal{V}_{\text{vbend}_c} &= \frac{1}{2} A_{\text{vbend}(x_b)}\, c_o \bar{w} && (509)
\end{aligned}
$$

$$\mathcal{V}_{\text{vbend}} = \mathcal{V}_{\text{vbend}_c} + \mathcal{V}_{\text{vbend}_b} \tag{510}$$
$$W_{\text{vbend}} = \rho_{\text{fuse}}\, g \mathcal{V}_{\text{vbend}} \tag{511}$$

3.3.10 Total Fuselage Weight

$$W_{\text{padd}} = W_{\text{pay}}\, f_{\text{padd}} \tag{512}$$
$$W_{\text{fuse}} = W_{\text{padd}} + W_{\text{shell}} + W_{\text{window}} + W_{\text{insul}} + W_{\text{floor}} + W_{\text{cone}} + W_{\text{hbend}} + W_{\text{vbend}} \tag{513}$$

3.4 Wing Sizing and Weight (Design only)

3.4.1 Wing Planform Sizing (at start-of-cruise point)

$$\rho_{\text{cabin}(h_c)} = \frac{1}{RT_{\text{cabin}}} \max\left(\, p_{\text{cabin}} \,,\, p_{0(h_c)} \,\right) \tag{514}$$
$$W_{\text{buoy}} = \left(\rho_{\text{cabin}} - \rho_{0(h_c)}\right) g\, \mathcal{V}_{\text{cabin}} \tag{515}$$
$$\bar{W}_c = W_c + W_{\text{buoy}} \tag{516}$$
$$V_c = M_{\text{CR}}\, a_{0(h_c)} \tag{517}$$
$$S = \frac{\bar{W}_c}{\frac{1}{2}\rho V_c^2\, C_{L_c}} \tag{518}$$
$$b = \sqrt{S\, AR} \tag{519}$$
$$c_o = \frac{S}{b} \frac{2}{2\eta_o + (1+\lambda_s)(\eta_s - \eta_o) + (\lambda_s+\lambda)(1-\eta_s)} \tag{520}$$
$$c_s = c_o\, \lambda_s \tag{521}$$

3.4.2 Exposed Wing Area and Wing-Centroid Offset

$$S_{\text{wing}} = c_o \frac{b}{2} \left[(1+\lambda_s)(\eta_s - \eta_o) + (\lambda_s+\lambda)(1-\eta_s)\right] \tag{522}$$
$$\Delta x_{\text{wing}} = \frac{1}{S}\, c_o \frac{b^2}{12} \tan\Lambda \left[(1+2\lambda_s)(\eta_s-\eta_o)^2 + (\lambda_s+2\lambda)(1-\eta_s)^2 + 3(\lambda_s+\lambda)(1-\eta_s)(\eta_s-\eta_o)\right] \tag{523}$$

3.4.3 Wing Root Loading

$$W_{\text{center}} = \begin{cases} W_{\text{pay}} + W_{\text{fuse}} + W_{\text{htail}} + W_{\text{vtail}} + \frac{1}{2} W_{\text{strut}} + W_{\text{totadd}} + W_{\text{eng}} & , \quad \text{fuse engines} \\ W_{\text{pay}} + W_{\text{fuse}} + W_{\text{htail}} + W_{\text{vtail}} + \frac{1}{2} W_{\text{strut}} + W_{\text{totadd}} & , \quad \text{wing engines} \end{cases} \tag{524}$$
$$\eta_o = \frac{b_o}{b} \tag{525}$$
$$\eta_s = \frac{b_s}{b} \tag{526}$$
$$C = 2\eta_o + (1+\lambda_s)(\eta_s - \eta_o) + (\lambda_s+\lambda)(1-\eta_s) \tag{527}$$

$$K_o = \frac{2}{AR\,C} \tag{528}$$

$$p_o = \frac{2}{b}\,\frac{N\,W_{\rm center} - L_{\rm htail}}{C + 2(f_{Ln}+f_{Lo})\eta_o + 4 f_{L_t} K_o \lambda^2} \tag{529}$$

$$p_s = p_o\,\lambda_s \tag{530}$$

3.4.4 Outer Surface (Wing or Tail) Structural Sizing

All the relations below apply to either the wing or a tail surface.

$$\bar{h}_{\rm rms} = \bar{h}\left[\,1 - \frac{2}{3}(1-r_h) + \frac{1}{5}(1-r_h)^2\,\right]^{1/2} \tag{531}$$

$$\mathcal{S}_s = \frac{p_o\,b}{4}\,(\lambda_s+\lambda)(1-\eta_s) \tag{532}$$

$$\mathcal{M}_s = \frac{p_o\,b^2}{24}\,(\lambda_s+2\lambda)(1-\eta_s)^2 \tag{533}$$

$$\bar{t}_{\rm web_s} = \frac{\mathcal{S}_s}{c_s^2\,\tau_{\rm web}}\,\frac{1}{2\,r_h\,\bar{h}}\,\frac{1}{\cos^2\Lambda} \tag{534}$$

$$\bar{h}_{\rm rms}^3 - (\bar{h}_{\rm rms} - 2\bar{t}_{\rm cap})^3 \equiv C = \frac{\mathcal{M}_s}{c_s^3\,\sigma_{\rm cap}}\,\frac{6\bar{h}}{\bar{w}}\,\frac{1}{\cos^4\Lambda} \tag{535}$$

$$\bar{t}_{\rm cap_s} = \frac{1}{2}\left(\bar{h}_{\rm rms} - \left(\bar{h}_{\rm rms}^3 - C\right)^{1/3}\right) \tag{536}$$

$$\bar{A}_{\rm cap_s} = 2\,\bar{t}_{\rm cap_s}\,\bar{w} \tag{537}$$

$$\bar{A}_{\rm web_s} = 2\,\bar{t}_{\rm web_s}\,r_h\,\bar{h} \tag{538}$$

3.4.5 Strut and Strut-Attach Location Loads

Cantilever wing case, no engine

In this case, there is no inner panel, with $\eta_o = \eta_s$. So $()_o = ()_s$ for all quantities.

$$\mathcal{R} = 0 \tag{539}$$

$$\mathcal{T} = 0 \tag{540}$$

$$\mathcal{P} = 0 \tag{541}$$

$$\mathcal{S}_o = \mathcal{S}_s \tag{542}$$

$$\mathcal{M}_o = \mathcal{M}_s \tag{543}$$

Cantilever wing case, with engine

In this case, the single engine weight provide the applied load $\mathcal{R}$, with no strut or compression loads present.

$$\mathcal{R} = N\,W_{\rm eng}/n_{\rm eng} \tag{544}$$

$$\mathcal{T} = 0 \tag{545}$$

$$\mathcal{P} = 0 \tag{546}$$

$$\mathcal{S}_o = \max\left\{\,\mathcal{S}_s\;,\;\mathcal{S}_s - \mathcal{R} + \frac{p_o\,b}{4}\,(1+\lambda_s)(\eta_s-\eta_o)\right\} \tag{547}$$

$$\mathcal{M}_o \;=\; \max\left\{ \mathcal{M}_s \;,\; \mathcal{M}_s \,+\, (\mathcal{S}_s - \mathcal{R})\frac{b}{2}\,(1{+}\lambda_s)(\eta_s{-}\eta_o) \,+\, \frac{p_o\,b^2}{24}\,(1{+}2\lambda_s)(\eta_s{-}\eta_o)^2 \right\} \quad (548)$$

The shear and moment limiting is to prevent negatively-tapered structure, which is not realistic for the download requirement.

Strut-braced wing case

In this case, the strut load is assumed to be such that $\mathcal{M}_o{=}\mathcal{M}_s$. For sizing the root web, $\mathcal{S}_o{=}\mathcal{S}_s$ is also assumed.

$$\mathcal{R} \;=\; \frac{p_o\,b}{12}\,(1{+}2\lambda_s)(\eta_s{-}\eta_o) \,+\, \mathcal{S}_s \quad (549)$$

$$\ell_s \;=\; \sqrt{z_s^2 \,+\, \frac{b^2}{4}(\eta_s{-}\eta_o)^2} \quad (550)$$

$$\mathcal{T} \;=\; \mathcal{R}\,\frac{\ell_s}{z_s} \quad (551)$$

$$\mathcal{P} \;=\; \mathcal{R}\,\frac{b/2}{z_s}(\eta_s{-}\eta_o) \quad (552)$$

$$\ell_{s_\perp} \;=\; \sqrt{z_s^2 \,+\, \frac{b^2}{4}\frac{(\eta_s{-}\eta_o)^2}{\cos^2\Lambda}} \quad (553)$$

$$\mathcal{T}_\perp \;=\; \mathcal{T}\,\frac{\ell_{s_\perp}}{\ell_s} \quad (554)$$

$$\mathcal{S}_o \;=\; \mathcal{S}_s \quad (555)$$

$$\mathcal{M}_o \;=\; \mathcal{M}_s \quad (556)$$

3.4.6 Inner Surface (Wing or Tail) Structural Sizing

$$\bar{t}_{\mathrm{web}_o} \;=\; \frac{\mathcal{S}_o}{c_o^2\,\tau_{\mathrm{web}}}\,\frac{1}{2\,r_h\,\bar{h}}\,\frac{1}{\cos^2\Lambda} \quad (557)$$

$$\bar{h}_{\mathrm{rms}}^3 - (\bar{h}_{\mathrm{rms}}{-}2\bar{t}_{\mathrm{cap}})^3 \;\equiv\; C \;=\; \frac{\mathcal{M}_o}{c_o^3\,\sigma_{\mathrm{cap}}}\,\frac{6\bar{h}}{\bar{w}}\,\frac{1}{\cos^4\Lambda} \quad (558)$$

$$\bar{t}_{\mathrm{cap}_o} \;=\; \frac{1}{2}\left(\bar{h}_{\mathrm{rms}} \,-\, \left(\bar{h}_{\mathrm{rms}}^3 - C\right)^{1/3}\right) \quad (559)$$

$$\bar{A}_{\mathrm{cap}_o} \;=\; 2\,\bar{t}_{\mathrm{cap}_o}\,\bar{w} \quad (560)$$

$$\bar{A}_{\mathrm{web}_o} \;=\; 2\,\bar{t}_{\mathrm{web}_o}\,r_h\,\bar{h} \quad (561)$$

3.4.7 Total Wing or Tail Surface Weight

$$\mathcal{V}_{\mathrm{cen}} \;=\; c_o^2\,b\,\eta_o \quad (562)$$

$$\mathcal{V}_{\mathrm{inn}} \;=\; c_o^2\,b\,\tfrac{1}{3}(1+\lambda_s{+}\lambda_s^2)(\eta_s{-}\eta_o)\,\cos\Lambda \quad (563)$$

$$\mathcal{V}_{\mathrm{out}} \;=\; c_o^2\,b\,\tfrac{1}{3}(\lambda_s^2+\lambda_s\lambda+\lambda^2)(1-\eta_s)\,\cos\Lambda \quad (564)$$

$$W_{\mathrm{cap}} \;=\; \rho_{\mathrm{cap}}\,g\left[\bar{A}_{\mathrm{cap}_o}\mathcal{V}_{\mathrm{cen}} \,+\, \tfrac{1}{2}\Big(\bar{A}_{\mathrm{cap}_o}{+}\bar{A}_{\mathrm{cap}_s}\Big)\mathcal{V}_{\mathrm{inn}} \,+\, \bar{A}_{\mathrm{cap}_s}\mathcal{V}_{\mathrm{out}}\right] \quad (565)$$

$$W_{\mathrm{web}} \;=\; \rho_{\mathrm{web}}\,g\left[\bar{A}_{\mathrm{web}_o}\mathcal{V}_{\mathrm{cen}} \,+\, \tfrac{1}{2}\Big(\bar{A}_{\mathrm{web}_o}{+}\bar{A}_{\mathrm{web}_s}\Big)\mathcal{V}_{\mathrm{inn}} \,+\, \bar{A}_{\mathrm{web}_s}\mathcal{V}_{\mathrm{out}}\right] \quad (566)$$

$$W_{\mathrm{wing}} \;=\; (W_{\mathrm{cap}} + W_{\mathrm{web}})(1{+}f_{\mathrm{wadd}}) \quad (567)$$

3.4.8 Strut Weight

$$W_{\text{strut}} \;=\; \rho_{\text{strut}}\, g A_{\text{strut}}\, 2\ell_{s_\perp} \tag{568}$$

3.5 Max-Fuel Weight (Design only)

$$\bar{h}_{\text{avg}} \;=\; \bar{h}\left[\,1-\frac{1}{3}(1-r_h)\,\right] \tag{569}$$

$$\bar{A}_{\text{fuel}} \;=\; \frac{A_{\text{fuel}}}{c_\perp^2} \;=\; (\bar{w}-2\bar{t}_{\text{web}})(\bar{h}_{\text{avg}}-2\bar{t}_{\text{cap}}) \tag{570}$$

$$(W_{\text{fuel}})_{\max} \;=\; \rho_{\text{fuel}}\, g\left[\bar{A}_{\text{fuel}_o}\mathcal{V}_{\text{cen}} \;+\; \tfrac{1}{2}\Big(\bar{A}_{\text{fuel}_o}+\bar{A}_{\text{fuel}_s}\Big)\mathcal{V}_{\text{inn}} \;+\; \bar{A}_{\text{fuel}_s}\mathcal{V}_{\text{out}}\right] \tag{571}$$

3.6 Horizontal and Vertical Tail Sizing and Weight (Design only)

$$l_{\text{h}} \;=\; x_{\text{htail}} \;-\; x_{\text{wing}} \tag{572}$$

$$l_{\text{v}} \;=\; x_{\text{vtail}} \;-\; x_{\text{wing}} \tag{573}$$

$$c_{\text{mac}} \;=\; \frac{c_o^2\, b}{S}\left[\,\eta_o \;+\; \tfrac{1}{3}(1+\lambda_s+\lambda_s^2)(\eta_s-\eta_o) \;+\; \tfrac{1}{3}(\lambda_s^2+\lambda_s\lambda+\lambda^2)(1-\eta_s)\right] \tag{574}$$

$$S_{\text{h}} \;=\; V_{\text{h}}\, S\, \frac{c_{\text{mac}}}{l_{\text{h}}} \tag{575}$$

$$b_{\text{h}} \;=\; \sqrt{S_{\text{h}}\, AR_{\text{h}}} \tag{576}$$

$$c_{o_{\text{h}}} \;=\; \frac{S_{\text{h}}}{b_{\text{h}}(1+\lambda_{\text{h}})/2} \tag{577}$$

$$S_{\text{v}} \;=\; V_{\text{v}}\, S\, \frac{b}{l_{\text{v}}} \tag{578}$$

$$b_{\text{v}} \;=\; \sqrt{S_{\text{v}}\, AR_{\text{v}}} \tag{579}$$

$$c_{o_{\text{v}}} \;=\; \frac{S_{\text{v}}}{b_{\text{v}}(1+\lambda_{\text{v}})/2} \tag{580}$$

3.6.1 Horizontal tail sizing and wing positioning (Design only)

$$\frac{\partial \mathcal{R}_M}{\partial S_{\text{h}}} \;=\; -\frac{\partial W}{W^2}\frac{W_{\text{htail}}}{S_{\text{h}}} \;+\; \frac{1}{C_L}\left[-(c_o C_{M_1}-x_{\text{wbox}})\frac{C_{L_{\text{h}}}}{S} + \frac{c_{o\text{h}}}{S} + (c_{o\text{h}} C_{M_1}-x_{\text{hbox}})\frac{C_{L_{\text{h}}}}{S}\right] \tag{581}$$

$$\frac{\partial \mathcal{R}_M}{\partial x_{\text{wbox}}} \;=\; \frac{1}{W}\left[r_{\text{fuel}}W_{\text{fuel}} + W_{\text{wing}} + W_{\text{strut}} + W_{\text{lgmain}}\right] \;-\; \frac{1}{C_L}\left[C_L - C_{L_{\text{h}}}\frac{S_{\text{h}}}{S}\right] \tag{582}$$

$$\frac{\partial \mathcal{R}_S}{\partial S_{\text{h}}} \;=\; -\frac{\partial W}{W^2}\frac{W_{\text{htail}}}{S_{\text{h}}} \;-\; (c_o\, C_{M\text{w}_1} - x_{\text{wbox}})\frac{1}{S}\frac{\partial C_{L_{\text{h}}}}{\partial C_L} \;+\; (c_{o\text{h}}\, C_{M\text{h}_1} - x_{\text{hbox}})\frac{1}{S}\frac{\partial C_{L_{\text{h}}}}{\partial C_L} \tag{583}$$

$$\frac{\partial \mathcal{R}_S}{\partial x_{\text{wbox}}} \;=\; \frac{1}{W}\left[r_{\text{fuel}}W_{\text{fuel}} + W_{\text{wing}} + W_{\text{strut}} + W_{\text{lgmain}}\right] \;-\; \left(1 - \frac{S_{\text{h}}}{S}\frac{\partial C_{L_{\text{h}}}}{\partial C_L}\right) \tag{584}$$

3.6.2 Horizontal tail trim (off-design only)

$$\frac{\partial \mathcal{R}_M}{\partial C_{L_\mathrm{h}}} = \frac{1}{C_L}\left[-(c_o C_{M_1} - x_{\mathrm{wbox}})\frac{S_\mathrm{h}}{S} + (c_{o\mathrm{h}} C_{M\mathrm{h}_1} - x_{\mathrm{hbox}})\frac{S_\mathrm{h}}{S}\right] \tag{585}$$

$$(C_{L_\mathrm{h}})_{\mathrm{new}} = C_{L_\mathrm{h}} - \frac{\mathcal{R}_M}{\partial \mathcal{R}_M / \partial C_{L_\mathrm{h}}} \tag{586}$$

3.6.3 Horizontal and Vertical Tail Loading

$$L_{\mathrm{h}_{\mathrm{max}}} = q_{NE} S_\mathrm{h} C_{L_\mathrm{h}} \tag{587}$$

$$L_{\mathrm{v}_{\mathrm{max}}} = q_{NE} S_\mathrm{v} C_{L_\mathrm{v}} \tag{588}$$

$$p_{o_\mathrm{h}} = \frac{L_{\mathrm{h}_{\mathrm{max}}}}{b_\mathrm{h}} \frac{2}{1+\lambda_\mathrm{h}} \tag{589}$$

$$p_{o_\mathrm{v}} = \frac{L_{\mathrm{v}_{\mathrm{max}}}}{b_\mathrm{v}} \frac{2}{1+\lambda_\mathrm{v}} \tag{590}$$

The max vertical tail lift $L_{\mathrm{v}_{\mathrm{max}}}$ is also used for sizing the tailcone and fuselage added bending material in the next iteration.

3.6.4 Horizontal Tail Structural Sizing and Weight

The horizontal-tail structural sizing and weight calculations are the same as for the wing, starting at (121), ultimately giving W_{htail}.

3.6.5 Vertical Tail Structural Sizing and Weight

The vertical-tail structural sizing and weight calculations are the same as for the wing and the horizontal tail, except that a real+image symmetrical vertical tail is first assumed by doubling the real vertical-tail span, area, and aspect ratio.

$$\hat{b}_{o_\mathrm{v}} = 2 b_{o_\mathrm{v}} \tag{591}$$

$$\hat{b}_\mathrm{v} = 2 b_\mathrm{v} \tag{592}$$

$$\hat{S}_\mathrm{v} = 2 S_\mathrm{v} \tag{593}$$

$$\hat{AR}_\mathrm{v} = 2 AR_\mathrm{v} \tag{594}$$

These are then used in the structural sizing and weight calculations, starting at (121). The resulting weight $\hat{W}_\mathrm{v}$ is then halved to give the weight of the single real vertical tail.

$$W_{\mathrm{vtail}} = \hat{W}_\mathrm{v}/2 \tag{595}$$

3.7 First-Iteration Total Max Takeoff Weight (Design only)

To allow performing aerodynamic and weight-burn calculations on the first iteration, an interim total weight is now computed using the sub-component weights defined above. The

estimated weight fractions for the engines, fuel, and of course the total-proportional fraction are also accounted for in the denominator.

$$W_{\text{MTO}} = \frac{W_{\text{fix}} + W_{\text{pay}} + W_{\text{fuse}} + W_{\text{wing}} + W_{\text{strut}} + W_{\text{htail}} + W_{\text{vtail}}}{1 - f_{\text{eng}} - f_{\text{fuel}} - f_{\text{apu}} - f_{\text{hpesys}} - f_{\text{lgnose}} - f_{\text{lgmain}}} \tag{596}$$

$$W_{\text{eng}} = W_{\text{MTO}}\, f_{\text{eng}} \tag{597}$$

$$W_{\text{fuel}} = W_{\text{MTO}}\, f_{\text{fuel}} \tag{598}$$

$$W_{\text{apu}} = W_{\text{MTO}}\, f_{\text{apu}} \tag{599}$$

$$W_{\text{hpesys}} = W_{\text{MTO}}\, f_{\text{hpesys}} \tag{600}$$

$$W_{\text{lgnose}} = W_{\text{MTO}}\, f_{\text{lgnose}} \tag{601}$$

$$W_{\text{lgmain}} = W_{\text{MTO}}\, f_{\text{lgmain}} \tag{602}$$

For the second and subsequent iterations, a similar but different weight update formula is used, as will be derived shortly.

3.8 Drag (Dissipation) Build-Up

3.8.1 Induced drag

$$C_{D_i} = \frac{C_L^2}{\pi\, AR\, e} \tag{603}$$

Any trim drag penalty is assumed to be included in the specified span efficiency e.

3.8.2 Fuselage profile drag

The wake-endpoint momentum area Θ_{wake} and trailing-edge kinetic energy area Θ^*_{TE} in the absence of BLI are obtained from the axisymmetric boundary layer solution.

$$\Theta_{\text{wake}} = \mathcal{F}(M_\infty, Re_\ell\,;\, A_{(x)}, b_{0(x)}) \tag{604}$$

$$\Theta^*_{TE} = \mathcal{F}(M_\infty, Re_\ell\,;\, A_{(x)}, b_{0(x)}) \tag{605}$$

The fuselage dissipation drag coefficient is then calculated as follows for any fuselage viscous defect ingestion fraction $f_{\text{BLI f}}$.

$$C_{\Phi_{\text{surf}}} = \frac{\Theta^*_{TE}}{S} \tag{606}$$

$$C_{\Phi_{\text{wake}}} = \frac{2\Theta_{\text{wake}}}{S} - \frac{\Theta^*_{TE}}{S} \tag{607}$$

$$C'_{D_{\text{fuse}}} = C_{\Phi_{\text{surf}}} + C_{\Phi_{\text{wake}}}(1 - f_{\text{BLI f}}) \tag{608}$$

3.8.3 Wing profile drag

The 2D-airfoil database giving the friction and profile drag coefficients as functions of the wing-normal lift coefficient, Mach number, and airfoil thickness/chord ratio.

$$c_{\ell_\perp} = C_L / \cos^2\Lambda \tag{609}$$

$$
\begin{aligned}
M_\perp &= M\,\cos\Lambda && (610)\\
\tau &= \bar{h} && (611)\\
\bar{c}_{d_f} &= \bar{c}_{d_f}(c_{\ell_\perp}, M_\perp, \tau) && (612)\\
\bar{c}_{d_p} &= \bar{c}_{d_p}(c_{\ell_\perp}, M_\perp, \tau) && (613)
\end{aligned}
$$

These are applied using infinite swept-wing relations, with the shock unsweep factor included.

$$
\begin{aligned}
f_{\text{Suns}} &= \frac{k_{\text{Suns}} c_o^2}{S_{\text{wing}}/2} && (614)\\
c_{d_o} &= \left\{\bar{c}_{d_f} \;+\; \bar{c}_{d_p}\left[f_{\text{Suns}} \;+\; (1-f_{\text{Suns}})\cos^2\Lambda\right]\cos\Lambda\right\}\left(\frac{Re_{c_o}}{Re_{\text{ref}}}\right)^{a_{Re}} && (615)\\
K_s &= \begin{cases} \dfrac{2}{2+a_{Re}}\dfrac{1-\lambda_s^{2+a_{Re}}}{1-\lambda_s^2} & , \quad |1-\lambda_s| > 0.02 \\ 1 \;-\; a_{Re}\,\dfrac{1-\lambda_s}{1+\lambda_s} & , \quad |1-\lambda_s| < 0.02 \end{cases} && (616)\\
K &= \begin{cases} \dfrac{2}{2+a_{Re}}\dfrac{\lambda_s^{2+a_{Re}}-\lambda^{2+a_{Re}}}{\lambda_s^2-\lambda^2} & , \quad |\lambda_s-\lambda| > 0.02 \\ 1 \;-\; a_{Re}\,\dfrac{\lambda_s-\lambda}{\lambda_s+\lambda} & , \quad |\lambda_s-\lambda| < 0.02 \end{cases} && (617)\\
C_{D_{\text{wing}}} &= \frac{c_o\, b/2}{S}\, c_{d_o}\left[(1+\lambda_s)(\eta_s-\eta_o)K_s \;+\; (\lambda_s+\lambda)(1-\eta_s)K\right] \qquad \text{(without BLI)} && (618)
\end{aligned}
$$

Any BLI on the wing is accounted for via the ingestion fraction $f_{\text{BLI w}}$.

$$
\begin{aligned}
r_{\Phi_{\text{wake}}} &= 0.15 && (619)\\
C_{\Phi_{\text{wake}}} &= r_{\Phi_{\text{wake}}}\, C_{D_{\text{wing}}} && (620)\\
C'_{D_{\text{wing}}} &= C_{D_{\text{wing}}} \;-\; C_{\Phi_{\text{wake}}} f_{\text{BLI w}} && (621)
\end{aligned}
$$

3.8.4 Tail profile drag

The dissipation drag of the horizontal and vertical tails is obtained the same way as for the wing, with zero BLI assumed. The 2D friction and pressure drag coefficients c_{d_f} and c_{d_p} are specified directly.

3.8.5 Strut profile drag

$$
\begin{aligned}
k_A &= 0.65 && (622)\\
c_{\text{strut}} &= \sqrt{\frac{A_{\text{strut}}}{k_A\,\bar{h}_{\text{strut}}}} && (623)\\
S_{\text{strut}} &= 2 c_{\text{strut}}\,\ell_{s_\perp} && (624)\\
\cos\Lambda_s &= \frac{\ell_s}{\ell_{s_\perp}} && (625)\\
C_{D_{\text{strut}}} &= \frac{S_{\text{strut}}}{S}\left(c_{d_f} \;+\; c_{d_p}\cos^3\Lambda_s\right) r_{V_{\text{strut}}}^3 && (626)
\end{aligned}
$$

3.8.6 Engine nacelle profile drag

$$\frac{V_{\mathrm{n}_{LE}}}{V_\infty} = \max\left(2r_{V_{\mathrm{nace}}} - \frac{M_2}{M_\infty}\ ,\ 0\right) \tag{627}$$

$$r^3_{V_{\mathrm{nsurf}}} = \frac{1}{4}\left[\frac{V_{\mathrm{n}_{LE}}}{V_\infty} + r_{V_{\mathrm{nace}}}\right]\left[\left(\frac{V_{\mathrm{n}_{LE}}}{V_\infty}\right)^2 + r^2_{V_{\mathrm{nace}}}\right] \tag{628}$$

$$C_{D_{\mathrm{nace}}} = f_{\mathrm{Snace}}\, C_{f_{\mathrm{wet}}}\, r^3_{V_{\mathrm{nsurf}}} \tag{629}$$

3.8.7 Total drag

$$C'_D = C_{D_i} + C'_{D_{\mathrm{fuse}}} + C'_{D_{\mathrm{wing}}} + C_{D_{\mathrm{tail}}} + C_{D_{\mathrm{strut}}} + C_{D_{\mathrm{nace}}} \equiv \mathcal{F}_{\mathrm{aero}}(C_L, M_\infty \ldots) \tag{630}$$

3.9 Engine Sizing and Weight (Design only)

3.9.1 Engine sizing

$$F'_e = \frac{\bar{W}_c}{n_{\mathrm{eng}}}\left(\frac{C'_D}{C_L} + \gamma_{\mathrm{CR}}\right)_c \tag{631}$$

$$\{A_2, A_{5\ldots}\} = \mathcal{F}_{\mathrm{eng}_1}(F'_e, T_{t_4}, OPR_{\mathrm{D}}, BPR_{\mathrm{D}\ldots}\,;\, M_\infty, p_\infty, T_\infty, K_{\mathrm{inl}\ldots}) \tag{632}$$

$$d_{\mathrm{f}} = \sqrt{\frac{4A_2}{\pi(1 - HTR^2_{\mathrm{f}})}} \tag{633}$$

3.9.2 Engine weight

$$W_{\mathrm{ebare}} = n_{\mathrm{eng}}\, W_{e_1}\,(\dot{m}, OPR_{\mathrm{D}}, BPR_{\mathrm{D}}) \tag{634}$$

$$W_{\mathrm{eadd}} = W_{\mathrm{ebare}}\, f_{\mathrm{eadd}} \tag{635}$$

$$S_{\mathrm{nace}_1} = r_{\mathrm{Snace}}\,\frac{\pi}{4}\,d^2_{\mathrm{f}} \tag{636}$$

$$W_{\mathrm{nace}} = n_{\mathrm{eng}}\, W_{n_1}\,(d_{\mathrm{f}}, S_{\mathrm{nace}_1}) \tag{637}$$

$$W_{\mathrm{pylon}} = (W_{\mathrm{ebare}} + W_{\mathrm{eadd}} + W_{\mathrm{nace}})\ f_{\mathrm{pylon}} \tag{638}$$

$$W_{\mathrm{eng}} = W_{\mathrm{ebare}} + W_{\mathrm{eadd}} + W_{\mathrm{nace}} + W_{\mathrm{pylon}} \tag{639}$$

$$f_{\mathrm{eng}} = \frac{W_{\mathrm{eng}}}{W_{\mathrm{MTO}}} \tag{640}$$

3.9.3 Nacelle wetted area fraction and skin friction coefficient

$$S_{\mathrm{nace}} = n_{\mathrm{eng}}\, S_{\mathrm{nace}_1} \tag{641}$$

$$f_{\mathrm{Snace}} = \frac{S_{\mathrm{nace}}}{S} \tag{642}$$

$$\ell_{\mathrm{nace}} = 0.15\, r_{\mathrm{Snace}}\, d_{\mathrm{f}} \tag{643}$$

$$Re_{\mathrm{nace}} = \frac{\rho_\infty V_\infty \ell_{\mathrm{nace}}}{\mu_\infty} \tag{644}$$

$$C_{f_{\mathrm{wet}}} = C_f\,(Re_{\mathrm{nace}}) \tag{645}$$

3.10 Specific Fuel Consumption

3.10.1 Engine performance

The turbofan model calculations give the $TSFC'$ from either a specified T_{t4}, or a specified thrust F'_e, or both.

$$TSFC' = \mathcal{F}_{\text{eng}_1}(T_{t_4}, F'_e \ldots) \quad \text{(cruise)} \tag{646}$$
$$TSFC' = \mathcal{F}_{\text{eng}_2}(T_{t_4} \ldots) \quad \text{(climb)} \tag{647}$$
$$TSFC' = \mathcal{F}_{\text{eng}_3}(F'_e \ldots) \quad \text{(descent)} \tag{648}$$

One of these functions is evaluated at each integration point over the mission.

3.10.2 Climb trajectory integration

The integration is performed over n discrete points which are uniformly spaced from takeoff altitude h_b start of cruise altitude h_c. The prescribed altitudes and corresponding atmospheric properties are calculated as follows.

$$h_i = h_b \frac{n-i}{n-1} + h_c \frac{i-1}{n-1} \tag{649}$$
$$\rho_i = \rho_{\text{atm}(h_i)} \tag{650}$$
$$p_i = p_{\text{atm}(h_i)} \tag{651}$$
$$a_i = a_{\text{atm}(h_i)} \tag{652}$$

A predictor-corrector scheme is used for the integration of equations (431) and (432), with the differentials dR and $d(\ln W)$ replaced by simple differences. For each point i along the trajectory, the effective drag coefficient C'_D and thrust F' are computed by calling the routines implementing the procedures outlined above. These calculations require as inputs the velocity V_i obtained from the specified $(C_L)_i$ and the current weight W_i.

$$\rho_{\text{cabin}(h_i)} = \frac{1}{RT_{\text{cabin}}} \max\left(p_{\text{cabin}}\ ,\ p_i\right) \tag{653}$$
$$W_{\text{buoy}_i} = (\rho_{\text{cabin}} - \rho_i)\, g\, \mathcal{V}_{\text{cabin}} \tag{654}$$
$$\bar{W}_i = W_i + W_{\text{buoy}_i} \tag{655}$$
$$V_i = \sqrt{\frac{2\bar{W}_i \cos\gamma_i}{\rho_i S (C_L)_i}} \tag{656}$$
$$M_i = \frac{V_i}{a_i} \tag{657}$$
$$(C'_D)_i = \mathcal{F}_{\text{aero}}((C_L)_i, M_i \ldots) \tag{658}$$
$$\{F'_i, TSFC'_i\} = \mathcal{F}_{\text{eng}_2}(T_{t4_i}, V_i \ldots) \tag{659}$$

Iteration for the flight path angle γ_i is performed during the corrector step described shortly, using equation (430).

The predicted range increment ΔR^* and predicted next weight W^*_{i+1} are next computed using forward Euler integration.

$$V^*_{i+1} = \sqrt{\frac{2\bar{W}_i \cos\gamma_i}{\rho_{i+1} S C_{L_{i+1}}}} \tag{660}$$

$$\Delta R^* = \left(h_{i+1} - h_i + \frac{(V^*_{i+1})^2 - V_i^2}{2g}\right)\left(\frac{F'}{\bar{W}}\frac{1}{\cos\gamma} - \frac{C'_D}{C_L}\right)^{-1}_i \tag{661}$$

$$\frac{W^*_{i+1}}{W_i} = \exp\left\{-\left(\frac{F'}{W}\frac{TSFC'}{V\cos\gamma}\right)_i \Delta R^*\right\} \tag{662}$$

The predicted weight W^*_{i+1} is then used to compute predicted integrands at point i+1, and the corrector integration step is then performed using the predictor-approximated trapezoidal integration. The range and time are also integrated.

$$\Delta R = \left(h_{i+1} - h_i + \frac{V^2_{i+1} - V_i^2}{2g}\right)\frac{1}{2}\left[\left(\frac{F'}{\bar{W}}\frac{1}{\cos\gamma} - \frac{C'_D}{C_L}\right)^{-1}_i + \left(\frac{F'}{\bar{W}}\frac{1}{\cos\gamma} - \frac{C'_D}{C_L}\right)^{-1}_{i+1}\right] \tag{663}$$

$$R_{i+1} = R_i + \Delta R \tag{664}$$

$$t_{i+1} = t_i + \frac{1}{2}\left[\frac{1}{V_i\cos\gamma_i} + \frac{1}{V_{i+1}\cos\gamma_{i+1}}\right]\Delta R \tag{665}$$

$$\frac{W_{i+1}}{W_i} = \exp\left\{-\frac{1}{2}\left[\left(\frac{F'}{W}\frac{TSFC'}{V\cos\gamma}\right)_i + \left(\frac{F'}{W}\frac{TSFC'}{V\cos\gamma}\right)_{i+1}\right]\Delta R\right\} \tag{666}$$

The integration then repeats for the next point i along the climb trajectory.

3.10.3 Cruise and Descent Angles, Distances

$$\gamma_{\text{CR}} = \left(\frac{C'_D}{C_L}\frac{p\,TSFC'}{\rho g V - p\,TSFC'}\right)_c \tag{667}$$

$$R_d = R_c + \frac{h_e - h_c - \gamma_{\text{DE}}(R_{\text{total}} - R_c)}{\gamma_{\text{CR}} - \gamma_{\text{DE}}} \tag{668}$$

$$h_d = h_c + \gamma_{\text{CR}}(R_d - R_c) \tag{669}$$

3.10.4 End-of-Cruise weight, time

$$\frac{W_d}{W_c} = \exp\left[-\frac{F'}{W}\frac{TSFC'}{V}(R_d - R_c)\right]_c \tag{670}$$

$$t_d = t_c + \frac{R_d - R_c}{V} \tag{671}$$

3.10.5 End-of-Descent weight, time

The descent integration proceeds in the same way as the climb, but with the prescribed angle γ_{DE}. The engine calculation is performed for the implied required thrust.

$$F'_{e_i} = \frac{\bar{W}_i}{n_{\text{eng}}}\left(\sin\gamma_{\text{DE}} + \frac{C'_D}{C_L}\cos\gamma_{\text{DE}}\right)_i \tag{672}$$

$$\{T_{t_{4_i}}\,;\, TSFC'_i, OPR_i, BPR_{i\cdots}\} = \mathcal{F}_{\text{eng}_3}(F'_{e_i}, A_2, A_{5\cdots}\,;\, M_i, p_i, T_i, K_{\text{inl}_i\cdots}) \tag{673}$$

The end result of the integration is the final mission weight and flight time.

$$\rightarrow \quad W_e \tag{674}$$
$$\rightarrow \quad t_e \tag{675}$$

3.11 Mission fuel

From the final landing weight W_e, the fuel burn and takeoff fuel weight can then be obtained.

$$W_{\text{burn}} = W_b - W_e \tag{676}$$
$$W_{\text{fuel}} = W_{\text{burn}}\,(1+f_{\text{reserve}}) \tag{677}$$
$$f_{\text{fuel}} = \frac{W_{\text{fuel}}}{W_{\text{MTO}}} \tag{678}$$

3.12 Overall Weight Iteration (Design)

$$\begin{aligned}(W_{\text{MTO}})_{\text{new}} = {} & W_{\text{fix}} + W_{\text{pay}} + W_{\text{padd}} + W_{\text{shell}} \\ & + W_{\text{window}} + W_{\text{insul}} + W_{\text{floor}} + W_{\text{hbend}} + W_{\text{vbend}} + W_{\text{cone}} \\ & + W_{\text{wing}} + W_{\text{strut}} + W_{\text{htail}} + W_{\text{vtail}} + W_{\text{eng}} \\ & + W_{\text{fuel}} + W_{\text{apu}} + W_{\text{hpesys}} + W_{\text{lgnose}} + W_{\text{lgmain}}\end{aligned} \tag{679}$$

However, this expression is <u>not</u> used as written. In order to accelerate the convergence, the components are first segregated into ones which are exactly or nearly constant, e.g.

$$W_{\text{fix}}\ ,\ \ W_{\text{pay}}\ ,\ \ W_{\text{padd}}\ ,\ \ W_{\text{shell}}\ ,\ \ W_{\text{window}}\ ,\ \ W_{\text{insul}}\ ,\ \ W_{\text{floor}}$$

and the remaining ones which are expected to be roughly proportional to the final weight itself. For the latter items, the latest weight fractions and their sum Σ_f are first computed using the best previous W_{MTO}.

$$\begin{aligned} f_{\text{cone}} &= W_{\text{cone}}/W_{\text{MTO}} \\ f_{\text{hbend}} &= W_{\text{hbend}}/W_{\text{MTO}} \\ f_{\text{vbend}} &= W_{\text{vbend}}/W_{\text{MTO}} \\ f_{\text{wing}} &= W_{\text{wing}}/W_{\text{MTO}} \\ f_{\text{strut}} &= W_{\text{strut}}/W_{\text{MTO}} \\ f_{\text{htail}} &= W_{\text{htail}}/W_{\text{MTO}} \\ f_{\text{vtail}} &= W_{\text{vtail}}/W_{\text{MTO}} \\ f_{\text{eng}} &= W_{\text{eng}}/W_{\text{MTO}} \\ f_{\text{fuel}} &= W_{\text{fuel}}/W_{\text{MTO}} \end{aligned} \tag{680}$$

$$\Sigma_f = f_{\text{cone}} + f_{\text{hbend}} + f_{\text{vbend}} + \ldots + f_{\text{fuel}} + f_{\text{apu}} + f_{\text{hpesys}} + f_{\text{lgnose}} + f_{\text{lgmain}} \tag{681}$$

Note that $f_{\text{apu}}, f_{\text{hpesys}}, f_{\text{lgnose}}, f_{\text{lgmain}}$ always stay fixed and do not need to be recomputed.

In summary, assuming that Σ_f stays fixed is equivalent to assuming that the new weight satisfies the following relation.

$$\begin{aligned}(W_{\text{MTO}})_{\text{new}} &= W_{\text{fix}} + W_{\text{pay}} + W_{\text{padd}} + W_{\text{shell}} + W_{\text{window}} + W_{\text{insul}} + W_{\text{floor}} \\ &\quad + (W_{\text{MTO}})_{\text{new}}\, \Sigma_f \end{aligned} \tag{682}$$

At this point, the fraction sum Σ_f is monitored to detect a weight divergence:

$$\Sigma_f \geq 1 \quad \rightarrow \quad \text{weight divergence, stop} \tag{683}$$

$$\Sigma_f < 1 \quad \rightarrow \quad \text{weight converging, continue} \tag{684}$$

For the normal second case, the new total weight can be computed explicitly from (682),

$$(W_{\text{MTO}})_{\text{new}} = \frac{W_{\text{fix}} + W_{\text{pay}} + W_{\text{padd}} + W_{\text{shell}} + W_{\text{window}} + W_{\text{insul}} + W_{\text{floor}}}{1 - \Sigma_f} \tag{685}$$

which is then used with the fractions to obtain the corresponding new component weights.

$$\begin{aligned} W_{\text{cone}} &= (W_{\text{MTO}})_{\text{new}}\, f_{\text{cone}} \\ W_{\text{hbend}} &= (W_{\text{MTO}})_{\text{new}}\, f_{\text{hbend}} \\ W_{\text{vbend}} &= (W_{\text{MTO}})_{\text{new}}\, f_{\text{vbend}} \\ W_{\text{wing}} &= (W_{\text{MTO}})_{\text{new}}\, f_{\text{wing}} \\ W_{\text{strut}} &= (W_{\text{MTO}})_{\text{new}}\, f_{\text{strut}} \\ W_{\text{htail}} &= (W_{\text{MTO}})_{\text{new}}\, f_{\text{htail}} \\ W_{\text{vtail}} &= (W_{\text{MTO}})_{\text{new}}\, f_{\text{vtail}} \\ W_{\text{eng}} &= (W_{\text{MTO}})_{\text{new}}\, f_{\text{eng}} \\ W_{\text{fuel}} &= (W_{\text{MTO}})_{\text{new}}\, f_{\text{fuel}} \\ W_{\text{apu}} &= (W_{\text{MTO}})_{\text{new}}\, f_{\text{apu}} \\ W_{\text{hpesys}} &= (W_{\text{MTO}})_{\text{new}}\, f_{\text{hpesys}} \\ W_{\text{lgnose}} &= (W_{\text{MTO}})_{\text{new}}\, f_{\text{lgnose}} \\ W_{\text{lgmain}} &= (W_{\text{MTO}})_{\text{new}}\, f_{\text{lgmain}} \end{aligned} \tag{686}$$

Updating via expressions (685) and (686) in effect assumes that the weight fractions and their sum Σ_f in the denominator will not change in the next iteration, in contrast to expression (679) which assumes that the weights themselves will not change. Since the former is a much better assumption, using (685) gives a significant improvement in convergence rate over what would be achieved if (679) was used instead. The convergence rates are compared in Figure 23. The improvement is greatest for long-range aircraft, for which the airframe and fuel weights are more strongly coupled.

A convergence factor of ~ 0.20 is typically observed, giving convergence to machine zero in 15–25 iterations. In light of this performance, the far greater complexity of the alternative Newton iteration method is simply not warranted. Its added cost of computing the Jacobian matrix would likely swamp the potentially fewer iterations that it offers.

The overall iteration procedure is shown in Figure 24. After convergence, the result is the aircraft characteristics and performance as functions of the input parameters.

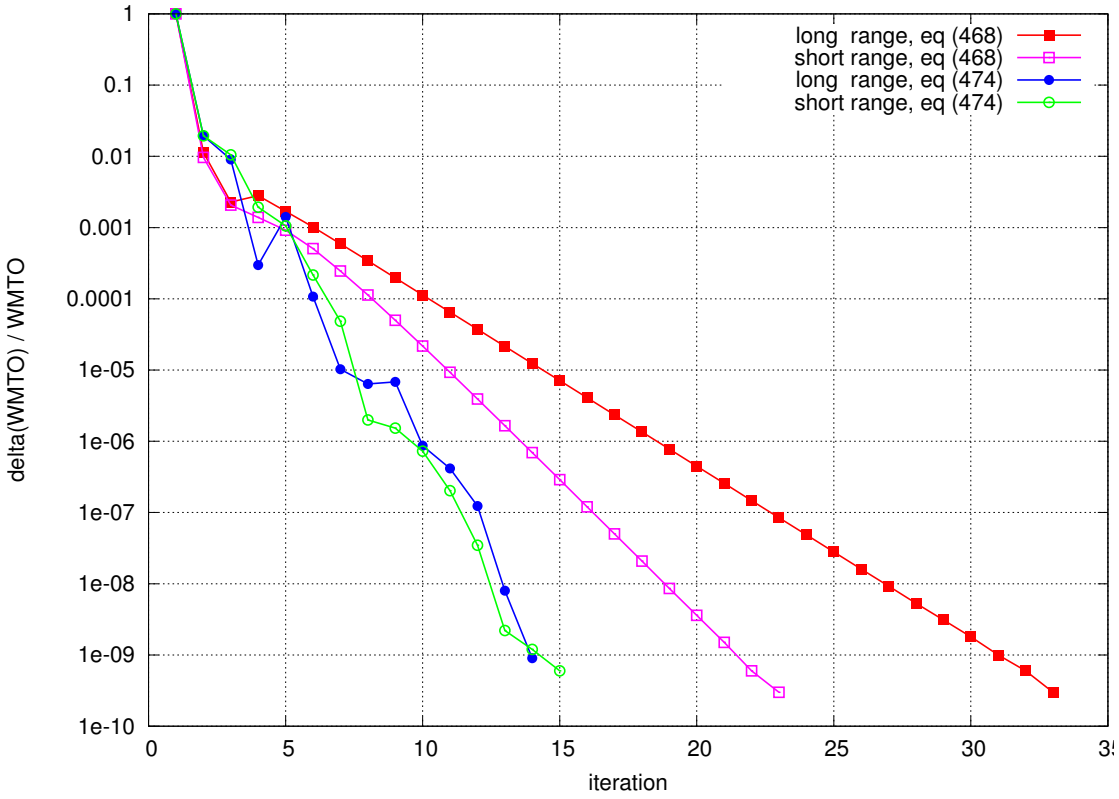

Figure 23: Weight-iteration convergence for long range and short range aircraft.

3.13 Overall Weight Iteration (Off-Design)

For the off-design case, only the fuel weight is updated, to give the takeoff weight W_{TO}.

$$\begin{aligned}(W_{\text{TO}})_{\text{new}} \;=\; & W_{\text{fix}} + W_{\text{pay}} + W_{\text{padd}} + W_{\text{shell}} + W_{\text{window}} + W_{\text{insul}} + W_{\text{floor}} \\ & + W_{\text{cone}} + W_{\text{hbend}} + W_{\text{vbend}} + W_{\text{wing}} + W_{\text{strut}} + W_{\text{htail}} + W_{\text{vtail}} \\ & + W_{\text{eng}} + W_{\text{fuel}} + W_{\text{apu}} + W_{\text{hpesys}} + W_{\text{lgnose}} + W_{\text{lgmain}}\end{aligned} \tag{687}$$

3.14 Takeoff Performance

The takeoff performance of the converged aircraft can be performed after the weight convergence, as a post-processing step. The takeoff quantities of interest are the obstacle-clearance takeoff distance ℓ_{TO}, the balanced field length ℓ_{BF}, and the balanced-field climb angle γ_{BF}. The calculation procedures for these quantities are described in the separate document "Balanced Field Length Calculation".

3.15 Noise Calculation

The mission calculations described above assume a smooth fixed-power climb immediately from takeoff, as shown in Figure 22. However, for takeoff noise calculations a modified noise-abatement initial climb profile is assumed, as shown in Figure 25. Full takeoff power

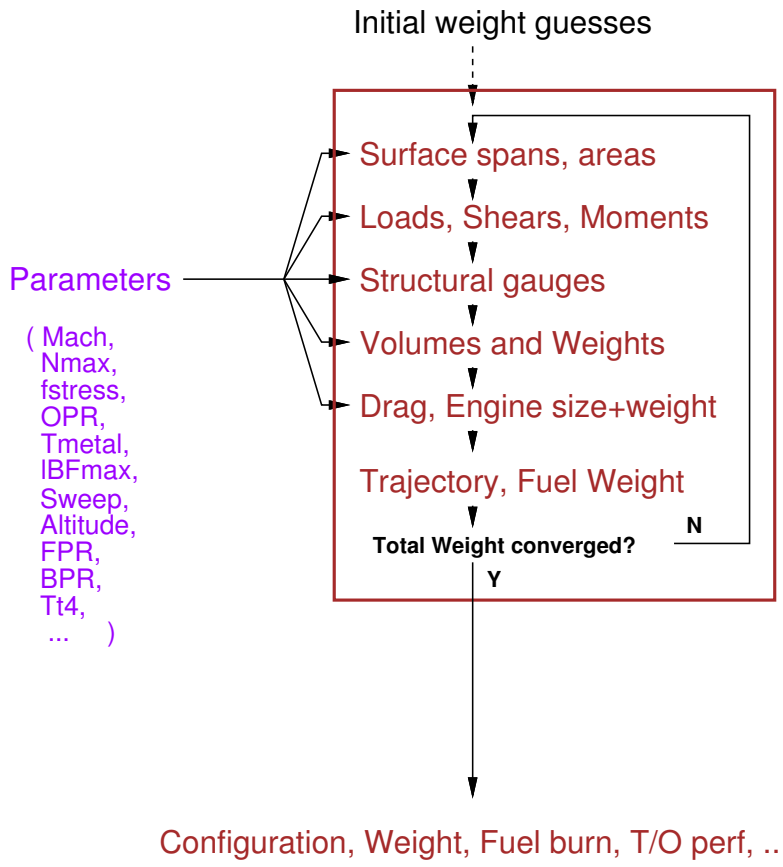

Figure 24: Weight-iteration procedure.

is assumed until the cutback point, which is implicitly specified by the cutback sight angle $\theta_{\rm CB}$. A reduced power is then specified, just enough to maintain the small cutback climb angle $\gamma_{\rm CB}$. The cutback-point location is then determined by geometry.

$$\Delta h_{\rm TO} \;=\; (l_{\rm obs} - l_{\rm TO})\,\frac{\tan\gamma_{\rm TO}}{1+\tan\gamma_{\rm TO}\cot\theta_{\rm CB}} \tag{688}$$

$$l_{\rm CB} \;=\; (l_{\rm obs} - l_{\rm TO})\,\frac{1}{1+\tan\gamma_{\rm TO}\cot\theta_{\rm CB}} \;+\; l_{\rm TO} \tag{689}$$

The sideline noise $dB_{\rm SL}$ is measured at the sideline position at aircraft liftoff point $l_{\rm TO}$ and 450 m laterally, with the aircraft at takeoff power. The cutback noise $dB_{\rm CB}$ is measured from the runway point, with the aircraft at the cutback point $l_{\rm CB}, h_{\rm TO}$ at takeoff power. The flyover noise $dB_{\rm FO}$ is measured from the runway point, with the aircraft directly overhead at cutback power. Optimization constraints can be applied on the three dB noise values to seek the optimum $\theta_{\rm CB}$, and the takeoff and cutback $T_{t\,4}$ values.

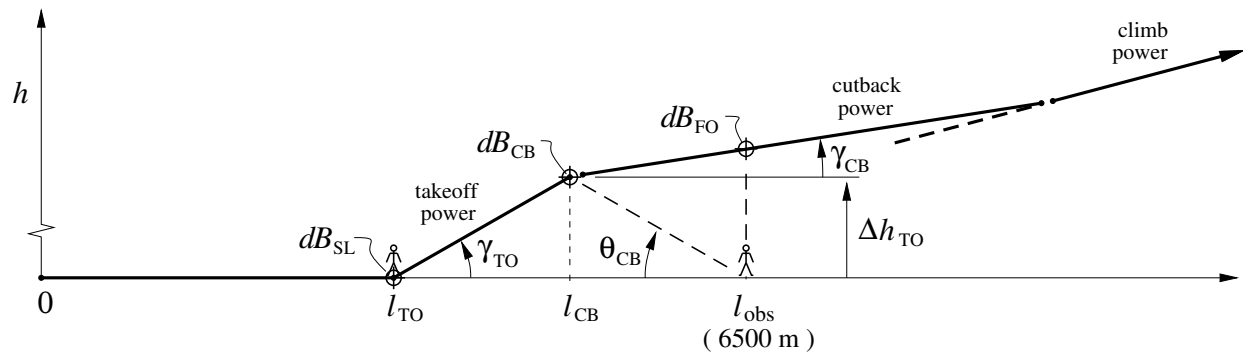

Figure 25: Noise-abatement climb profile.

4 Optimization

The parametric sizing, weight, and performance estimation method described so far is now subjected here to an optimization process, where a selected subset of the model parameters are *computed* via optimization, instead of being explicitly prescribed. The result is a considerable reduction in the number of independent model parameters which need to be considered and manually examined.

4.1 General Theory

Consider an objective function $F_{(q)}$ which depends on a number of independent model parameter quantities q. Now partition these q into two groups v and p,

$$\{q\} = \{v, p\} \tag{690}$$

$$F_{(q)} = F_{(v,p)} \tag{691}$$

where

1. The influence of v on F is non-monotonic, i.e. $\partial F/\partial v = 0$ somewhere in the model parameter space $\{q\}$. In optimization terminology, these v are called *Design Variables*.

2. The influence of p on F is monotonic, i.e. $\partial F/\partial p$ has the same sign throughout the model parameter space $\{q\}$. In optimization terminology, these p are called *Design Parameters*.

The Design Variables v are now explicitly determined by imposing the optimality equations for F with respect to v. These particular v values are denoted by $v^*{}_{(p)}$.

$$\left.\frac{\partial F_{(v,p)}}{\partial v}\right|_{v^*} = 0 \quad \rightarrow \quad v^*{}_{(p)} \tag{692}$$

The corresponding values of F are a simplified function F^* of only the Design Parameters p.

$$F_{(v,p)} \quad \rightarrow \quad F(v^*{}_{(p)}, p) \equiv F^*{}_{(p)} \tag{693}$$

The result is a reduction of the effective design space which needs to be explored, from the original $\{v, p\}$ to the smaller $\{p\}$.

4.2 Present Application

One objective-function output of the present sizing and weight estimation method is the fuel energy consumption per payload-range,

$$F \equiv E_{\rm sp}(AR, \sigma, \ldots) = \frac{W_{\rm fuel}\, h_{\rm fuel}}{W_{\rm pay}\, R_{\rm total}} \tag{694}$$

also known as "*PFEI*". This can be generalized to a fleet-wide fuel consumption, by weight-summing the quantities over any number of fleet missions of varying payload and range,

$$F \equiv E_{\rm sp}(AR, \sigma, \ldots) = \frac{\sum_k w_k\, W_{{\rm fuel}_k}\, h_{{\rm fuel}_k}}{\sum_k w_k\, W_{{\rm pay}_k}\, R_{{\rm total}_k}} \tag{695}$$

where k is the mission index and w_k is the mission weighting factor. Different fuels used for different missions can also be considered, via their different specific heating values $h_{{\rm fuel}_k}$

In the objective function's arguments, AR is the specified aspect ratio, σ represents any one of the material allowable-stress values, and "$\ldots$" denotes the remaining parameters which will be ignored in this example. Clearly, $\partial E_{\rm sp}/\partial\sigma$ will be strictly monotonic negative, since the stronger the material the lighter the aircraft and the less fuel energy it will require, regardless of all the other parameter values. However, $\partial E_{\rm sp}/\partial AR$ is expected to be zero somewhere, since energy requirements increase if AR is too small (C_{D_i} excessive), or if AR is too big ($W_{\rm wing}$ excessive). Therefore it's possible to determine $AR = AR^*$ and corresponding $E^*_{\rm sp}$ where the optimality condition $\partial E_{\rm sp}/\partial AR = 0$ is met, with the result that AR no longer needs to be specified. This reduces the parameter space by one dimension, from $\{AR, \sigma, \ldots\}$ to $\{\sigma, \ldots\}$, as pictured in Figure 26, which a considerable simplification.

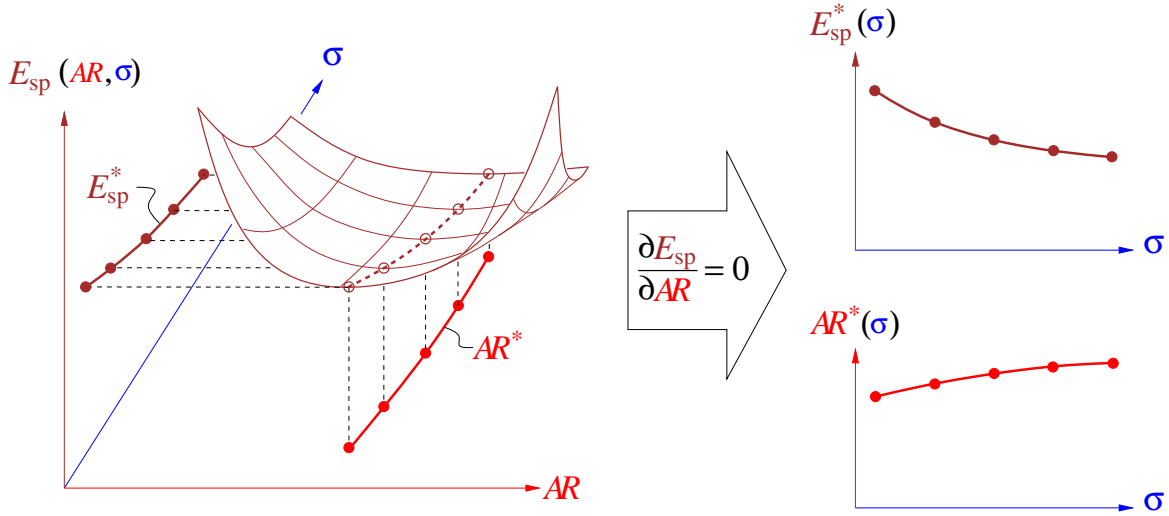

Figure 26: 2D function $E_{\rm sp}(AR, \sigma)$ replaced with two 1D functions $E^*_{\rm sp}(\sigma)$ and $AR^*(\sigma)$ when the $\partial E_{\rm sp}/\partial AR|_{AR^*} = 0$ optimality requirement is imposed.

4.3 Chosen Design Variables

The following quantities have been identified as suitable design variables for the present sizing and weight model.

h_c	start-of cruise altitude
$C_{L_{\rm CR}}$	cruise lift coefficient
AR	aspect ratio
Λ	wing sweep
$\bar{h}$	wing box height/chord ratio (airfoil t/c)
$FPR_{\rm D}$	design fan pressure ratio (also denoted by $\pi_{\rm f_D}$)
$BPR_{\rm D}$	design bypass ratio
$T_{t\,4_{\rm TO}}$	takeoff turbine inlet temperature
$T_{t\,4_{\rm CR}}$	cruise turbine inlet temperature

The remaining quantities are then the independent design parameters which need to be individually or combinatorially sampled to discern their effect on the objective function, and also on the design variables.

The overall iteration procedure with the embedded optimization is shown in Figure 27. After convergence, the results are the aircraft characteristics (including the optimized design variables) and the performance as functions of the input design parameters.

In order to reduce the size of the design parameter space, it is desirable to move as many of the design parameters inside the optimization loop, by declaring them as design variables. This typically requires higher-level fidelity models which can properly capture the effect of the moved variables on the fuel-burn objective function.

4.4 Constraints

The sub-optimization procedure also provides a convenient way to incorporate constraints which the aircraft must meet. One example is the requirement of a minimum balanced field length, $l_{\rm BF} \le l_{\rm BF_{max}}$. The simplest way to implement one or more of such constraints is via penalty functions. For example, the modified objective function would be

$$F \;\equiv\; E_{\rm sp(AR,\sigma,...)} \;+\; K \left\{ \max\left[\, 0 \,,\; l_{\rm BF(AR,\sigma,...)} - l_{\rm BF_{max}} \,\right] \right\}^2 \tag{696}$$

where K is a suitable weighting factor. The optimization procedure will then drive the design variables so that $l_{\rm BF}$ exceeds $l_{\rm BF_{max}}$ by at most a small tolerance, depending on the magnitude of K. Other constraints can also be included by adding similar additional one-sided quadratic terms.

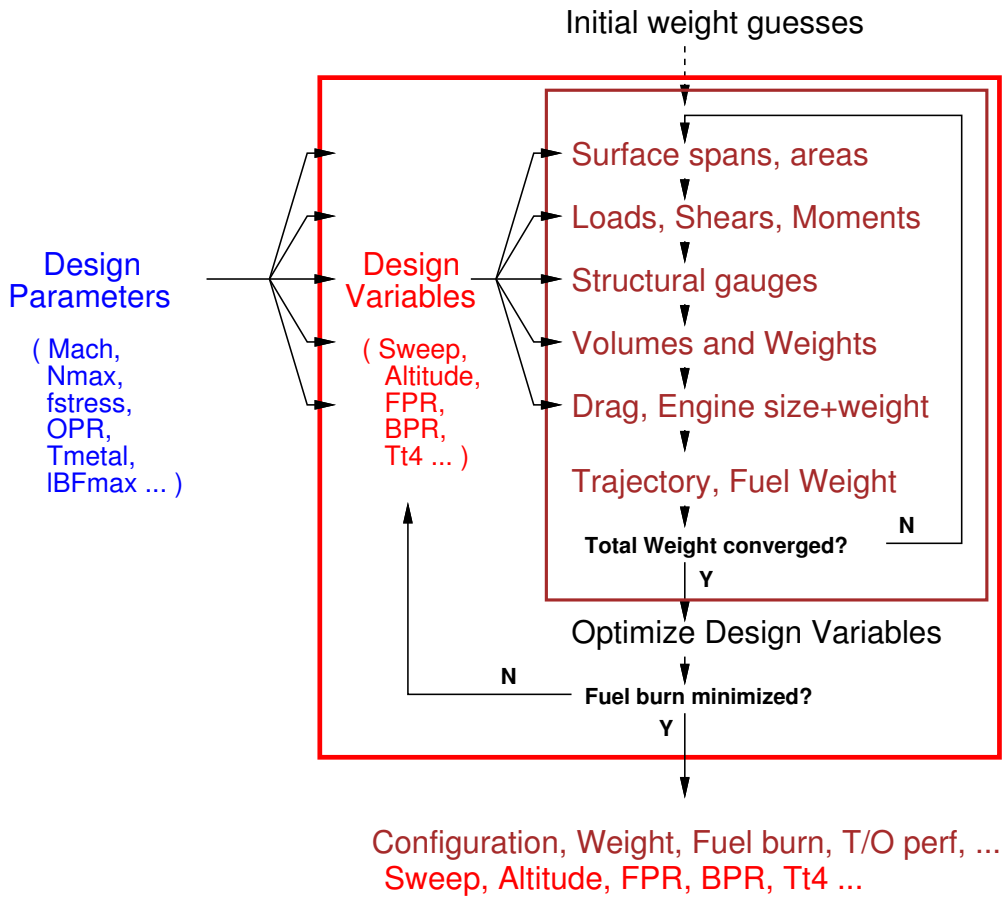

Figure 27: Weight-iteration procedure combined with optimization of the identified design variables.

5 Parameter Sampling

In the optimization process described in the previous section, the Design Parameters remain as independent quantities which can be arbitrarily set. These are typically quantities which are not under the designer's immediate control, such as specified payload and range, material properties, field-length requirements, etc. It is of considerable interest to determine the sensitivity of the optimized aircraft and performance to these external parameters.

An effective way to discern the effect of the parameters is to simply sample them at specified intervals and compute and display the resulting aircraft and performance outputs. The optimization can be optionally performed inside this sampling loop. Sampling up to two parameters (called "i" and "j" parameters) is effective, since the resulting two-dimensional data can be effectively displayed on contour plots or multiple line plots. The overall method organization is shown in Figure 28.

References

[1] J. Roskam. *Airplane Design.* DAR Corporation, Lawrence, Kansas, 2000.

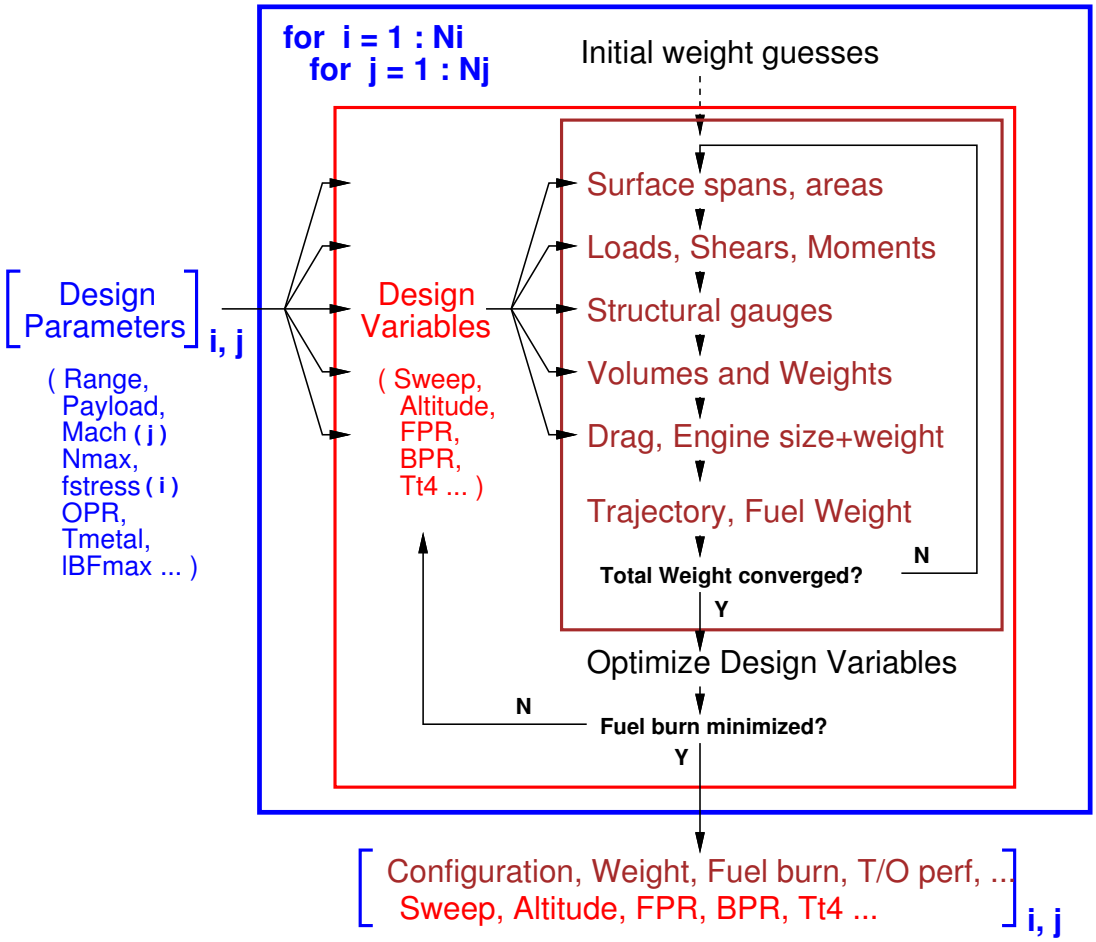

Figure 28: Two-dimensional parameter sampling sweep, wrapped around optimization and weight-iteration loops. The outputs are obtained in a two-dimensional i,j grid.

[2] E. Torrenbeek. *Synthesis of Subsonic Airplane Design*. Delft University Press, 1988.

[3] D.P. Raymer. *Aircraft Design: A Conceptual Approach*. AIAA Education Series. AIAA, 1992.

[4] S. Jayaram, A. Myklebust, and P. Gelhausen. ACSYNT — A standards-based system for parametric computer aided conceptual design of aircraft. AIAA Paper 92-1268, Feb 1992.

[5] W.H. Mason and T.K. Arledge. ACSYNT aerodynamic estimation — An examination and validation for use in conceptual design. AIAA Paper 93-0973, Feb 1993.

[6] M.D. Ardema, M.C. Chambers, A.P. Patron, A.S. Hahn, M. Hirokazu, and M.D. Moore. Analytical fuselage and wing weight estimation of transport aircraft. NASA TM 110392, May 1996.

[7] M.B. Knapp. Applications of a nonlinear wing planform design program. Master's thesis, MIT, Aug 1996.

[8] S. Wakayama. *Lifting Surface Design Using Multidisciplinary Optimization*. PhD thesis, Stanford, June 1994.

[9] S. Wakayama. Blended-wing-body optimization setup. AIAA Paper 00-4740, Sept 2000.

[10] I. Kroo. PASS, Program for Aircraft Synthesis Studies. Software Package, Desktop Aeronautics, Palo Alto, CA, 2005.

[11] J.L. Kerrebrock. *Aircraft Engines and Gas Turbines, 2nd Ed.* The MIT Press, Cambridge, 1996.

[12] M. Drela. Power balance in aerodynamic flows. *AIAA Journal*, 47(7):1761–1771, July 2009. Also AIAA Paper 09-3762, San Antonio Conference, June 2009.

[13] J.K.C. Low. Ultra-high bypass ratio jet noise. NASA Contractor Report NASA CR-195394, NASA, 1994.

[14] J.R. Stone, D.E. Groesbeck, and C.L. Zola. Conventional profile coaxial jet noise prediction. *AIAA Journal*, 21(3), Mar 1983.

[15] M.R. Fink. Airframe noise prediction method. Report FAA-RD-77-29, FAA, 1977.

[16] J. Wolkovitch. The joined wing: An overview. *Journal of Aircraft*, 23(3), Mar 1986.

[17] R. Liebeck. Design of the Blended Wing Body subsonic transport. *Journal of Aircraft*, 41(1), Jan 2004.

[18] M.N. Beltramo, D.L. Trapp, B.W. Kimoto, and D.P. Marsh. Parametric study of transport aircraft systems cost and weight. Technical Report NASA CR 151970, NASA, April 1977.

[19] M. Drela and M.B. Giles. Viscous-inviscid analysis of transonic and low Reynolds number airfoils. *AIAA Journal*, 25(10):1347–1355, Oct 1987.